Radio propagation for the next generation mobile communication system

Hejselbæk, Johannes

DOI (link to publication from Publisher):
10.5278/vbn.phd.tech.00049

Publication date:
2018

Document Version
Publisher's PDF, also known as Version of record

RADIO PROPAGATION FOR THE NEXT GENERATION MOBILE COMMUNICATION SYSTEM

BY
JOHANNES HEJSELBÆK

DISSERTATION SUBMITTED 2018

AALBORG UNIVERSITY
DENMARK

Radio propagation for the next generation mobile communication system

Ph.D. Dissertation

Johannes Hejselbæk

Dissertation submitted: September 7, 2018

Dissertation submitted:	September 7, 2018
PhD supervisor:	Prof. Gert Frølund Pedersen Department of Electronic Systems Aalborg University
Assistant PhD supervisor:	Assoc. Prof. Wei Fan Department of Electronic Systems Aalborg University
PhD committee:	Associate Professor Jan Hvolgaard Mikkelsen (chair.) Aalborg University
	Associate Professor Andrés Alayón Glazunov University of Twente
	Professor Rodney Grant Vaughan Simon Fraser University
PhD Series:	Technical Faculty of IT and Design, Aalborg University
Department:	Department of Electronic Systems

ISSN (online): 2446-1628
ISBN (online): 978-87-7210-260-3

Published by:
Aalborg University Press
Langagervej 2
DK – 9220 Aalborg Ø
Phone: +45 99407140
aauf@forlag.aau.dk
forlag.aau.dk

Printed in Denmark by Rosendahls, 2018

Curriculum Vitae

Johannes Hejselbæk

Johannes Hejselbæk received his B.Sc. E.E. with a specialization in communication systems in 2013 and an M.Sc. E.E. with a specialization in wireless communication systems in 2015. Both degrees were obtained from Aalborg University. His M.Sc. thesis was a result of research conducted in collaboration with Intel Mobile Communications Denmark where he was employed in a part-time position, along with his studies, from 2013 to 2015. Since 2015 he has been employed as a PhD Fellow in the section for Antennas, Propagation and Millimetre-wave Systems (APMS) in the Department of Electronic Systems at Aalborg University. In 2018 he was a visiting junior fellow at Tokyo Institute of Technology, where he collaborated with Takada Laboratory on the topic of 5G propagation. The focus of his current work is on channel characterization by empirical studies and electromagnetic modelling.

Curriculum Vitae

Abstract

The mobile communication industry is moving towards the fifth generation mobile communication system (5G). This thesis presents contributions to the understanding of what is expected to be the radio propagation channel for this next generation mobile communication system. One of the expected attributes of 5G is the support of a very high data rate by exploiting parts of the less utilized radio frequency spectrum above 6 GHz. The 3–30 GHz spectrum is also known as the super high frequency (SHF) or centimetre-wave band, while 30–300 GHz as the extremely high frequency (EHF) or millimetre-wave band. Lately, the frequency range from 6 GHz and up have been referred to as the mm-wave frequencies especially by the industry. These frequencies are very high compared to the ones used for today's mobile communication, which is one of the main reasons for the rekindled interest in the study of the radio propagation channel.

The thesis starts with an introduction to some of the early history of radio communication and the transition to what we today call mobile communication. The introduction is then used as motivation for the research objectives defined for the PhD study. The main focus of the work is collecting propagation data for the future 5G radio channel, investigating the user impact on mm-wave channels and study device-to-device communication in a forest environment.

The reason for focusing on the collection of propagation data is to contribute to the development of radio propagation virtualization tools. These virtualization tools are needed for an efficient development and implementation of 5G in relation to both antenna and transceiver design, as well as radio network planning. The virtualization is achieved by applying a number of channel propagation models. Before these, either existing or newly developed, channel models can be verified there is a need to characterize the radio channel. This characterization is done by performing channel sounding measurements aiming at capturing the different channel characteristics. Especially the transition from the sub 6 GHz to the so-called mm-wave frequencies suggested for 5G have posed questions to which channel parameters prove out to emphasise.

Abstract

The thesis includes a description of the development of a channel sounding system capable of characterizing the propagation channel at both the legacy and newly proposed frequencies for 5G. By applying the developed sounding system it is possible to highlight some of the differences and similarities between the two frequency bands. The sounding system is also used to validate different channel sounding techniques by empirical studies.

A study of the user impact on the mm-wave channel is also a part of this thesis. The study is conducted utilizing a state-of-the-art channel sounder together with a mock-up handset including a linear array operating at 21.5 GHz. Using the measurement setup, an indoor radio channel is investigated both with and without a user holding the handset. This is done to identify the direct impact of the user and the feasibility of adopting beamforming from the handset.

Finally, the thesis presents the development of a measurement system and a measurement campaign aiming at characterizing the propagation channel for device-to-device narrow-band internet-of-things type communication. The measurement campaign, conducted in a forest, is utilized as a basis for comparing the performance of different suggested models including both path-loss and foliage-loss.

Resumé

Mobil kommunikations industrien arbejder imod den femte generation mobil kommunikations system (5G). Denne afhandling præsentere bidrag til forståelsen af hvad der kan forventes af radio udbredelses kanalen for dette næste generations mobil kommunikations system. En af de forventede egenskaber for 5G er dets understøttele af meget høje data rater ved udnyttelse af dele af det mindre udnyttede radio spektrum over 6 GHz. Frekvens spektret fra 3-30 GHz er også kendt som super high frequency (SHF) båndet eller centimeter-bølge båndet, mens 30–300 GHz er kendt som extremely high frequency (EHF) båndet eller millimeter-bølge båndet. På det seneste er frekvenser over 6 GHz alle blevet refereret til som millimeter-frekvenser specielt af industrien. Disse frekvenser er meget høje sammenlignet med dem der anvenders til mobil kommunikation i dag, hvilket er en af hovedårsagerne til den fornyede interesse i at studere radioudbredelses kanalen.

Denne afhandling starter med en introduktion til noget af den tidlige historie omkring radio kommunikation og udviklingen frem til det vi i dag kalder for mobil kommunikation. Introduktionen anvendes som motivation for de forskningsmål der er defineret for dette Ph.d. studie. Hovedfokus for dette studie har være på indsamlingen af radioudbredelses data for den fremtidige 5G radio kanal, undersøgelse af brugeres indflydelse på mm-bølge kanalen og undersøgelse af enhed-til-enhed kommunikation i et skov miljø.

Grundet til der er fokus på indsamling af radioudbredelses data er for at kunne bidrage til udvikling af radioudbredelses virtualiserings værktøjer. Disse værktøjer er nødvendige for effektivt at kunne udvikle of implementere 5G i forbindelse med både antenne og transceiver radio såvel som radio netværksplanlægning. Virtualiseringen opnås gennem en række radioudbredelsesmodelleer. Før disse, enten eksisterende eller nyudviklede, kanalmodeller kan verificeres er det nødvendigt at karakterisere radiokanalen. Denne karakterisering gennemgøre ved at foretage kanalmålinger med det formål at karakterisere kanalens forskellige egenskaber. Specielt skiftet fra frekvenser under 6 GHz til de såkaldte mm-bølge frekvenser der er foreslået til anvendelse af 5G har stillet spørgsmål til hvilke kanal egenskaber der har størst betydning.

Denne afhandling indeholder en beskrivelse af udviklingen af et radiokanal målesystem i stand til at karakterisere radioudbredelseskanalen ved både de nutidige of fornyeligt foreslåede frekvenser til 5G. Ved at anvende det udviklede målesystem er det muligt at tydeligøre nogle af de forskelle og ligheder der er mellem de to frekvensbånd. Målesystemet er også anvendt til at verificere forskellige radiokanal måleteknikker gennem empiriske undersøgelser

Et studie af bruger påvirkningen af mm-bølge kanalen er også en del af denne afhandling. Studiet er gennemført ved at anvende et state-of-the-art radiokanal målesystem sammen med et model håndsæt indeholdende et lineært array tunet til 21.5 GHz. Ved at anvender denne måleopstilling undersøges et indendørs radiomiljø med og uden en bruger der holder håndsættet. Dette er gjort for at identificere den direkte påvirkning brugeren har og anvendeligheden af beamforming fra håndsættet.

Slutteligt præsentere afhandlingen også udviklingen af et målesystem og en målekampagne med det formål at karakterisere radioudbredelseskanalen for enhed-til-enhed smal-bånds internet-of-things kommunikation. Målekampagnen, gennemført i en skov, anvendes som udgangspunkt for en sammenligning af præstationen af forskellige foreslåede kanalmodeller der inkludere både udbredelses og vegetations tab.

Contents

Thesis Details

Thesis Title:	Radio propagation for the next generation mobile communication system
PhD Candidate:	Johannes Hejselbæk
Supervisors:	Prof. Gert Frølund Pedersen - Aalborg University Assoc. Prof. Wei Fan - Aalborg University

This thesis is submitted as partial fulfilment of the requirements for the degree of Doctor of Philosophy (PhD) from Aalborg University, Denmark. The thesis is compiled as a collection of papers resulting in the main part of the thesis being scientific papers published in, or submitted to, peer-reviewed journals and conferences. The work presented in the thesis is the result of three years of research, in the period September 2015 – August 2018, as a PhD fellow in the Section of Antennas, Propagation and Millimetre-wave Systems (APMS), Department of Electronic Systems, Aalborg University.

The PhD stipend (nr. 8-15048) has been funded as a part of the VIRTUOSO project. The Innovation Fund Denmark have together with Aalborg University and industry partners; Telenor, Keysight, and Intel Mobile Communications financed this project.

The main body of this thesis consist of the following papers:

A. Johannes Hejselbæk, Wei Fan, Gert F. Pedersen, "Ultrawideband VNA Based Channel Sounding System for Centimetre and Millimetre Wave Bands.", *IEEE 27th Annual International Symposium on Personal, Indoor, and Mobile Radio Communications (PIMRC)*, 2016

B. Johannes Hejselbæk, Yilin Ji, Wei Fan, Gert F. Pedersen, "Channel Sounding System for MM-Wave Bands and Characterization of Indoor Propagation at 28 GHz." *International Journal of Wireless Information Networks*, Vol. 24, Nr. 3, p. 204-216, 2017

C. Johannes Hejselbæk, Anders Karstensen, Jesper Ø. Nielsen, Wei Fan, Gert F. Pedersen, "Validation of Emulated Omnidirectional Antenna

Output Using Directive Antenna Data." *11th European Conference on Antennas and Propagation (EuCAP). IEEE*, p. 131-135., 2017

D. Johannes Hejselbæk, Jesper Ø. Nielsen, Wei Fan, Gert F. Pedersen, "Measured 21.5 GHz Indoor Channels With User-Held Handset Antenna Array", *IEEE Transactions on Antennas and Propagation*, Vol. 65, Nr. 12, p. 6574 - 6583., 2017

E. Johannes Hejselbæk, Jesper Ø. Nielsen, Christian Drewes, Wei Fan, Gert F. Pedersen, "Propagation Measurements for Device-to-Device Communication in Forest Terrain." *12th European Conference on Antennas and Propagation (EuCAP). IEEE*, 2018.

F. Johannes Hejselbæk, Jesper Ø. Nielsen, Wei Fan, Gert F. Pedersen, "Empirical Study of Near Ground Propagation in Forest Terrain for Internet-of-Things type Device-to-Device Communication.", *IEEE Access*, SUBMITTED 2018

According to the Ministerial Order no. 1039 of August 27, 2013, regarding the PhD Degree § 12, article 4, statements from each co-author about the PhD students contribution to the above-listed papers have been provided to the PhD school for approval prior to the submission of this thesis. These co-author statements have also been presented to the PhD committee and included as a part of their assessment.

In addition to the listed papers as the main content of this thesis, the following papers were also either authored or co-authored during the PhD studies. As these papers are not a part of the main body of this thesis they have not been included in print. The reader is therefore kindly referred to their respective publishing channels as listed hereafter.

1. Johannes Hejselbæk, Anders Karstensen, Jesper Ø. Nielsen, Gert F. Pedersen, "Angular Power Distribution Measurements and Modelling of Outdoor Urban Environment Using Ray-tracing at 2 and 18 GHz." *10th European Conference on Antennas and Propagation (EuCAP). IEEE*, 2016.

2. Johannes Hejselbæk, Igor A. Syrytsin, Patrick C. F. Eggers, "Measurements of UWB Pulse Propagation Along a Wind Turbine Blade at 1 to 20 GHz" *12th European Conference on Antennas and Propagation (EuCAP). IEEE*, 2018.

3. Yilin Ji, Johannes Hejselbæk, Wei Fan, Gert F. Pedersen, "A Map-Free Indoor Localization Method Using Ultrawideband Large-Scale Array Systems." *IEEE Antennas and Wireless Propagation Letters*, 2018

4. Panawit Hanpinitsak, Johannes Hejselbæk, Kentaro Saito, Wei Fan, Junichi Takada, Gert F. Pedersen, "Frequency Dependency Analysis of Geometry based Clusters in Indoor Environments at SHF Bands", *International Journal of Antennas and Propagation*,
DRAFTED 2018

5. Samantha Caporal Del Barrio, Johannes Hejselbæk, Art Morris, Gert F. Pedersen, "Combining Antenna and Ground Plane Tuning to Efficiently Cover Tv White Spaces on Handsets." *11th European Conference on Antennas and Propagation (EuCAP). IEEE*, p. 2964-2968., 2017

6. Marie Mbeutcha, Wei Fan, Johannes Hejselbæk, Gert F. Pedersen, "Evaluation of massive MIMO systems using time-reversal beamforming technique." *27th Annual International Symposium on Personal, Indoor, and Mobile Radio Communications (PIMRC): Workshop: Inclusive Radio Communication Networks for 5G and Beyond (IRACON2016)*, 2016.

Preface

I enjoy a challenge and always strive to finish what I have started. However, when I first started at Aalborg University (AAU) in 2010 I had no plans what so ever spending the next eight years there. In fact, my plan was to get my engineering degree as fast as possible as a Diploma-Engineer and then find a job. The first step to change this was the introduction to the almost magical world of electromagnetics. Understanding how invisible electrical fields together with their magnetic counterpart could transfer energy and information has triggered an urge for exploration. I have had this urge for exploring and experimenting since my childhood. I needed to understand this new field of knowledge and it soon became clear to me that would require enrolling as a master student and prolonging my studies. During my master studies, I realized that the best way of continuing my exploration was to aim for a PhD stipend which was encouraged by Prof. Gert Frølund Pedersen.

The encouragement of Prof. Gert Frølund Pedersen together with some persistence from my side resulted in my PhD stipend with him as the main supervisor. I am grateful for both the opportunity and the support I have received, all this would have not been possible without you.

I also have to give a special thank you to my co-supervisor Assoc. Prof. Wei Fan for putting up with my stubbornness and at times very different ways of working while still guiding me throughout my time as a PhD student. Thank you for supporting me even when I chose to follow directions which lead me away from the path I think you intended me to follow.

Another person who requires the utmost gratitude is Assoc. Prof. Jesper Ødum Nielsen who has been a very large part of my work the last three years. Without your expertise and willingness to mentor me I would never have obtained my current knowledge and insights in the field of channel sounding. As you know I hope to continue my academic endeavour with you as my mentor and I am grateful that you accepted this proposal.

I would also like to extend my gratitude to all my colleagues which have put up with me for the last three years. I thank you all for fruitful discussions, your help with all kind of problems and most of all for listening to me when I needed to complain. I do hope that some of my efforts, advice and other

help can serve as repayment for all I have received from you.

I also need to thank my family and friends for unconditionally supporting my endeavour in obtaining a PhD degree. This even when it was not clear to them why I chose this path out of the many and perhaps, even more perplexing, stuck to it. I look forward to being able to spend more time with all of you.

Finally, I would like to add a quote which has helped me smile, even when I felt there was no progress in my research. It reminds me that the path towards knowledge, which I still follow, is full of twists and turns.

An expert is a person who has found out by his own painful experience all the mistakes that one can make in a very narrow field — Niels Bohr

Johannes Hejselbæk
Aalborg University, September 3, 2018

Part I

Introductory Chapters

Chapter 1 - Introduction

This chapter serves as an introduction to the main contents of this thesis. The first two sections provide a brief summary of the early start of wireless communication and the history of mobile communication. This is followed by a presentation of the research objectives for the work laying the foundation for this theses. Lastly, a section is included to give an overview of the thesis structure.

1.1 The birth of wireless communication

Do you know when it first saw the light, this electric telegraph, one of the most marvellous applications of modern science?

It was in that memorable year, 1822: Oersted, a Danish physicist, held in his hands a piece of copper wire, joined by its extremities to the two poles of a Volta pile. On his table was a magnetized needle on its pivot, and he suddenly saw (by chance you will say, but chance only favours the mind which is prepared) the needle move and take up a position quite different from the one assigned to it by terrestrial magnetism. A wire carrying an electric current deviates a magnetized needle from its position. That, gentlemen, was the birth of the modern telegraph.

— Louis Pasteur, 1854 [1]

In fact, Hans Christian Ørsted discovered that an electric current produces a magnetic field already in 1820 [2,3]. The new evidence of a connection between electricity and magnetism encouraged André Marie Ampère to start formulating a combined theory of electricity and magnetism the very same year [4]. Another scholar, Michael Faraday, also picked up an interest for electromagnetism and described the electromagnetic forces as lines [4]. The idea of lines of force lead James Clerk Maxwell to the unification of the electric and magnetic forces in the famous Maxwell's equations published in 1861-1862 [5]. What most consider as Maxwell's equations are in fact the reformulated versions as derived by Oliver Heaviside in 1884-1885 [6].

Maxwell had theorized the existence of airborne electromagnetic waves but it was Heinrich Rudolf Hertz who proved their existence with experi-

ments performed between 1886 and 1889 [7].

The application of Hertzian (radio) waves for wireless telegraphy was predicted in 1892 by William Crookes [8]. In 1893 Nikola Tesla was giving lectures at the Franklin Institute in Philadelphia on the transmission of electromagnetic energy at high-frequency [9]. The following year in 1894 Oliver Lodge and Alexander Muirhead demonstrated wireless signalling using radio waves at Oxford University Museum of Natural History [10]. The same year Jagadish Chandra demonstrated the application of wireless signalling with wavelengths in the millimetre range in India [11].

In 1894 Guglielmo Marconi began his work on commercializing wireless telegraphy. In July 1896 he sent signals a 1.6 km over central London and in September 3.2 km across Salisbury Plain. In May 1897 he transmitted across the Bristol Channel and in December same year from the Isle of Wight to a ship in the English Channel [10]. Marconi was committed to prove the commercial possibilities and in December 1901 he received his famous tree dots (morse code for S) send from England at Signal Hill in Newfoundland, Canada. This cross Atlantic transmission was made possible not only by the entrepreneurship of Marconi by also by applying Tesla coil oscillators developed by Nikola Tesla and a receiver (coherer) developed by Jagadish Chandra Bose making this a world-class achievement in more than one aspect [9,12].

In 1901 the papers of Karl Ferdinand Braun on wireless transmission was published [13]. Especially one of the inventions described herein was important for the advance of wireless communication. Until this point, the generation of the transmission signal was conducted by connecting an antenna directly to a spark gap generator. This meant that the mismatch of the impedance between the antenna and generator would quickly dampen the oscillations, resulting in losses in signal strength. Braun designed a coupled resonant circuit with an inductive coupling to the antenna which improved the efficiency of the transmitter greatly. In 1899 he went to Cuxhaven to conduct experiments which proved to be a success with regular wireless transmissions over distances of 62 km to the island of Heligoland [14]. In 1898 he applied for a patent on his sparkless oscillator in Germany and a year later in 1899 for a patent in the United States which was granted to him in 1904 [15,16].

In 1909 Braun and Marconi jointly received the Nobel Prize for their contributions to the development of wireless telegraphy. At this time the field of wireless telegraphy was of great interest and numerous discoveries and inventions had already, or would in the following decades, contribute to the progress towards what we today know as wireless communication [17].

1.2 Introduction of mobile communication

What could be seen as early commercial mobile communication emerged already in the 1920s after the end of the first world war. At this time Bell labs and others tested car-based mobile radios together with transportable teleradios developed during the war [18]. However, these radios where one or two-way radios connected to the land-based telephone system by an operator. In this text, the concept of a mobile communication system is defined to be a system designed specifically for mobile telephones. Mobile phones, also often denoted as cellular phones, needed the passing of the Second World War before the technology matured [19].

In 1947 the concept of a cell divided system was coined by Douglas H. Ring and William R. Young form Bell labs in a company memorandum [20]. They described the idea of providing wireless service to a wide area by dividing it into a set of smaller regions or cells. Each of these cells should have a transceiver covering its own area with a number of frequency channels for its users as well as having frequency channels allocated to communicate with neighbouring cells. This idea of frequency reuse and planning was addressing already then the problem of limited available radio frequency spectrum.

Through the 1950s to the 70s different smaller mobile communication networks emerged. In 1969 the concept of handover was introduced and in 1972 a cellular system including handovers was patented [21,22]. The first handheld mobile phone was designed by Martin Cooper from Motorola in 1973 [23]. The first large-scale cellular mobile communication network was deployed in Tokyo by Nippon Telegraph and Telephone Corporation (NTT) in 1979 [24]. This network was followed by the first fully automatic cellular phone system Nordic Mobile Telephony (NMT) which was first deployed in 1981 in Saudi Arabia. The same year the NMT network was deployed in Sweden and Norway and the following year in Denmark and Finland. The four Scandinavian countries were the first to offer roaming made available through the use of the common network standard [25]. Both the NTT and NMT network was based on analogue technology which is referred to as the first generation mobile communication network or abbreviated as 1G.

The migration from analogue towards digital technology occurred with the second generation mobile communication network (2G) emerging in the early 90s [26]. With the introduction of a digital network, the path was open for a new service, mobile data. Until this point, mobile communication was only used for voice. Mobile data would revolutionize the way mobile phones were used and it started with the simple popular feature of Global System for Mobile communications (GSM); Short Messaging Service (SMS). GSM was developed by the European Telecommunications Standards Institute (ETSI) and have become the most used 2G standard worldwide with more than 9

billion connected devices [27]. To put that in perspective, that is more than the number of people on earth. In 1996 Nokia introduced the Communicator 9000 which is considered to the be the first early smartphone [28].

The rapid increase in demand for data service initiated the development of the third generation mobile communication network (3G). Already in the mid-80s a concept denoted International Mobile Telecommunications-2000 (IMT-2000) was promoted by the International Telecommunication Union (ITU) [29]. The main idea was to obtain a worldwide interoperability providing the capability of seamless global roaming. In the year 2000, a unanimous decision was taken by the members of ITU to follow the IMT-2000 for 3G. In the European Union, the 3G standard chosen was Universal Mobile Telecommunications System (UMTS) which since 1999 have been managed by the 3rd Generation Partnership Project (3GPP). The first UMTS network was launched in Oslo, Norway in 2001 [19].

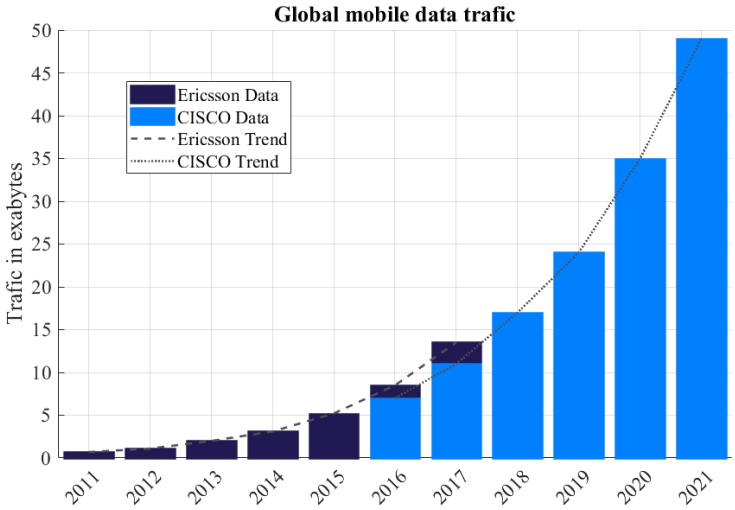

Fig. 1.1: Global mobile data trafic in exabytes (10^{18} bytes). 2011 - 2017 from Ericsson based on measurements [30]. 2016 - 2021 from Cisco based on predictions [31].

The introduction of mobile broadband with 3G drove the demand for mobile data even further. As a result, 3GPP released the first version of Long Term Evolution (LTE) in 2009 [32]. Some describe LTE as the fourth generation mobile communication network (4G) but it does not completely fulfil the requirement of e.g. 1 Gbit/s data rates listed by ITU in their definition of 4G, denoted IMT-Advanced [33]. Talking about 4G has therefore been quite diffuse and it has been more convenient to refer to the releases of LTE by 3GPP. LTE release 10 in 2011 provided the LTE-Advanced (LTE-A) standard which provides major enhancements in data rates as compared to LTE [32]. However, the demand for mobile broadband data is increasing exponentially as

seen in Fig. 1.1 resulting in the industry still having an incentive to improve the mobile communications standards.

The LTE-A standard is continuously evolving to take advantage of new developments and technologies. However, the requirement of backwards comparability is in some aspects limiting the development taking full advantages of recent research efforts. This has made the industry look towards a fifth generation mobile communication network (5G). In 2015 the ITU approved the IMT-2020, a framework for 5G, which besides providing vast improvements in mobile broadband throughputs also addresses new communication use cases as low latency, high reliability and very high number of connected devices [34]. A comparison between the requirements of IMT-Advanced (4G) and IMT-2020 (5G) is shown in Fig. 1.2a. Fig. 1.2b shows the three main development directions from IMT-Advanced to IMT-2020 and their applications. The use of a triangle in Fig. 1.2b illustrates the fact that these three directions to some extent counteract each other. An example on this is the gigabytes in a second application whose implementation will most likely require a sacrifice in latency and number of devices connected.

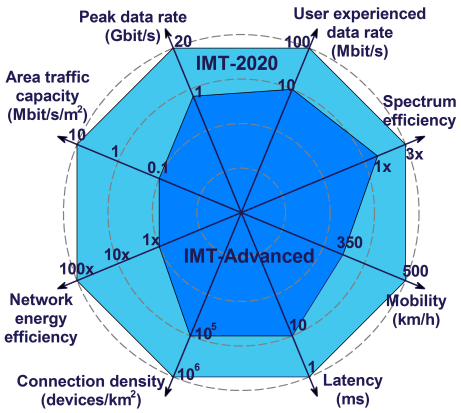

(a) Comparison between IMT-Adcanced and IMT-2020

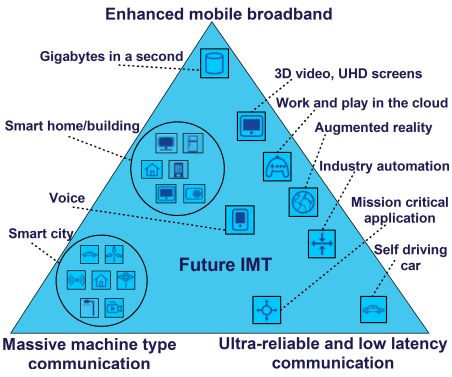

(b) The three main directions for 5G and example applications.

Fig. 1.2: Illustrations of ITUs vision for 5G, redrawn from [34].

Enabling the next generation mobile communication network requires a monumental effort from both academia and the mobile industry. One of these work efforts is the *VIRTUalized envirOnment for communication System development and Optimization* (VIRTUOSO) project which initiated in 2014. This project is a result of collaboration between The Innovation Fund Denmark, Aalborg University and industry partners; Telenor, Keysight, and Intel Mobile Communications. The contents of this thesis is a result of the contributions made by the author as a part of this project.

1.3 Research Objectives

The VIRTUOSO project, which this PhD project is a part of, focuses on the ability to virtualize the testing of mobile systems performance. To enable a virtualization of the radio channel, a deep understanding of all involved propagation mechanisms is needed.

The focus of this PhD study has been on the characterization of the wireless radio channels intended for 5G. 5G is expected to support a very high data rate by exploiting parts of the less utilized spectrum above 6 GHz together with the spectrum already allocated for mobile communication. Some of these newly suggested frequency allocations, in general referred to as mm-wave frequencies, are very high compared to the ones used for current mobile networks. Due to this, there is an interest in investigating these new frequency ranges to highlight the differences and similarities in propagation behaviour to legacy frequency bands. Further on, multiple new use cases have been defined for 5G which in some scenarios introduces new or less known radio channels. The propagation characteristics of these radio channels are also investigated. This is quite a broad definition of the research focus and as a result, a number of sub research objectives have been defined as shown in the following.

1) **Collection of propagation data.**
   When this PhD started only a few measurements were available describing the expected early mm-wave channels located close to 28 GHz. As a result, the first objective was to provide measurement data by utilization of channel sounding. To perform channel sounding of high quality it was needed to develop measurement systems and procedures. To allow for comparison between legacy and new frequency bands the developed measurement system needed to be able to operate on a very broad frequency span. The aim of the comparison measurements was to identify what channel properties changed significantly and what knowledge perhaps could be shared between the two bands. More specifically, there is an interest in studying the relation between Angle of Arrival (AoA) and the evolution of clusters for the two frequency bands. The result of this study is to be utilized for channel modelling efforts related to the virtualization of the radio channel.

2) **Study of the user impact on a mm-wave channel.**
   User shadowing/blocking is a known phenomenon at e.g. 60 GHz from the studies conducted in relation to the IEEE 802.11ad standard which is used for short-range indoor to indoor communication. Another known phenomenon is the absorption due to the user's hand/head close to the handset antenna. The objective of this research item was therefore to

perform a measurement capable of capturing the radio channel with a user holding a handset operating close to the expected mm-wave channel at 28 GHz. The aim was to see to which extend the user would block the signal or significantly change the dominant signal path in an indoor scenario. The measurements, therefore, had to be done both with and without a user for comparison. The findings from this study serve as input to the development of virtualization tools.

3) **Investigation of Device-to-Device communication in forest terrain.** One of the emerging technologies related to 5G is the use of Device-to-Device (D2D) communications as a way of either offloading the network or extending its range into rural areas etc. The technology is also interesting in relation to internet-of-things (IoT) where small devices might be deployed in areas where they would need a powerful transceiver to connect with the cellular network. By applying D2D communication they could form an ad hoc network which would reduce their cost and power consumption. The objective of this research item was to investigate the coverage range with a near-ground deployment of a D2D system in a forest utilizing Narrow Band IoT (NB-IoT). An NB-IoT system should be able to operate with a path-loss of 164 dB as specified by its standard. Conducting measurements with this high path-loss required the development of a special measurement system. The aim was to measure the path-loss in a forest and compare the results to known models. This study is to provide knowledge needed for the implementation of a link-level virtualization tool for NB-IoT.

1.4 Thesis Structure

This thesis consists of two parts. The first part contains introductory chapters while the second contains scientific papers produced by the author.

The first part includes four chapters. Chapter 1 serves to provide the reader with some insights into the history of mobile communication and also introduce the objective of the research presented in this thesis. Chapter 2 provides some background knowledge related to the research topics presented in the thesis. Chapter 3 briefly describes motivation, contents and main findings of the contributions included in the second part of the thesis. Finally, chapter 4 serves as a summary and concludes this work.

The second part includes the main content of this thesis in the form of 6 scientific papers (A to F).

References

[1] L. Pasteur, *Inaugural Address as newly appointed Professor and Dean (Sep 1854) at the opening of the new Faculté des Sciences at Lille (7 Dec 1854). In René Vallery-Radot, The Life of Pasteur, translated by Mrs. R. L. Devonshire, Page 76*, 1911.

[2] H. C. Oersted, "Experiments on the effect of a current of electricity on the magnetic needle," *Annals of Philosophy*, vol. 16, pp. 273–277, 1820.

[3] ——, "Experimenta circa effectum conflictus electrici in acum magneticam," *Johannis Christianus Orsted*, Jul. 1820.

[4] N. Forbes and B. Mahon, *Faraday, Maxwell, and the Electromagnetic Field - How two men revolutionized physics*. Prometheus Books, 2014, ISBN: 987-1-61614-942-0.

[5] J. C. Maxwell, "On physical lines of force; part 1-4," *Philosophical Magazine*, vol. 21 & 23, 1861.

[6] O. Heaviside, "Electromagnetic induction and its propagation, sec. 4," *Electrician*, 1885.

[7] H. Hertz, "On electromagnetic effects produced by electrical disturbances in insulators," *Electric Waves*, pp. 96–106, 1888.

[8] W. Crookes, "Some possibilities of electricity." *Fortnightly Review*, vol. 51, p. 173–181, 1892.

[9] M. J. Seifer, *Wizard - The Life and times of Nikola Tesla, Biography of a genius*. Prometheus Books, 2014, ISBN: 987-1-61614-942-0.

[10] S. Hong, *Wireless : from Marconi's black-box to the audion*. MIT Press, 2001, ISBN: 0-262-08298-5.

[11] Indian National Science, *Pursuit and Promotion of Science The Indian Experience (Chapter 2)*, 2001.

[12] P. K. Bondyopadhyay, "Sir j.c. bose diode detector received marconi's first transatlantic wireless signal of december 1901 (the 'italian navy coherer' scandal revisited)," *Proceedings of the IEEE*, vol. 86, no. 1, pp. 259–285, Jan 1998.

[13] K. F. Braun, *Drahtlose Telegraphie durch Wasser und Luff*. Leipzig Verlag von Veit & Comp., 1901.

[14] ——, "Electrical oscillations and wireless telegraphy," Nobel Lecture, Dec. 1909, - Available Online: https://www.nobelprize.org/nobel_prizes/physics/laureates/1909/braun-lecture.pdf.

[15] ——, "Schaltungsweise des mit einer luftleitung verbundenen gebers für funkentelegraphie," Deutsche Republik Patent 111 578, 1898.

[16] ——, "Wireless electric transmission of signals over surfaces," U.S. Patent US750 429A, 1899.

[17] M. Salazar-Palma, A. Garcia-Lamperez, A. Garcia-Lampérez, T. K. Sarkar, and D. L. Sengupta, "The father of radio: A brief chronology of the origin and development of wireless communications," *IEEE Antennas and Propagation Magazine*, vol. 53, no. 6, pp. 83–114, Dec 2011.

[18] Federal Communications Commission, "A short history of radio," Inside Focus on Mobile Radio, 2003.

[19] T. Farley, "Mobile telephone history," *Telektronikk*, vol. 3/4, pp. 022–034, 2005.

[20] D. H. Ring, "Mobile telephony - wide area coverage - case 20564," Cover Sheet for Technical Memoranda, Bell Telephone Laboratories, Dec. 1947.

[21] C. E. Paul, "Telephones aboard the metroliner," *Bell Laboratories Record*, vol. 77, pp. 76–84, Mar. 1969.

[22] A. E. Joel, "Mobile communication system," U.S. Patent US3 663 762, 1972.

[23] E. Gregersen, "Martin cooper - american engineer," *Encyclopædia Britannica*, 2017.

[24] A. F. Molisch, *Wireless communications*. IEEE Press, 2005, ISBN: 978-0-470-84888-3.

[25] J. Meurling and R. Jeans, *The mobile phone book: the invention of the mobile telephone industry*. London: Communications Week International on behalf of Ericsson Systems, 1994, ISBN: 0952403102.

[26] T. S. Rappaport, *Wireless communications - Principles and Practice*. Prentice Hall, 2002, ISBN: 0-13-042232-0.

[27] The GSM Association, - Available Online: https://www.gsma.com/.

[28] Nokia, *Towards Telecommunications - Nokia since 1865*, Aug. 2000.

[29] International Telecommunication Union, "About mobile technology and imt-2000," 2011, - Available Online: https://www.itu.int/osg/spu/imt-2000/technology.html.

[30] Ericsson, "Ericsson mobility report," 2018, - Available Online: http://www.ericsson.com/mobility-report.

[31] Cisco, "Cisco Visual Networking Index: Global Mobile Data Traffic Forecast Update, 2016–2021 White Paper," Feb. 2017, - Available Online: http://www.cisco.com/c/en/us/solutions/collateral/service-provider/visual-networking-index-vni/white_paper_c11-520862.html.

[32] The 3rd Generation Partnership Project (3GPP), - Available Online: http://www.3gpp.org/.

[33] ITU, *Requirements related to technical performance for IMT-Advanced radio interface(s)*, ITU-R M.2134, 2008.

[34] ——, *Framework and overall objectives of the future development of IMT for 2020 and beyond*, ITU-R M.2083, 2015.

Chapter 2 - Technical Content

This chapter provides some background knowledge and discussions related to the research topics presented in this thesis. The first section introduces the definition of the radio propagation channel and some of the methods used to describe and model this. The second section describes the principal of channel sounding and the application of different methods and techniques.

2.1 The radio propagation channel

The radio propagation channel is a description of the physical path the radio wave signal travels/propagates to provide a connection between the entities of the radio system. The radio wave is emitted and captured by the antennas, hence the antennas inherently are a part of the radio propagation channel. As a result, in this text it is chosen to subdivide, the radio propagation channel into the pure propagation channel and the radio channel also including the antennas as shown in Fig. 2.1.

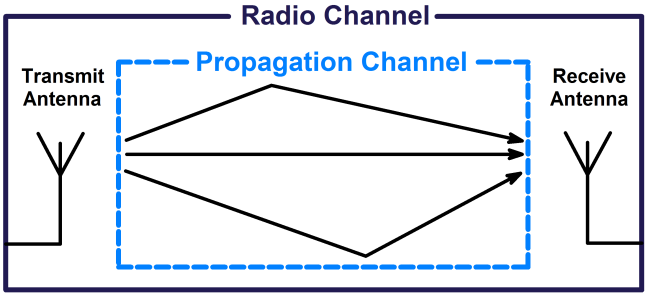

Fig. 2.1: Definition of radio and propagation channel.

In the simplest form, a radio system consists of a transmitter and receiver where the transmit (Tx) antenna has to radiate enough power to impose its signal at the receive (Rx) antenna. For most radio systems the antennas will not change their behaviour during operation but the propagation channel

will vary due to changes in the surrounding environment. These variations are dependent on multiple parameters as the distance between Tx and Rx antenna, the speed of movement of the systems entities or change in the environment. Understanding the impact of these variations is important for the design of a radio system. As a result, great effort is put into modelling the radio propagation channel.

2.1.1 Channel modelling methods

Channel models are needed to virtualize the radio propagation channel by development of simulation tools. These simulation tools are comprised of a range of channel models dependent on their application. For all of them, the accuracy of the simulation output is therefore completely dependent on the validity and quality of the applied channel models. The choice of channel model is a tradeoff between accuracy and simplicity. Hence, the goal of a channel model is often to describe the aspects that are of importance for a given wireless system without it being too complex resulting in it being easy to implement and use.

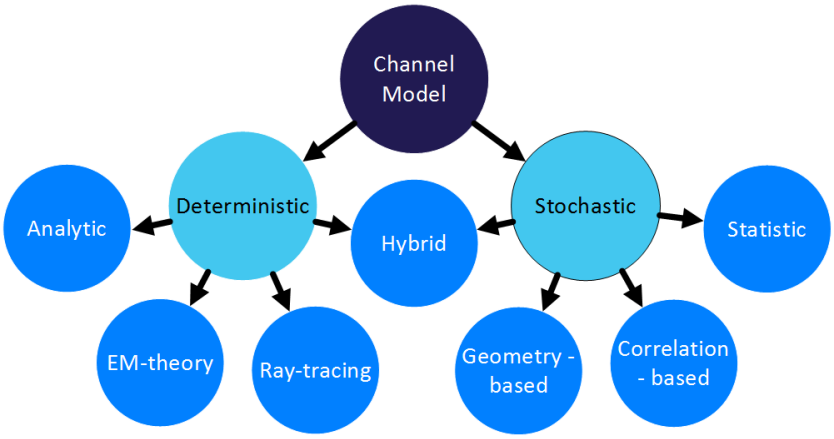

Fig. 2.2: Channel model types and hierarchy.

In general, channel modelling is divided into two groups: deterministic and stochastic as seen in Fig. 2.2. The deterministic models will provide the same answer each time for the same parameters while the stochastic, due to their random variables, will provide different answers. Sometimes a channel model consists of a combination of deterministic and stochastic parts resulting in a hybrid model.

The deterministic models cover the analytic subset which is derived from physical and mathematical laws. An example is the fundamental free-space path-loss and two-ray model. The benefit of these models is their relatively

low number of variables and thereby low complexity. The disadvantage of the models is that they are only valid for a very specific scenario. A method of applying these models in other scenarios is to adjust their variables utilizing empirical data. An example of such an empirical model is the simplified path-loss model shown in (2.1).

$$P_{Rx} = P_{Tx}\, G_{Tx}\, G_{Rx} \left(\frac{\lambda}{4\pi d_0}\right)^2 \left(\frac{d_0}{d}\right)^{\gamma} \quad [W] \quad (2.1)$$

$$P_{Rx} = P_{Tx} + G_{Tx} + G_{Rx} + 20\, log_{10}\left(\frac{4\pi d_0}{\lambda}\right) + \gamma\, 10\, log_{10}\left(\frac{d}{d_0}\right) \quad [dBm] \quad (2.2)$$

where P_{Tx} and P_{Rx} are the power at Tx and Rx in either linear or logarithmic units. G_{Tx} and G_{Tx} are the antenna gains. d is the propagated distance and d_0 is the reference distance for the antennas far field. The constant γ is the approximated path-loss exponent which is found via empirical measurements. Different values for γ dependent on the environment are showed in TABLE 2.1

Environment	γ range
Urban macrocells	3.7 - 6.5
Urban microcells	2.7 - 3.5
Office building (same floor)	1.6 - 3.5
Office building (multiple floor)	2 - 6
Store	1.8 - 2.2
Factory	1.6 - 3.3
Home	3

Table 2.1: Typical path loss exponents [1]

In complex environments where an analytical solution is not applicable the channel can be modelled utilizing either the electromagnetic (EM) theory (Maxwell's equations) or its approximation ray-tracing. Both of the methods describe the propagation of the electromagnetic waves by applying models for the path-losses (dissipation loss, atmospheric absorption, penetration losses etc.) and solving the resulting field or ray for each interaction. The interactions of the electromagnetic wave are beside propagation/transmission divided into three mechanisms: reflection, diffraction, and scattering all resulting in a different impact on the propagation channel as illustrated in Fig. 2.3.

The benefit of EM-theory and Ray-tracing is that it can provide very accurate and detailed information about the radio channel. The disadvantage is that it also requires very accurate and detailed information about the environment which often results in very computationally heavy simulations. The high level of details also makes the methods site-specific, which makes them better suited for static cases in a specific environment.

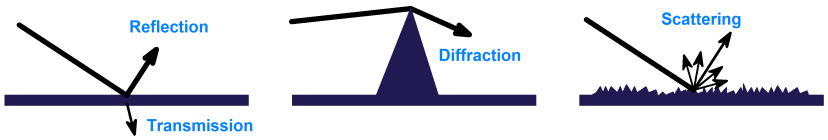

Fig. 2.3: Illustration of reflection, diffraction and scattering.

The stochastic model builds upon statistical information which allows for the models to be more generic. A simple example is to add a Gaussian random variable to the simplified path-loss model (2.2) and thereby take the large-scale fading (shadowing) due to obstructing objects into account. The Gaussian random variable in general has a standard deviation ranging from 4 dB to 10 dB dependent on the environment [2]. The benefit of these added statistical properties to the analytical models is the simplicity while the disadvantage is the need for a large dataset to provide the statistical parameters for a given environment.

Correlation-based models describe the correlation properties of the channel which is especially interesting in relation to multiple-input-multiple-output (MIMO) systems. This can be done using a correlation matrix of all the Tx Rx combinations which however can require a large number of parameters. Due to this simplified models as the Kronecker model is more widely used [3]. The benefit of these models is the ability to efficiently model a MIMO channel with many channels. The disadvantage is the need for a large number of parameters or knowledge about at least one set of channel parameters.

The geometry-based channel models emulate the spatial properties of the channel by applying point scatterers in geometrical positions determined by statistical distributions. These randomly placed scatters are assigned different statistical properties and can thereby model the multipath-components (MPC) seen in a channel response of a radio channel. Due to the ability to model both the temporal and spatial domain, geometry-based channel models are widely used. Some of the more known are the Spatial Channel Model (SCM/SCME) by 3GPP [4], the IMT-Advanced by ITU [5] and the WINNER model by CEPT [6]. The benefit of these models is the inherently included spatial properties which make it easier to relate the model parameters to the physical propagation mechanisms. The directive properties of the channel models also allow for de-embedding of the antenna gains. The disadvantage of the statistical models is that they require an extensive effort to obtain the datasets, which are achieved usually by empirical studies. Applicable statistical information will then make use of the obtain datasets.

The application of a stochastic based channel model realisation does not necessarily resemble any real physical situation, specific location or area. To account for this, a hybrid method denoted map-based channel models has

been proposed. These models combine information about the physical environment by means of e.g ray-tracing and then apply stochastic models to account for e.g moving objects or diffused scattering. One of these models is proposed by the Mobile and wireless communications Enablers for Twenty-twenty (2020) Information Society (METIS) project [7]. The METIS project has now been extended to METIS II which is a part of The 5G Infrastructure Public Private Partnership (5GPPP) which focuses on delivering solutions and standards for the next generation communication infrastructures in the coming decade [8].

2.1.2 What is new for 5G?

As seen in the previous radio section, propagation modelling is a huge and active field and has been so for decades. This leads to the question of what is new about the radio propagation channel for the fifth generation mobile communication system (5G).

The increasing demand for mobile broadband data, described in section 1.2, drives the mobile industry to move in new directions to facilitate the increase in data rate. If one is to think of the data needed to be moved from the network to the user as water, an analogy can be used to explain the possible ways they can choose. The radio channel can be seen as a pipe wherein the water flows and if the water flow needs to be increased, one can choose to do the following three things:

- Increase the speed/pressure in the pipe
- Increase the number of pipes.
- Increase the volume of the pipe.

Increasing the speed of the water flow in the pipe is equivalent to improving the modulation scheme or code efficiency. The spectral efficiency of existing schemes and codes is already approaching the Shannon–Hartley limit leaving the foreseen improvement here not enough for the requirements of 5G. Increasing the number of pipes is equivalent to adding more radio channels which is exactly what is already adopted for 4G (LTE-Advance) as diversity and MIMO. For this method to significantly increase the data rate, the different radio channels need to be decorrelated. In some scenarios, it is difficult to ensure decorrelated channels and the small size of a handset also limits the possibility to distribute the antennas over a large area which otherwise would help. This leaves the option of increasing the volume of the pipe which is equivalent to increase the bandwidth of the radio channel. This approach is in fact also already applied for 4G as carrier aggregation. However, aggregating the available spectrum currently allocated to mobile communication is still not sufficient for the realization of 5G.

Numerous wireless systems are operating utilizing different parts of the radio wave spectrum. To avoid conflicts between these systems their allocations in the spectrum is regulated by both international and national laws and agreements. In Denmark, it is the Danish Ministry of Energy, Utilities and Climate which controls the frequency allocations. Fig. 2.4 gives an overview of the allocations and the complexity of the figure indicates the scarceness of unused spectrum. The lack of available radio frequency spectrum around the current frequency range used for mobile communication is the main reason for exploring new frequency ranges for allocation to mobile communication.

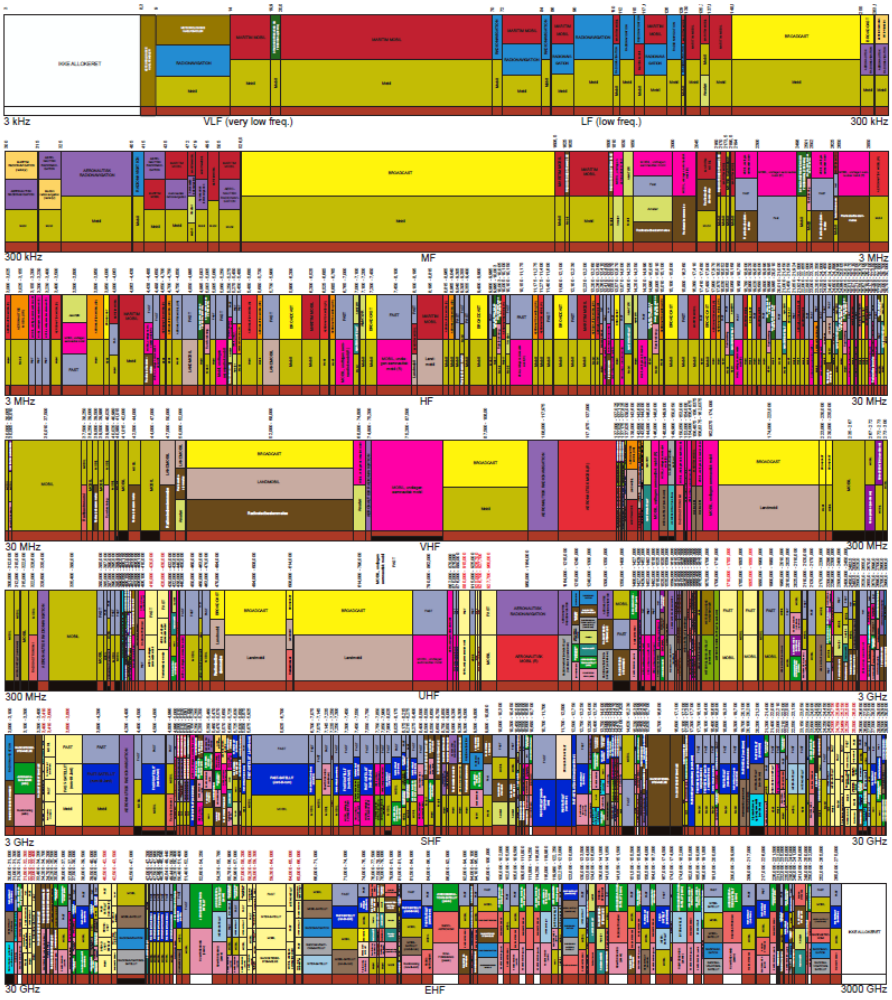

Fig. 2.4: Overview of frequency allocations in Denmark, for details see: [9].

The inclusion of the so-called mm-waves frequencies is one of the largest steps in a new direction for the industry. Current mobile communication systems are generally deployed at frequencies below 6 GHz while 5G is also suggested to utilize frequencies in the range 10 – 80 GHz [10,11]. Strictly speaking, many of these newly proposed frequencies are in fact in the cm-wave region if one is to follow the ITU frequency band division. This denotes the frequency range 3 – 30 GHz as the super-high-frequency (SHF) band and the frequency range 30 – 300 GHz as the extremely high-frequency (EHF) band, the former having wavelengths in the range of centimetres and later in the range of millimetres.

The proposed new 5G spectrum is as seen in Fig. 2.4 already allocated but efforts are being made to either reallocate the services there or allow for coexistence with 5G. The services allocated in the frequency range are today mostly allocated for point to point systems, Radio-location/navigation and satellite communication. Common for all of these is that they in principal are line-of-sight (LOS) systems with either short range or utilizing high gain antennas. A reason for this is that the higher frequencies in general experience greater attenuation. The mm-waves frequencies (10 – 80 GHz) suffer from a higher penetration loss, more significant shadowing due to obstructing objects and a larger free-space path-loss when assuming constant gain antennas.

To overcome the higher attenuation, high gain antennas and beamforming are described as an enabling technology for 5G when implemented in the mm-wave region [12–17]. Utilizing high gain antennas would compensate for the additional attenuation but would also make the antennas and thereby the radio channel highly directive. The relation between gain and directivity is described further in section 2.1.3.

The directivity would change the behaviour of the radio propagation channel. A highly directive antenna as seen from the transmit (Tx) side would only illuminate a subset of the surrounding environment and likewise would a highly directive receive (Rx) antenna only "see" in the direction it is pointed. These dynamics of the radio propagation channel have to lead to the development of signal models also including angular information as further described in section 2.1.4.

Another consequence of the application of mm-wave frequencies is that the phenomena of diffused scattering becomes more pronounced. Diffused scattering is in this context defined as the scattering caused by the surface structure of the interacting objects [18,19]. As the frequency is increased the wavelength is decreased and at some point, the wavelength starts to be comparable to the surface structure. When this happens the interacting object cannot be modelled using a simple smooth surface any more. The laws of reflection are well defined for a plane/smooth surface. The reflected field depends on the wavelength, incident angle and the EM material properties

(Permittivity ϵ, Permeability μ and Conductivity σ). If the surface instead is irregular/rough with periodic or random variations in surface height, then there is no general solution [20–22]. Therefore the diffused field is only described by exact formulations for very restricted scenarios or by approximations based on empirical studies [23,24].

In summary, a channel model applicable for 5G deployed in the mm-wave frequencies does not only have to predict the power for a given point but also has to predict where the power is coming from. This can be done by including spatial information as the angle of arrival. It is also now needed to account for the additional transmission and penetration loss as well as the level of diffused scattering. In the end, all the proposed channel models need validation against real measured channels. Providing this, empirical data and studies are the main objectives for the papers included in Part II of this thesis.

2.1.3 Friis equation and its relation to directive antennas

The Friis transmission equation describes the relationship between Tx and Rx power in free-space as (2.3) provided (2.4), know as the far field criteria, is fulfilled [25].

$$\frac{P_{Rx}}{P_{Tx}} = \left(\frac{A_{Rx}\, A_{Tx}}{d^2\, \lambda^2} \right) \tag{2.3}$$

$$d \geq \frac{2\, a^2}{\lambda} \tag{2.4}$$

where P_{Tx} and P_{Rx} are the powers at the transmitter and receiver of same unit. A_{Tx} and A_{Rx} are the effective areas of the Tx and RX antenna. d, λ and a are respectively the distance between transmitter and receiver, the wavelength and the largest dimension of the antenna aperture, all given in the same units.

The effective area of a directive antenna is given by (2.5). The maximum effective area of an isotropic antenna is given by (2.6) as the directivity and efficiency of an isotropic antenna is defined to be 1.

$$A_{dir} = \epsilon\, D(\theta, \phi)\, \frac{\lambda^2}{4\, \pi} \tag{2.5}$$

$$A_{iso} = \frac{\lambda^2}{4\, \pi} \tag{2.6}$$

where $D(\theta, \phi)$ is the and directivity for the (θ, ϕ) direction and ϵ is the antenna efficiency.

The directivity is a unit-less description of the relation between the radiation intensity for a given direction and the total radiated power as given in

(2.7).

$$D(\theta,\phi) = \frac{4\pi\, U(\theta,\phi)}{P_{rad}} \tag{2.7}$$

where $U(\theta,\phi)$ is the radiation intensity and P_{rad} is the radiated power.

From (2.7) it is seen that confining the radiated power over a smaller area will increase the directivity. This high intensity direction of the antenna radiation pattern is often referred to as beams.

An antenna is often described only by its gain. The gain is proportional to the directivity as expressed in (2.8) for a given direction and (2.9) for the direction of maximum directivity (D_0).

$$G(\theta,\phi) = \epsilon\, D(\theta,\phi) \tag{2.8}$$

$$G_{max} = \epsilon\, D_0 \tag{2.9}$$

From this follows that the maximum gain of an antenna is in the direction of maximum directivity. This direction if often referred to as the main beam of the antenna.

The maximum antenna gain can also be described using the effective area as shown in (2.10) [26].

$$G_{max} = \frac{4\pi\, \epsilon_{ap}\, A_{phys}}{\lambda^2} \tag{2.10}$$

where ϵ_{ap} is the antenna's aperture efficiency and A_{phys} is the physical area of the aperture.

An interesting observation from (2.10) is that the maximum gain will increase proportionally to an increase of the physical area of the antenna, if the wavelength is kept constant and vice versa if the physical area of the antenna is kept constant. As the physical area needed for an efficient antenna decreases with the wavelength, this means that the gain of an antenna would increase at the same rate if the area utilized for the antenna is kept constant. This frequency-dependency increase in gain would counteract the increase in free-space path-loss (FSPL) given in (2.11).

$$L_{FSPL} = \left(\frac{\lambda}{4\pi\, d}\right)^2 \quad [w] \tag{2.11}$$

$$L_{FSPL} = 20\, log_{10}\left(\frac{4\pi d}{\lambda}\right) \quad [dB] \tag{2.12}$$

Effectively the increase in FSPL due to an increase in frequency can be fully compensated by allowing the maximum effective area of the antennas to also increase with frequency.

2.1.4 The Power-Angular-Delay-Profile

In the context of this work, the radio propagation channel is assumed to be terrestrial meaning the surrounding environment would impact the propagation. This impact effectively makes free-space assumptions not valid for all scenarios where the distance between the Tx and Rx antennas are greater than the distance to surrounding objects or the ground. The radio waves' interaction with objects on their path presents itself as time dispersion in the wideband channel impulse response (CIR) [27]. The CIR in the stationary case is expressed as (2.13) [28].

$$h(\tau) = \sum_{k=1}^{K} a_k \, \delta\left(\tau - \tau_k\right) \, e^{j\varphi_k} \tag{2.13}$$

where K is the total number of resolvable multipath components (MPC). a_k, τ_k and φ_k are respectively the amplitude, arrival time, and phase for the kth component. $\delta(\cdot)$ denotes a Dirac delta function.

If the orientation of the antennas is to be included, (2.13) can be expanded to an expression for the double-directional radio channel as given in (2.14) [29].

$$\begin{aligned} h\left(\tau, \phi^{Rx}, \theta^{Rx}, \phi^{Tx}, \theta^{Tx}\right) = \sum_{k=1}^{K} a_k \, \delta\left(\phi^{Rx} - \phi_k^{Rx}\right) \delta\left(\theta^{Rx} - \theta_k^{Rx}\right) \\ \delta\left(\phi^{Tx} - \phi_k^{Tx}\right) \delta\left(\theta^{Tx} - \theta_k^{Tx}\right) \delta\left(\tau - \tau_k\right) \, e^{j\varphi_k} \end{aligned} \tag{2.14}$$

where ϕ and θ are the azimuth and elevation angles for either the receiver (Rx) or transmitter (Tx) antenna.

Expression (2.14) is for the case with directional antennas at both Tx and Rx side of the link. In case where one of the antennas is omnidirectional and the antennas are restricted in the same elevation plane, the expression simplifies to (2.15).

$$h\left(\tau, \phi\right) = \sum_{k=1}^{K} a_k \, \delta\left(\phi - \phi_k\right) \delta\left(\tau - \tau_k\right) \, e^{j\varphi_k} \tag{2.15}$$

The time dispersion for a given radio channel is often described via its power-delay-profile (PDP). A common assumption is that the PDP will have an exponentially decaying tail [28]. This tail is a result of interactions with the surroundings which includes the low powered dense multipath components and the diffused scattering. The PDP is defined the statistically average of the CIR for a small area as given in (2.16). An example of a PDP is shown in Fig. 2.5.

$$P(\tau) = |h(\tau)|^2 \tag{2.16}$$

where the PDP to a given time instance, τ, often is given in dB.

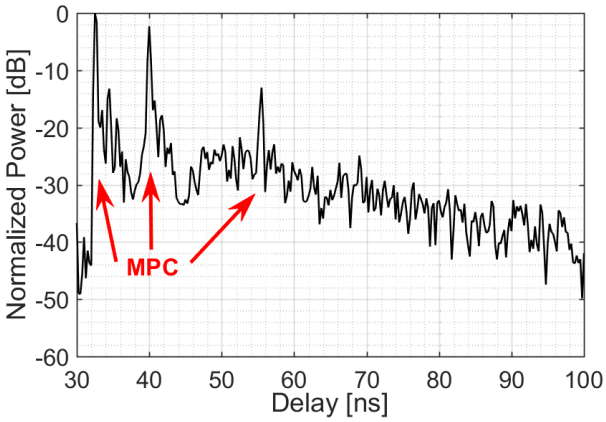

Fig. 2.5: Example PDP with three multipath components (MPC) showing. The power level is normalized to the maximum power of the first MPC.

The tail of each MPC is clearly seen for the first two MPCs in Fig. 2.5. It can also be seen that it takes some time until the normalized power level returns to the power level before the first MPC at approximately -50 dB. This time is also known as the reverberation time from the concept of room electromagnetics [23].

As for the CIR, the PDP can also be defined in the angular domain. To do this, the concept of the Power-Angular-Delay-Profile (PADP) is introduced. Plotting this requires an additional dimension for the angular domain which is why the PADP is often plotted as e.g. temperature/surface maps. Fig. 2.6 is an example of a PADP where the angular domain is the angle of arrival (AoA) for at a given location.

2.2 Channel Sounding

As stated in section 1.3 the aim of this PhD project is to provide some of the empirical data and studies needed to characterize the wireless radio channels intended for 5G. Due to this, the majority of the time throughout the project period has been spent on the development of channel sounding systems and performing measurements with these.

Channel sounding or just sounding can be simply explained as the principal of transmitting a known signal and then at either another location or time instance receive it and its echoes. The received signal can then be studied as a representation of the radio channel it has traversed. In principal channel sounding is conducted in either the frequency or time domain wherein the aim is to represent received power for a given frequency or time instance [30].

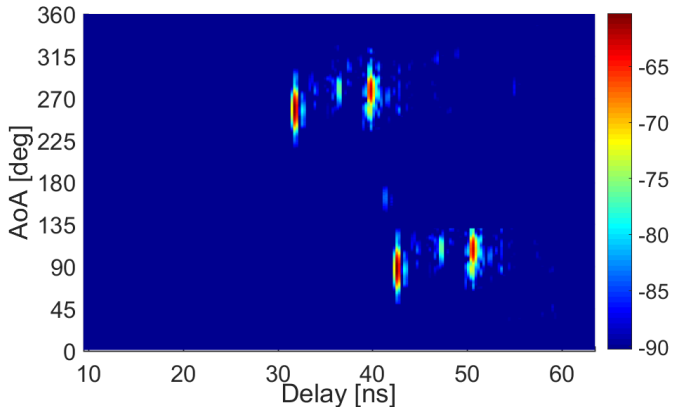

Fig. 2.6: Example PADP with four multipath components (MPC) showing. The power is given in dBm.

In the time domain, this is often represented as the CIR or PDP as described in section 2.1.4. A benefit of investigating the channel in the time domain is that the time of flight or propagation time can be related to the physical surroundings by applying geometric optics or simple ray-tracing.

2.2.1 Measurement systems for channel sounding

For the work related to this thesis three types of hardware platforms have been utilized as a basis for the sounding system.

- Spectrum Analyser.
- Vector Network Analyser (VNA).
- Dedicated correlation based channel sounder.

By utilizing a spectrum analyser it is possible to investigate the radio channel in the frequency domain. A spectrum analyser is fundamentally a highly adjustable and sensitive receiver. This means that the spectrum analyser normally does not include a transmitter and therefore an external signal generator is needed to transmit the sounding signal. This division of transmitter and receiver in a spectrum analyser based sounding system allows for greater freedom to deploy and move the transmitter and receiver for different types of measurements.

The spectrum analyser measures the signal magnitude for a small sub-band of the frequency span determined by the chosen resolution bandwidth (RBW). This is very efficient for determining relative received power at a given frequency but does not provide phase information of the received signal as the spectrum analyser does not track the phase. This means that temporal information for the propagation channel can only be extracted with a

spectrum analyser based sounding system by applying some type of modulation to the sounding signal. This modulation could be implemented in numerous ways but should at least either provide timestamps in the received signal or some other form of synchronization between the transmitter and receiver.

A vector network analyser (VNA) inherently provides synchronization between the transmitter and receiver as they are both included in the same hardware. This means the power and delay between transmitter and receiver can be measured as absolute values. The VNA also has the advantage as compared to the spectrum analyser that it tracks the phase of the signal which allows for direct transformation between frequency and time domain.

The VNA measures the magnitude and phase for a given frequency with a chosen RBW. The VNA sweeps the transmit/sounding signal over a chosen frequency range while it simultaneously records the channel response. This means that the measurement, as for the spectrum analyser is conducted in the frequency domain. However, the measurement of the frequency span, in general, takes longer for the VNA as compared to the spectrum analyser due to the VNAs need to also sweep the transmit frequency and aligning of the phase [30].

Channel sounding including phase information is especially important in relation to the concept of beamforming. The phase information is as an example needed to adjust the complex weights determining the direction of the main beam of a linear array [31,32]. The capability of measuring the phase also allows for the application of real and virtual antenna arrays which can be utilized to capture the spatial properties of the radio channel as described further in section 2.2.2.

In general, the frequency sweep type measurements have one large drawback and that is the time each frequency sweep takes. The chosen frequency band is swept with a continuous wave (CW) sounding signal. The sounding signal is generated by an oscillator in either an external signal generator or the VNA itself which for each frequency step has to reset and align the phase etc. This process is not optimized for speed but for accuracy which for most applications is the dominant parameter for measurement equipment. The problem with the sweep time is that the radio channel in principal should be static during the frequency sweep but, due to the delay in transmitting the sounding signal, could change. This makes the VNA based sounding systems unsuitable for time-varying channels with a large bandwidth and thereby sweep time is to be measured [33].

Even though the VNA based sounding systems are only capable of measuring static or quasi-static channels they are very popular due to their relatively simple implementation. This can be seen by the number of publications presented in literature related to 5G channel measurements of which a few are listed here [33–36]. Similar for all of these is that the measurement

systems due to high losses in the cables, as a result of the high frequencies proposed for 5G, only measures channel of relatively short distance. The high losses in the cables have been proposed overcome with up and down conversion of the CW signal and introduction of fiberoptic solutions [37–39].

For time-varying channels, direct pulse measurements in the time domain are more suitable as they are not restricted by the frequency sweep time. The sounding pulse can be seen in the frequency domain as a chirp or pseudo-random noise. Common for these is that dedicated hardware has to be utilized. This makes the dedicated channel sounders less versatile and more cumbersome to modify for different frequencies or bandwidth.

Dedicated channel sounders capable of sounding real time-varying channels is, of course, the most desired solution. However, especially the cost of constructing these sounders have limited them in availability and capabilities. The capability of measuring multiple channels in parallel is naturally one of the most expensive as each additional channel in principal needs its own additional sounder.

Like for the VNA based channel sounders, the dedicated channel sounders is challenged with the very large bandwidth needed for high accuracy time resolution. For the chirp sounders, the difference in transmit power for the different frequencies and the transmission time of the frequency modulated continuous wave (chirp) at some points needs consideration [40,41]. For the correlation based sounders, the generation of the pseudo-noise sequence (PNS) needed to cover the frequency span increases with bandwidth and with this the effort needed by either computational or hardware de-correlation of it also increases [42,43].

Some of the state-of-the-art channel sounders utilised for 5G measurements have been presented in [44–48]. It can be noted that many of these channel sounders have been developed in parallel with the work presented in this thesis.

2.2.2 Directional Channel Sounding

To capture the spatial properties of the radio channel it becomes necessary to also sample in the spatial domain besides sampling the power and delay domain. The spatial properties related to antennas are often given using polar coordinates resulting in angular information for azimuth (ϕ) and elevation (θ). Due to this, the channel is described using the power-angular-delay-profile (PADP) as described in section 2.1.4.

The sampling in the spatial domain is often conducted in angular steps by either physical directional antennas or by beamforming (spatial filtering). The beamforming can be archived by using either a virtual or real antenna array. By rotating the highly directive antenna gain pattern around either one or both azimuth and elevation axis it is possible to sample either the two

or three-dimensional spatial domain. The accuracy of the spatial sampling depends on the directivity and sidelobes of the antenna gain pattern as well as limitations posed by the used channel sounder system [49].

The simplest technique to sample the spatial domain is to mechanically rotate a directive physical antenna like a horn antenna. The benefit of this technique is that only one sounding link is needed which means it fits well with the VNA based sounding systems. Dependent on the type of mechanical positioning system and directivity of the used antennas', different levels of angular resolution can be archived. Due to the simplicity, this method is widely used but it has some clear drawbacks. An apparent drawback is the measurement time of each angular scan as not only the measurement systems e.g. frequency sweep but also positioning takes time. During the entire measurement, the radio channel has to stay static which limits the applicable measurement scenarios.

Another technique is instead of mechanically rotating directive antennas which can be limited in directivity or have high sidelobes to create an antenna array and apply beamforming. Multiple arrangements of the antenna arrays exist, as uniform linear or circular array (ULA/UCA), all having different algorithms for the needed signal processing. The benefit of utilizing beamforming is that it is possible to achieve higher resolution in the angular domain than by using physical antennas. If the antennas used for the array are omnidirectional the technique also removes the need for de-embedding the effect of the antennas gain pattern for 2D cases [50–52].

The antenna array can be created virtually by mechanically moving one antenna to the needed positions and conducting the measurements in sequence. The advantage of creating a virtual array is that there is only need for one sounding link which greatly reduces the cost and complexity of the sounding system. Another benefit of the virtual array is the lack of mutual coupling between antenna elements which can be difficult to account for by the beamforming algorithms [26]. The disadvantage is, like for the directional antennas, the measurement time which again also includes positioning time.

When mechanically moving antennas around during the measurement, problems with phase stability can emerge. At high frequency, the cables connecting the entities of the sounding systems becomes sensitive to bending and stretching. This is simply due to the change in physical dimensions of the cable that starts to become significant as compared to the wavelength of the signal running in the cable. Another problem with the very wideband measurements is that the phase centre of an antenna is usually frequency dependent and difficult to estimate. This means that the phase centre of the antenna could move during the frequency sweep which introduces some ambiguity to where e.g. the rotational centre of the UCA is located [53–55].

To significantly reduce the measurement time and avoid movement of the antennas and cables a real physical antenna array can be used instead

of the mechanically positioning system. The array could in simple form be a collection of directional antennas positioned such that they cover either one or both angular domains. An example of such a system is given in [56] and [57] which however have not been utilized for 5G measurements. Another method could be to realize either a ULA or UCA with all the needed elements. The obvious reason these type of channel sounders are not widely used especially at mm-wave frequencies is the high cost of having multiple parallel sounding links. However, with the current progress towards a wider use of mm-wave systems, some MIMO mm-wave sounders exist as the one presented in [44].

References

[1] A. Goldsmith, *Wireless communications*. Cambridge University Press, 2005, ISBN: 978-0-521-83716-2.

[2] A. F. Molisch, *Wireless communications*. IEEE Press, 2005, ISBN: 978-0-470-84888-3.

[3] J. P. Kermoal, L. Schumacher, K. I. Pedersen, P. E. Mogensen, and F. Frederiksen, "A stochastic mimo radio channel model with experimental validation," *IEEE Journal on Selected Areas in Communications*, vol. 20, no. 6, pp. 1211–1226, Aug 2002.

[4] T. 3rd Generation Partnership Project (3GPP), *Technical Specification Group Radio Access Network - Spatial channel model for Multiple Input Multiple Output (MIMO) simulations*, Technical Report TR 25.996, 2003.

[5] ITU, *Guidelines for evaluation of radio interface technologies for IMT-Advanced*, ITU-R M.2135, 2009.

[6] P. Kyösti, J. Meinilä, L. Hentilä, X. Zhao, T. Jämsä, C. Schneider, M. Narandzić, M. Milojević, A. Hong, J. Ylitalo, V.-M. Holappa, M. Alatossava, R. Bultitude, Y. de Jong, and T. Rautiainen, "WINNER II Channel Models," The European Conference of Postal and Telecommunications Administrations - CEPT, IST-4-027756 WINNER II D1.1.2 V1.2, Final Report, 2007.

[7] J. Medbo, P. Kyosti, K. Kusume, L. Raschkowski, K. Haneda, T. Jamsa, V. Nurmela, A. Roivainen, and J. Meinila, "Radio propagation modeling for 5g mobile and wireless communications," *IEEE Communications Magazine*, vol. 54, no. 6, pp. 144–151, June 2016.

[8] The 5G Infrastructure Public Private Partnership (5G PPP), - Available Online: https://5g-ppp.eu/.

[9] Danish Ministry of Energy, Utilities and Climate, *Spectrum auctions, frequency legislation and frequency planning.*, 2017, - Available Online: https://ens.dk/en/our-responsibilities/spectrum.

[10] S. Methley, W. Webb, S. Walker, and J. Parker, "Study on the suitability of potential candidate frequency bands above 6ghz for future 5g mobile broadband

systems," Quotient Associates Limited, Compass House, Vision Park, Chivers Way Histon, Cambridge, CB24 9AD, UK, Technical Report, March 2015.

[11] Ofcom, "Spectrum above 6 ghz for future mobile communications," Ofcom UK, Riverside House, 2a Southwark Bridge Road, London, Consultation Report, January 2015.

[12] P. Demestichas, A. Georgakopoulos, D. Karvounas, K. Tsagkaris, V. Stavroulaki, J. Lu, C. Xiong, and J. Yao, "5g on the horizon: Key challenges for the radio-access network," *Vehicular Technology Magazine, IEEE*, vol. 8, no. 3, pp. 47–53, Sept 2013.

[13] Z. Pi and F. Khan, "An introduction to millimeter-wave mobile broadband systems," *IEEE Communications Magazine*, vol. 49, no. 6, pp. 101–107, June 2011.

[14] C.-X. Wang, F. Haider, X. Gao, X.-H. You, Y. Yang, D. Yuan, H. Aggoune, H. Haas, S. Fletcher, and E. Hepsaydir, "Cellular architecture and key technologies for 5g wireless communication networks," *Communications Magazine, IEEE*, vol. 52, no. 2, pp. 122–130, February 2014.

[15] S. Rangan, T. Rappaport, and E. Erkip, "Millimeter-wave cellular wireless networks: Potentials and challenges," *Proceedings of the IEEE*, vol. 102, no. 3, pp. 366–385, March 2014.

[16] W. Roh, J.-Y. Seol, J. Park, B. Lee, J. Lee, Y. Kim, J. Cho, K. Cheun, and F. Aryanfar, "Millimeter-wave beamforming as an enabling technology for 5g cellular communications: theoretical feasibility and prototype results," *Communications Magazine, IEEE*, vol. 52, no. 2, pp. 106–113, February 2014.

[17] S. Han, C. l. I, Z. Xu, and C. Rowell, "Large-scale antenna systems with hybrid analog and digital beamforming for millimeter wave 5g," *IEEE Communications Magazine*, vol. 53, no. 1, pp. 186–194, January 2015.

[18] C. Kloch and J. B. Andersen, "Radiosity-an approach to determine the effect of rough surface scattering in mobile scenarios," in *IEEE Antennas and Propagation Society International Symposium 1997. Digest*, vol. 2, July 1997, pp. 890–893 vol.2.

[19] O. Franek, J. B. Andersen, and G. F. Pedersen, "Diffuse scattering model of indoor wideband propagation," *IEEE Transactions on Antennas and Propagation*, vol. 59, no. 8, pp. 3006–3012, Aug 2011.

[20] P. Beckmann and A. Spizzichino, *The Scattering of Electromagnetic Wave from Rough Surfaces*. Pergamon Press, Oxford: International Series of Monographs on Electromagnetic Waves, 1963, vol. 4.

[21] J. A. Ogilvy, *Theory of Wave Scattering from Random Rough Surfaces*. England, Bristol: IOP, 1991, no. ISBN: 0-7503-0063-9.

[22] N. Pinel and C. Bourlier, *Electromagnetic Wave Scattering from Random Rough Surfaces*. Wiley, 2013, ISBN: 978-1-84821-471-2.

[23] J. B. Andersen, J. O. Nielsen, G. F. Pedersen, G. Bauch, and J. M. Herdin, "Room electromagnetics," *IEEE Antennas and Propagation Magazine*, vol. 49, no. 2, pp. 27–33, April 2007.

[24] G. Steinböck, T. Pedersen, B. H. Fleury, W. Wang, and R. Raulefs, "Distance dependent model for the delay power spectrum of in-room radio channels," *IEEE Transactions on Antennas and Propagation*, vol. 61, no. 8, pp. 4327–4340, Aug 2013.

[25] H. T. Friis, "A note on a simple transmission formula," *Proceedings of the IRE*, vol. 34, no. 5, pp. 254–256, May 1946.

[26] C. Balanis, *Antenna Theory: Analysis and Design*. John Wiley & Sons, 2005, ISBN: 9780471667827.

[27] A. F. Molisch, "Ultrawideband propagation channels-theory, measurement, and modeling," *IEEE Transactions on Vehicular Technology*, vol. 54, no. 5, pp. 1528–1545, Sept 2005.

[28] H. Hashemi, "The indoor radio propagation channel," *Proceedings of the IEEE*, vol. 81, no. 7, pp. 943–968, Jul 1993.

[29] M. Steinbauer, A. F. Molisch, and E. Bonek, "The double-directional radio channel," *IEEE Antennas and Propagation Magazine*, vol. 43, no. 4, pp. 51–63, Aug 2001.

[30] S. Salous, *Radio Propagation Measurement and Channel Modelling*, 2013, ISBN: 978-0-470-75184-8.

[31] F. Zhang, W. Fan, and G. F. Pedersen, "Analytic and experimental investigation of beamforming algorithms for mm-wave channel characterization," in *2017 11th European Conference on Antennas and Propagation (EUCAP)*, March 2017, pp. 146–150.

[32] F. Zhang, W. Fan, J. Zhang, and G. F. Pedersen, "Virtual large-scale array beamforming analysis using measured subarray antenna patterns," *IEEE Access*, vol. 5, pp. 19 812–19 823, 2017.

[33] A. M. Street, L. Lukama, and D. J. Edwards, "Use of vnas for wideband propagation measurements," *IEE Proceedings - Communications*, vol. 148, no. 6, pp. 411–415, Dec 2001.

[34] W. Fan, I. Carton, J. . Nielsen, K. Olesen, and G. F. Pedersen, "Measured wideband characteristics of indoor channels at centimetric and millimetric bands," *EURASIP Journal on Wireless Communications and Networking*, vol. 2016, no. 1, p. 58, Feb 2016.

[35] R. Naderpour, J. Vehmas, S. Nguyen, J. Järveläinen, and K. Haneda, "Spatio-temporal channel sounding in a street canyon at 15, 28 and 60 ghz," in *2016 IEEE 27th Annual International Symposium on Personal, Indoor, and Mobile Radio Communications (PIMRC)*, Sept 2016, pp. 1–6.

[36] R. J. C. Bultitude, R. F. Hahn, and R. J. Davies, "Propagation considerations for the design of an indoor broad-band communications system at ehf," *IEEE Transactions on Vehicular Technology*, vol. 47, no. 1, pp. 235–245, Feb 1998.

[37] S. S. Ghassemzadeh, R. Jana, C. W. Rice, W. Turin, and V. Tarokh, "A statistical path loss model for in-home uwb channels," in *Ultra Wideband Systems and Technologies, 2002. Digest of Papers. 2002 IEEE Conference on*, May 2002, pp. 59–64.

[38] J. Conrat, P. Pajusco, and J. Thiriet, "A multibands wideband propagation channel sounder from 2 to 60 ghz," in *2006 IEEE Instrumentation and Measurement Technology Conference Proceedings*, April 2006, pp. 590–595.

[39] K. Sarabandi, N. Behdad, A. Nashashibi, M. Casciato, L. Pierce, and F. Wang, "A measurement system for ultrawide-band communication channel characterization," *IEEE Transactions on Antennas and Propagation*, vol. 53, no. 7, pp. 2146–2155, July 2005.

[40] X. Raimundo, S. Salous, and A. A. Cheema, "Indoor radio propagation measurements in the v-band," in *Radio Propagation and Technologies for 5G (2016)*, Oct 2016, pp. 1–5.

[41] S. Salous, S. M. Feeney, X. Raimundo, and A. A. Cheema, "Wideband mimo channel sounder for radio measurements in the 60 ghz band," *IEEE Transactions on Wireless Communications*, vol. 15, no. 4, pp. 2825–2832, April 2016.

[42] R. J. Pirkl and G. D. Durgin, "Optimal sliding correlator channel sounder design," *IEEE Transactions on Wireless Communications*, vol. 7, no. 9, pp. 3488–3497, September 2008.

[43] D. Ferreira, R. F. S. Caldeirinha, and N. Leonor, "Real-time high-resolution radio frequency channel sounder based on the sliding correlation principle," *IET Microwaves, Antennas Propagation*, vol. 9, no. 8, pp. 837–846, 2015.

[44] J. Ødum Nielsen, W. Fan, P. C. F. Eggers, and G. F. Pedersen, "A channel sounder for massive mimo and mmwave channels," *IEEE Communications Magazine*, 2018.

[45] P. B. Papazian, C. Gentile, K. A. Remley, J. Senic, and N. Golmie, "A radio channel sounder for mobile millimeter-wave communications: System implementation and measurement assessment," *IEEE Transactions on Microwave Theory and Techniques*, vol. 64, no. 9, pp. 2924–2932, Sept 2016.

[46] R. Müller, D. A. Dupleich, C. Schneider, R. Herrmann, and R. S. Thomä, "Ultra-wideband 3d mmwave channel sounding for 5g," in *2014 XXXIth URSI General Assembly and Scientific Symposium (URSI GASS)*, Aug 2014, pp. 1–4.

[47] T. S. Rappaport, G. R. MacCartney, M. K. Samimi, and S. Sun, "Wideband millimeter-wave propagation measurements and channel models for future wireless communication system design," *IEEE Transactions on Communications*, vol. 63, no. 9, pp. 3029–3056, Sept 2015.

[48] X. Zhao, S. Li, Q. Wang, M. Wang, S. Sun, and W. Hong, "Channel measurements, modeling, simulation and validation at 32 ghz in outdoor microcells for 5g radio systems," *IEEE Access*, vol. 5, pp. 1062–1072, 2017.

[49] S. M. Amjadi and K. Sarabandi, "Superresolution doa estimation with circular arrays using signal segregation algorithm in conjunction with a nulls-synthesis method," *IEEE Transactions on Antennas and Propagation*, vol. 66, no. 6, pp. 3108–3121, June 2018.

[50] H. Duan, B. P. Ng, C. M. S. See, and J. Fang, "Spatial resolutions of the broadband nonredundant and minimum redundancy arrays," *IEEE Signal Processing Letters*, vol. 14, no. 11, pp. 852–855, Nov 2007.

[51] Y. Ji, X. Yin, H. Wang, S. X. Lu, and C. Cao, "Antenna de-embedded characterization for 13–17-ghz wave propagation in indoor environments," *IEEE Antennas and Wireless Propagation Letters*, vol. 16, pp. 42–45, 2017.

[52] H. Xu, V. Kukshya, and T. S. Rappaport, "Spatial and temporal characteristics of 60-ghz indoor channels," *IEEE Journal on Selected Areas in Communications*, vol. 20, no. 3, pp. 620–630, April 2002.

[53] F. Zhang, W. Fan, and G. F. Pedersen, "Frequency-invariant uniform circular array for wideband mm-wave channel characterization," *IEEE Antennas and Wireless Propagation Letters*, vol. 16, pp. 641–644, 2017.

[54] S. S. Zhekov, A. Tatomirescu, and G. F. Pedersen, "Modified biconical antenna for ultrawideband applications," in *2016 10th European Conference on Antennas and Propagation (EuCAP 2016)*, April 2016.

[55] I. Carton, W. Fan, and G. F. Pedersen, "A frequency invariant beamformer for channel parameter estimation in millimeter wave bands," in *2015 International Symposium on Antennas and Propagation (ISAP)*, Nov 2015, pp. 1–4.

[56] A. Yamamoto, T. Sakata, K. Ogawa, K. Olesen, J. . Nielsen, and G. F. Pedersen, "Radio channel sounding using a circular horn antenna array in the horizontal plane in the 2.3 ghz band," in *Proceedings of the 2012 IEEE International Symposium on Antennas and Propagation*, July 2012, pp. 1–2.

[57] K. Kalliola, H. Laitinen, L. I. Vaskelainen, and P. Vainikainen, "Real-time 3-d spatial-temporal dual-polarized measurement of wideband radio channel at mobile station," *IEEE Transactions on Instrumentation and Measurement*, vol. 49, no. 2, pp. 439–448, April 2000.

Chapter 3 - Contributions

This chapter presents the main contributions of this thesis together with brief summaries of the motivation, work and findings of the papers included in Part II.

This PhD project included three objectives as described in section 1.3.

1. Collection of propagation data.
2. Study of the user impact on the mm-wave channel.
3. Investigation of Device-to-Device communication in forest terrain.

The first objective is very wide and therefore it could relate to all the papers included in this theses. However, for mm-waves, it relates to Paper A, B and C. The second objective is addressed in Paper D while the third objective relates to paper E and F.

The main contributions of this thesis can be listed as below where the corresponding paper(s) are indicated in parentheses.

1. Development and validation of channel sounding system capable of operating at both legacy and mm-wave frequencies. (A, B)
2. Theoretical and practical analysis of channel estimation methods. (C)
3. Practical investigation of the user impact on the propagation channel. (D)
4. Feasibility study of handset beamforming. (D)
5. Development and validation of a channel sounding system with a high dynamic range operating in active frequency bands. (E)
6. Validation of path-loss models by measurement data for D2D low elevation systems. (F)
7. Providing measured propagation data for future 5G radio channels. (A, B, D, E, F)

3.1 Paper A

Ultrawideband VNA Based Channel Sounding System for Centimetre and Millimetre Wave Bands.
Johannes Hejselbæk, Wei Fan, and Gert Frølund Pedersen
Published at the *IEEE 27th Annual IEEE International Symposium on Personal, Indoor and Mobile Radio Communications* - (PIMRC), 2016.

Motivation

At the time of this paper, there was no clear allocation in the frequency spectrum for mm-wave 5G. As a result, channel sounding campaigns where conducted at multiple bands as there was a need to identify possible differences in different bands. A VNA based channel sounding system capable of measuring mm-wave frequencies was at the time of the start of this PhD project purchased by the section for Antennas, Propagation and Millimetre-wave Systems (APMS) at Aalborg University (AAU). The measurement system was utilized for various measurement campaigns [1,2]. During one of the validation measurements before one of these campaigns, some large deviations in the frequency sweep were discovered. The vendor of the equipment did not have a clear answer to why this occurred and therefore no solution. As a result, there was a need to resolve this problem and verify the accuracy of the measurement system.

Paper content

The paper presents the problem of magnitude error at specific frequencies of the existing sounding system. The problem is identified to be a mismatch between internal shifts to harmonic frequencies of the purchased measurement equipment. The problem is solved by forcing the equipment to align its shifts in harmonic tones. By controlling the use of harmonics it is also possible to lower the distributed local oscillator (LO) frequency which extends the possible range of the system by reducing the frequency dependent losses in the distribution cables.

The improved measurement system is used for a multi-band measurement campaign of the power-angular-delay-profile (PADP) in both line-of-sight (LOS) and obstructed-LOS (OLOS) in an indoor scenario. The measurement is conducted using a mechanically steered horn antenna sweeping the azimuth angular plane. The PADP does therefore not include elevation information.

Main results

The cause of the magnitude error in the measurement system was identified and a solution was proposed. The improved measurement system is capable

of sounding in the frequency range from 2 to 50 GHz with a power drift of less than 0.5 dB at ranges of up to 30 m. A multi-band measurement campaign conducted at 18-20 GHz, 25-27 GHz, 28-30 GHz and 38-40 GHz showed that there was no significant difference in the PADP between these different bands.

3.2 Paper B

Channel Sounding System for MM-Wave Bands and Characterization of Indoor Propagation at 28 GHz.
Johannes Hejselbæk, Yilin Ji, Wei Fan, and Gert Frølund Pedersen
Published in the *International Journal of Wireless Information Networks* Vol. 24, Issue 3, pp. 204–216, 2017.

Motivation

Based on Paper A an invitation was received to submit an extended version to the Journal of Wireless Information Networks. At this time a new measurement campaign was planned to aim at measuring the channel with both a virtual array and by rotating a directional antenna. The plan was to compare the performance in obtaining the PADP using the two methods as well as study the evolution of the channel when moving the receiver through an indoor scenario.

Paper content

The paper describes the measurement system also presented in Paper A but with some extensions. In this paper, the measurement system's magnitude and phase stability over an extended time are also validated. When utilizing a virtual array it is important that not only the channel but also the measurement system does not change during each measurement snapshot. This paper also proposes to extend the existing measurement system to have two parallel receivers hence making it a single-input-multiple-output (SIMO) channel sounder. Further, the new SIMO sounder is adopting the use of a reference mixer to compensate for non-linearities in the used mixers and cables.

Using the new proposed system an indoor measurement campaign is conducted measuring 41 receiver locations distributed through a lab environment. The measurement is conducted with a frequency sweep from 26-30 GHz transmitted from an omnidirectional antenna while both a directional antenna and a virtual uniform circular array (UCA) antenna element are simultaneously recording the channel response.

By applying the maximum likelihood estimator with successive interference cancellation (MLE-SIC) algorithm described in [3] on the obtained data, the cluster evolution is studied.

Main results

The presented SISO channel sounder is validated for the frequency range 2-30 GHz showing a drift of less than 0.5 dB in magnitude and 1° in phase drift over 1 hour. The PADP resulting from the simultaneous channel sounding performed with the directional horn and the virtual UCA show good agreement. This helps validate the measurements presented in the literature using both virtual and directional antennas.

It was also shown in the paper that it is possible to track dominant paths throughout the measurement route consisting of the 41 measurement positions using the MLE-SIC algorithm. For the measured laboratory environment, the delay spread was found to be up to 6.5 ns and the angular spread up to 56°.

Recently the measurement system has also been applied to measurements utilizing a cubical virtual array as presented in [4].

3.3 Paper C

Validation of Emulated Omnidirectional Antenna Output Using Directive Antenna Data.
Johannes Hejselbæk, Anders Karstensen, Jesper Ødum Nielsen, Wei Fan, and Gert Frølund Pedersen
Published at the *2017 11th European Conference on Antennas and Propagation* - EuCAP 2017.

Motivation

In the design of receivers for communication systems, there is a need to know the power-delay-profile (PDP) of a given channel to account for the possible repetitions of the communication signal. The PDP for a given location is a sum of all the contributions from the surrounding interacting objects in the given environment. Therefore the PDP is often recorded utilizing omnidirectional antennas. However, to overcome the high attenuation of 5G mm-wave signals, directional antennas with high gain are often used. As a result, the omnidirectional PDP has to be constructed from a subset of channel measurements. The question is what difference does the angular resolution of the channel measurement have on the synthesised PDP.

Paper content

The paper presents a measurement campaign aiming at validating a synthesizing method for emulating an omnidirectional antenna. The paper then presents the derivations of a directional channel impulse response (CIR)

model and proposes an approximation of an omnidirectional PDP. The proposed method is validated against measurements conducted at the same location using both a real omnidirectional antenna and a rotated directional antenna. The measurement was conducted in both LOS and NLOS in the frequency range from 26 to 30 GHz using angular step sizes varying from 1 to 30 degrees.

Main results

It is found that the overall characteristics of the PDP is similar regardless of the choice of angular increments of the directional antenna. It is however also found that oversampling the angular domain by using angular step sizes of less than the half power beam width (HPBW) results in an overestimation of the received power. Conclusively, it is suggested that the best choice is to sample the angular domain using angular increments equivalent to the HPBW.

3.4 Paper D

Measured 21.5 GHz Indoor Channels With User-Held Handset Antenna Array.
Johannes Hejselbæk, Jesper Ødum Nielsen, Wei Fan, and Gert Frølund Pedersen
Published in the *IEEE TRANSACTIONS ON ANTENNAS AND PROPAGATION* Vol. 65, Issue 12, pp. 6574–6583, 2017.

Motivation

It is already known that the user has a large impact on the performance of a mobile communication system due to the added attenuation they cause by handling the handsets and at higher frequencies blocking signals. At the time of this work, multiple measurement campaigns were emerging in the literature but almost all of them not include a user. Due to this, it was desired to measure the channel at a frequency much higher than the ones utilized by legacy mobile communication generations. The aim was to study both the directional properties of the channel and the general impact on the received power by adding a user holding the handset.

Paper content

The paper presents a measurement system consisting of a mock-up handset with a linear 7 element array matched at 21.5 GHz, the AAU MIMO channel sounder and a dual polarized horn antenna. The AAU MIMO channel sounder is further described in [5] but it was configured here to perform 2

by 7 MIMO channel sounding, resulting in a full channel matrix between the handset array and the dual polarized horn antenna. Indoor measurements where performed using 10 different locations each measured with the handset pointing in 4 different directions. The measurements were conducted with the handset in free-space and with 5 different test persons.

The reason for including both free-space and users was to study if the difference in received power could be directly linked to the user. The reason for having different users was to gain knowledge about the users themselves or whether a user, in general, was the dominant factor in potential differences in received power. As beamforming from the handset side is suggested as a method to overcome the high attenuation at mm-wave frequencies, a study of the branch power ratio (BPR) between the 7 array elements was also conducted. This was done in order to investigate how many elements could potentially be used in an efficient manner for the beamforming. The difference in received power when transmitting in the two different polarizations have also been performed. Finally, the 4 directions were included to see to which extent body blocking would impact the received power level. Due to the large dataset generated by the large number of measurement variables and repetitions, most of the presented studies in the paper are conducted using statistics.

Main results

The measurement campaign showed that the mean impact of the users varied significantly, up to 12 dB, dependent on the location and orientation. This makes sense as the user at some locations and orientations will block the signal while in others might even help the signal by acting as a scatter, reflecting the power towards the handset antenna. The last finding that the measured power while the user is present in the channel was at some points higher than in free-space was a bit surprising, as the user, at legacy frequencies have not been seen causing this. The small wavelength of the signal can, however, explain this due to the size of the user starting to become significant, effectively making the user a large scatter. The difference in received power between the 5 users was within ± 4 dB. Effectively this means that the user is not always degrading the link quality as long as they do not directly affect the radiation properties of the handset antenna, as they where intentionally restricted from by the design of the used mock-up handset.

The study of the BPR showed large variations of up to 10 dB between the different elements. This high difference between elements' power effectively limits the available beamforming to only use a subset of the elements with highest or most uniform power. This is due to the otherwise high cost and complexity of equalizing the branch power by either power consuming amplification or SNR degrading attenuation. Conclusively, beamforming from

the handset side would be difficult even when the movement of the handset by the user is restricted to a minimum.

Investigations of the differences in received power dependent on the used polarization of the dual polarized horn antenna showed large variations of ± 10 dB. This shows that a large gain can be obtained by utilizing both polarizations. The difference in received power dependent on polarization is a result of the interactions with the surroundings. In the measured indoor case, the angles of the corridor walls could favour one polarization of a reflection which could become more pronounced with multiple interactions. After a number of interactions, the difference between received power in the two polarizations could become negligible. However, the relatively short distances of mm-wave systems due to the high attenuation of the signal suggests that both polarizations should be used for maximum possible power transfer.

The findings in this paper are to our knowledge very early if not the first related to the direct impact on the propagation channel by users at frequencies intended for 5G.

3.5 Paper E

Propagation Measurements for Device-to-Device Communication in Forest Terrain.
Johannes Hejselbæk, Jesper Ødum Nielsen, Christian Drewes, Wei Fan, and Gert Frølund Pedersen
Published at the *2018 12th European Conference on Antennas and Propagation* - EuCAP 2018.

Motivation

For device-to-device (D2D) communication so-called narrowband internet-of-things (NB-IoT) have been specified in standardization to operate with path-losses of up to 164 dB. The question is then what does these 164 dB correspond to with respect to distance in a forest with antennas placed at low elevation.

Paper content

The paper presents an overview of the allocations in LTE band 8 (880 - 960 MHz) as this is where NB-IoT is intended to be implemented. The paper includes a description of a spectrum analyser based channel sounding system for measuring received power levels after large losses. The measurement system is then used for a measurement campaign conducted in one of the state forests in Denmark. During the measurement, omnidirectional antennas at an elevation of 1.5 m where used at both the transmit and receive sides of the link. The measurements are conducted at 71 measurement positions

distributed over a range of up to 2580 m.

Main results

A spectrum analyser based channel sounding system capable of measuring a path-loss of more than 164 dB was developed and utilized for measurements. The measurement conducted in a typical forest terrain in Denmark showed that a link range of approximately 2000 m could be expected for an NB-IoT D2D system.

3.6 Paper F

Empirical Study of Near Ground Propagation in Forest Terrain for Internet-of-Things type Device-to-Device Communication.
Johannes Hejselbæk, Jesper Ødum Nielsen, Wei Fan, and Gert Frølund Pedersen
Submitted to *IEEE ACCESS*, 2018.

Motivation

Predicting the communication range of D2D NB-IoT systems in different environments by applying channel models is important for the development of commercial systems. Due to this the measurement results, also described in Paper E, is compared to existing path-loss models to validate their performance. Further, the impact of choosing different antenna elevations is investigated.

Paper content

The paper examines the relevant path-loss models form fundamental models to some of the latest proposals published in standardization work. The presented models are compared to each other to identify their relation. The paper also presents a summary of related measurements and their properties in relation to D2D scenarios. A subset of the presented path-loss models is compared to the measurement data also partly presented in Paper E together with an additional dataset with the transmit antenna at an elevation of 3.5 m and the receive antenna at 2.5 m. As none of the included path-loss models showed a direct fit with the measurement data, a combination of models is examined.

Main results

The comparison of the measurement data from the 1.5 m to 1.5 m and 3.5 m to 2.5 m measurement campaign showed that there was no significant difference in measured power. This is a result of the antennas at both antenna elevations

still being immersed in the foliage and the fact that the shifts in terrain are greater than the highest antenna elevation. As concluded in the paper the foliage and terrain loss, therefore, become the dominant factor. This means that if one antenna would be raised above the foliage the expected path-loss would be lower.

By combining different path-loss and foliage loss models it is shown that the power can be predicted with an RMS error of less than 8.1 dB. It is also found that a fairly simple model is capable of predicting the received power with an RMS error of less than 7.6 dB if only compared to the measurements from 200 m and to the maximum distance of 2580 m.

Empirical data with similar long measurement distance of 2580 m and maximum path-loss measured up to 180 dB for antennas with elevations down to 1.5 m have not been found other places in the literature.

References

[1] W. Fan, I. C. Llorente, and G. F. Pedersen, "Comparative study of centimetric and millimetric propagation channels in indoor environments," in *2016 10th European Conference on Antennas and Propagation (EuCAP 2016)*, April 2016.

[2] A. Karstensen, W. Fan, I. C. Llorente, and G. F. Pedersen, "Comparison of ray tracing simulations and channel measurements at mmwave bands for indoor scenarios," in *2016 10th European Conference on Antennas and Propagation (EuCAP 2016)*, April 2016.

[3] Y. Ji, W. Fan, and G. F. Pedersen, "Channel characterization for wideband large-scale antenna systems based on a low-complexity maximum likelihood estimator," *IEEE Transactions on Wireless Communications*, pp. 1–1, 2018.

[4] A. W. Mbugua, W. Fan, Y. Ji, and G. F. Pedersen, "Millimeter wave multi-user performance evaluation based on measured channels with virtual antenna array channel sounder," *IEEE Access*, vol. 6, pp. 12 318–12 326, 2018.

[5] J. Ødum Nielsen, W. Fan, P. C. F. Eggers, and G. F. Pedersen, "A channel sounder for massive mimo and mmwave channels," *IEEE Communications Magazine*, 2018.

Chapter 4 - Conclusion

The overall theme for this PhD was radio propagation for the next generation mobile communication systems which is quite a broad definition. As a result, the scope of the research has been focused on three main subjects being: collecting propagation data for future 5G radio channels, investigating the user impact on mm-wave channels and a study of device-to-device communication in a forest environment. Contributions have been made in all of the three research areas as it is briefly summarized as follows:

The thesis contributes to the understanding of the need for the introduction of the fifth generation mobile communication system (5G) and provides an overview of the suggested improvements as compared to the current mobile communication systems. A summary of different channel modelling and sounding approaches in relation to 5G is presented providing insights into the current state-of-the-art in the research field.

A channel sounding system capable of capturing both the temporal and spatial channel characteristics at frequencies from 2 to 50 GHz is presented in paper A and B. The measurements conducted with the sounding system showed that the radio propagation environment at the frequencies suggested for 5G (18-40 GHz) becomes highly directive. The measurements presented in paper A showed that no significant difference in the power-angular-delay-profile (PADP) could be identified for four measured bands, 18-20 GHz, 25-27 GHz, 28-30 GHz and 38-40 GHz. In paper B the sounding system is shown capable of simultaneous recording of two channels. In paper B it is also concluded that is it possible to track the dominant paths while moving through an indoor scenario. Using the developed simultaneously sounding of the two channels system, a synthesizing method for emulating an omni-directional antenna is validated using empirical data as presented in paper C.

The user impact on an indoor radio channel at 21.5 GHz was studied in Paper D. It is found that the user, as expected, in some cases introduces additional attenuation. However, it is also found that the user can provide a gain as compared to the channel with no user. This is a result of the directive channel and the finding that the user can be seen as an added scatter, which

in some scenarios can reflect the power towards the handset antenna. Further more a study of the branch power ration of the handset's 7 element array showed large variations. This indicates that beamforming from the handset side would be difficult without either only using a subset of the array or extensive power equalization.

To investigate the expected range of a narrowband Internet-of-Things (NB-IoT) in a forest environment, a measurement system, with a dynamic range of up to 180 dB has been developed as described in Paper E. Using the developed system a measurement campaign was conducted in LTE band 8 showing an expected range at 164 dB path-loss of 2 km. In paper F the obtained measurement data is further studied and compared to predictions of path-loss models specific to the scenario. The investigation of the path-loss models resulted in a proposal for a best practice of combining path-loss and foliage loss models.

As a whole, this PhD study has contributed to the advance of knowledge related to radio propagation channels as expected for the next generation mobile communication system - 5G.

Part II

Papers

Paper A

Ultrawideband VNA Based Channel Sounding System for Centimetre and Millimetre Wave Bands

Johannes Hejselbæk, Wei Fan and Gert Frølund Pedersen

The paper has been published at the
IEEE 27th Annual IEEE International Symposium on Personal, Indoor and Mobile Radio Communications - (PIMRC)

Abstract

Channel characterization of multipath channels at centimetre and millimetre wave bands is of interest from both academia and industry, especially for the frequency bands that are under consideration for 5G mobile communication systems. In this paper, we first demonstrate the limitations of an existing vector network analyzer (VNA) based channel sounding system in terms of frequency range and measurement range. After that, an improved system is proposed to address these limitations. The proposed system is capable of measuring from 2 to 50 GHz at 30 meters distances. A measurement campaign utilizing the proposed setup equipped with rotational directive horn antennas, with a focus on multi-band power-angle-delay profiles, was performed. The measured frequency bands are 18 - 20 GHz, 25 - 27 GHz, 28 - 30 GHz and 38 - 40 GHz.

I Introduction

The increasing growth in demand for mobile data drives the industry towards a fifth-generation mobile network (5G) [1]. To facilitate the demand for higher data rates, there is a need for unused radio spectrum. The super-high-frequency (SHF) bands (3 – 30 GHz) and the extremely high-frequency (EHF) bands (30 – 300 GHz), also referred to as centimetre- and millimetre-wave bands have the potential to provide the needed bandwidth [2].

To enable the system design for the 5G mobile network, understanding of the propagation channels is essential [3,4]. One of the important channel characteristics is the Angle-of-Arrivals (AoAs) of multipath channels. The possible utilization of high frequency for 5G systems enables the implementation of massive antenna arrays due to the small antenna element. This enables 5G systems to excessively utilize the spatial dimension via e.g., beamforming algorithms, which can boost the system performance significantly in terms of data rate and signal strength levels [5,6]. Therefore, knowledge of the AoAs of the propagation environments is the focus of this paper.

Channel characterization above 6 GHz for various propagation environments has attracted huge research attention in recent years. To ensure the realism of the modelled propagation channels, many measurement campaigns were carried out for various bands above 6 GHz. For the unlicensed frequency band at 60 GHz, used for IEEE 802.11ad, there are significant available studies [7,8]. The 60 GHz system is mainly for short range indoor to indoor communication due to the high path-loss introduced by oxygen absorption. For longer range systems, e.g. the potential 5G cellular systems, lower bands are suggested [3,9,10]. More specifically, there is an interest in the 28 - 30 GHz band, where some experimental measurements have been conducted [11–14].

In the literature, there are mainly two types of channel sounding systems [15]. The first, known as direct pulse measurements, utilizes a dedicated correlative channel sounder and operates in time-domain and the other, known as swept frequency measurements, utilizes a Vector Network Analyser (VNA) based system, and it operates in frequency-domain. The correlative channel sounders are capable of recovering an estimate of the channel impulse response (CIR) very fast [16]. This is an advantage for collecting large datasets for time-variant scenarios. However, the complexity of generating the sounding pulse poses limitations to the obtainable bandwidth of these systems [17]. A VNA based system do not have this limitation as it sweeps the chosen frequency band while the channel frequency response is measured between two ports of the VNA. This allows for very large bandwidths to be measured and hence it is a popular method especially for Ultra-wideband (UWB) applications [18,19].

Large bandwidths are expected for the future 5G mobile communication system, which encourages the use of a VNA for measurements. As it is difficult to assess the possible frequency bands over which the mm-wave systems are expected to operate at this stage, various frequency bands above 6 GHz are proposed and under investigation. Therefore, it is beneficial to record the channel over the whole interested band and understand the frequency dependence of channel parameters scenarios for future mm-Wave systems. This knowledge would help operators decide which frequency bands are preferable and how to utilize the channels best at different frequency bands. The VNA based channel sounding system is often adopted for mm-Wave channel measurements, due to high cost and complexity of the dedicated channel sounder [15,17]. However, there are some well-known limitations with the VNA system. The measurement system is limited in range (i.e. distance between transmitter (TX) and receiver (RX)), especially for mm-Wave systems. TX/RX signals are carried via RF cables, which introduce a power loss. Furthermore, the measurement scenario should be static as it takes time for VNA system to sweep over frequency domain for multiple locations. Hence, channel sounding using a VNA is normally used for short range indoor scenarios [15].

VNA based channel sounding systems have been extensively used for low-band (below 6GHz) and high-band (above 6GHz) in the literature. For frequencies below 6 GHz, there are publications addressing the measurement range issue. In [20], a system capable of supporting a TX-RX separation of up to 45 meters was presented. A system utilizing optics for extending the range up to 100 meters is presented in [18] for frequency below 6GHz as well. In [21], the measurement range up to 1000 meters was demonstrated with two synchronized VNAs. For systems operating above 6 GHz, most of the proposals are for systems operating at 60 GHz and therefore not intended for longer range measurements. A system operating at 26 GHz sweeping a 5

GHz bandwidth (24 to 29 GHz) is presented in [22]. However, this system is only operated in a range of 5 meters. In [23] a system operating at 28 GHz is presented which have a range of 7 meters, but only sweeping 1 GHz (27.5 - 28.5 GHz). The same frequency and bandwidth are used for the system presented in [24], where the range is here 30 meters. For larger bandwidths used in multi-band measurements, a system is presented in [14,25,26]. This has a limited range of about 10 meters and is restricted in which frequency bands it can measure, 2 - 4 GHz, 14 - 16 GHz and 28 - 30 GHz. This paper presents the cause of these limitations and a proposal for an improved measurement setup with an extended frequency range and also capable of extending the operational range.

This paper is organized as follows. Section II describes the existing VNA-based channel sounding system and presents the limitations of the system. This is followed by a presentation of the proposed new measurement system and its capabilities. Section III presents new multi-band power-angle-delay measurements. Section IV summarizes this work.

II Channel Sounding System

To extend the physical range of measurements conducted using a VNA, the VNA is used together with mixers. The basic principle is that via down-converting the signals with a mixer, the cable loss, which is the main limiting factor for measurement range, can be reduced.

Limitations of Existing System

The existing system presented in [14,25,26] is based on a mixer solution from Agilent. This solution is consisting of the following three elements:

- Distribution unit for the local oscillator and intermediate frequency.
- Reference mixer.
- Test mixer.

The distribution unit is in principle just an amplifier and splitter of the LO (Local Oscillator) from the VNA (PNA) to the mixers, as depicted in Fig. B.1. It also provides amplification of the IF (Intermediate Frequency) from the mixers along with demultiplexing of the IF from the test mixer.

The purpose of both the test mixer and reference mixer is to down-convert the received high-frequency signal to IF. The main difference between the test mixer and the reference mixer is that the test mixer multiplexes the IF on the LO resulting in only one cable having to go from distribution unit to mixer. The reference mixer uses separate lines for the LO and IF and also

provides feedback for the ALC (Automatic Level Control) in the distribution unit. Using the reference mixer enables the system to utilize leveled output power.

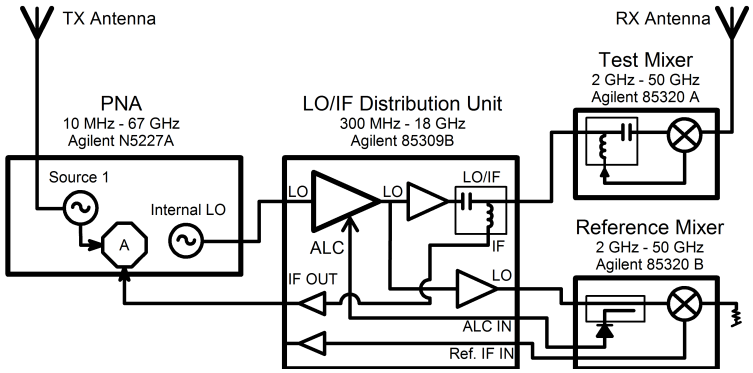

Fig. A.1: Block diagram of the existing measurement system.

A measurement is conducted to test the stability of the system. In this test the TX port is connected directly to the test mixer input. Following the manufacturer specified warm up period a normalization/calibration is performed. This procedure sets the trace to zero in the chosen frequency span from 2 GHz to 30 GHz (1001 points). The VNA was set to continuous sweeping, while the drift from the normalization is recorded. The drift after 10 sweeps is shown in Fig. B.2. It is clear that power variations exist, especially for frequency band from 2-6 GHz and 18-26.5 GHz. The lower band at 2-6 GHz shows deviations up to 1 dB and the higher band at 18-26.5 GHz shows deviations up to 3 dB. Below, these deviations in the measurement system are investigated.

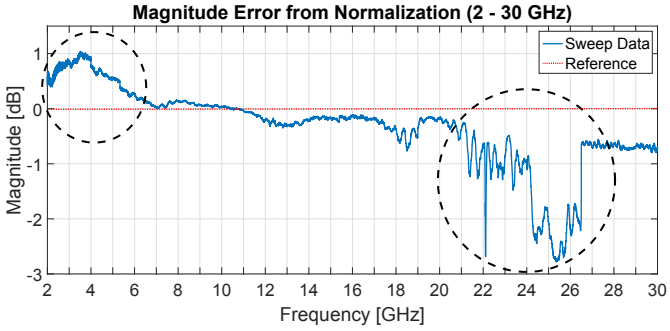

Fig. A.2: Deviation from the normalization/calibration curve for the frequency sweep from 2 to 30 GHz using the existing system.

As shown in Fig. B.1, the internal LO output from the PNA is ported to

the distribution unit. This setting was chosen as it was the most straightforward way to use and did not require any additional setup of the PNA. However, by measuring the output of the internal LO, it became evident that it only utilizes the fundamental frequency up to 26.5 GHz before it switches to operate on 3rd harmonics of the frequency. This is problematic, as the amplifiers in the distribution unit only have a frequency range from 300 MHz to 18 GHz. As a result, the required amplification of the LO from 18 to 26.5 GHz does not exist, which results in large power variations within 18-26.5 GHz, as shown in Fig. B.2.

The power variations within 2-6 GHz were found to be a result of to high LO power at the test mixer, for the lower frequencies. The purpose of the reference mixer is to control the LO power levels by using the ALC to compensate the frequency dependent loss of the cable connecting the mixers to the distribution unit. In the existing VNA system, two cables of different types and lengths are used to connect between the distribution unit and the two mixers. As a result, the ALC did not function as intended for the low band.

Proposed Improvement of Existing System

As discussed in Section A., the existing measurement system in general had two problems:

1. Over-powering at lower frequencies
2. Under-powering at higher frequencies

To address the under-powering at higher frequencies, an alternative source for the LO has to be used. The PNA is equipped with two source oscillators (signal generators), as depicted in Fig. B.3. The two oscillators are locked to each other, but it is possible to introduce a frequency offset between them. In the proposed setup, one oscillator is connected to the TX antenna (source 1), while the other oscillator (source 2) is used as LO and set to operate on a lower harmonic of the desired frequency. For example, source 1 can be set to sweep from 2 GHz to 30 GHz, while source 2 can sweep from 2/3 GHz to 10 GHz, using the 3rd harmonics. This ensures that the system operates within the frequency limits of the amplifiers of the distribution unit. The lowered frequency also reduces the cable losses which can improve the operational range of the system. It could be tempting to lower the LO frequency further by using higher harmonics. However, using harmonics have the cost of the sensitivity of the mixers and using higher harmonics will decrease the sensitivity level further.

As seen in Fig. B.3, the reference mixer is terminated at its input. Even though it is not needed to use a long cable for the reference mixer, this is

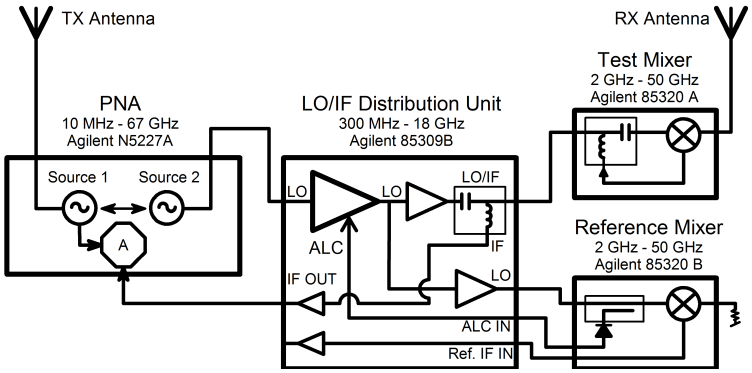

Fig. A.3: Block diagram of the proposed measurement system.

a solution to address the over-powering at lower frequencies. By using the same type and length of cabling to the reference mixer as for the test mixer, it is possible for the ALC to provide the same LO power over the selected frequency band.

Using the same settings as for the sweep shown in Fig. B.2, a sweep with the proposed solutions is conducted. The resulting magnitude error is shown in Fig. B.4. A significant improvement is achieved in terms of power variations. The only significant variations are seen close to 2.5 GHz, which is due to the settling time of the ALC. This settling time introduces a variation of up to 0.5 dB at the low frequency, aside from this a variation of less than 0.1 dB is seen.

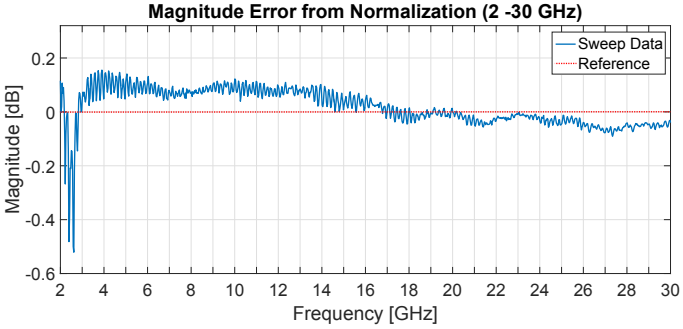

Fig. A.4: Deviation from the normalization/calibration curve for the frequency sweep from 2 to 30 GHz using the proposed system.

Improved System Capability

With the proposed systems, the measurement system capability in terms of measurement range and frequency range can be greatly improved. The frequency range of the used mixers is 2 to 50 GHz, which becomes the limiting factor as the PNA have a larger span. The measurement range is limited by the link budget. Below, the system link budget is discussed separately for the RF chain and in-the-air propagation loss.

The sensitivity level for the test mixer sets the limit for the lowest detectable power at its RF input. When operating the test mixers with 3rd harmonic, the sensitivity level for RF input is -118 dBm for 2 GHz to 18 GHz, -103 dBm for 18 GHz to 40 GHz and -100 dBm for 40 GHz to 50 GHz, respectively. This is on the condition that the LO input power at the mixer is at +12 to +17 dBm. To investigate the link budget of the RF chain, the most critical frequency 50 GHz is selected, as an example for measurement range. As discussed earlier, 3rd harmonics (i.e. 16.67 GHz) would be utilized for 50 GHz. According to the specifications, the maximum LO output power from the distribution unit is +23.5 dBm in the frequency range from 6.2 to 18 GHz when given an input signal at +6 dBm. This leaves $23.5 - 12 = 11.5$ dB for cable loss between distribution unit and mixer as illustrated in Fig. A.5.

The PNA is capable of delivering +18 dBm (@16.5 GHz), leaving 12 dB for cable loss between PNA and distribution unit. The used LO cable has a loss of 0.78 dB/m (@16.5 GHz), giving that at least $12/0.78 = 15.3$ m can be used for the cable from PNA to distribution unit and $11.5/0.78 = 14.7$ m of cable can be used from the distribution unit to the test mixer. In total, this gives an operational range of 30 meters when measuring at 50 GHz. When measuring at lower frequencies, the LO frequency will also be lower, allowing for longer cables to be used. As an example, the operational range is 41 meters when measuring at 30 GHz. The range of the LO distribution system could be extended by introducing further amplification.

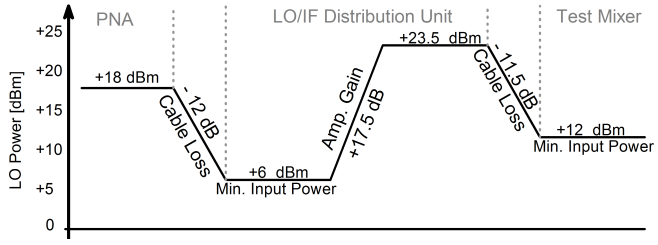

Fig. A.5: Link-budget for the LO power distribution.

Additional to the RF chain loss, the signals also suffer from in-the-air propagation loss. The path loss, however, highly depends on the measure-

ment scenario, e.g. Line-Of-Sight (LOS) or Non-LOS, together with the frequency measured. For the proposed measurement system, the maximum leveled output power from source 1 when sweeping up to 50 GHz is 9 dBm. The sensitivity of the test mixer is -100 dBm, which gives a maximum path loss of 109 dB. Using Friis free space propagation loss for LOS scenario and assuming 0 dB TX/RX antenna gains, the maximum transmission range is 32.6 meters for 50 GHz. If sweeping to a maximum of 30 GHz the leveled output power can be increased to 12 dBm while the sensitivity level of the test mixer is lowered to -103 dBm. This gives that the range will be 34.6 meters in same LOS scenario for 30 GHz. The transmission range can be further improved utilizing high gain antennas.

III Angular Power Measurement using New Proposed System

Using the presented measurement system, a multi-band measurement has been conducted aiming at capturing the power-angle-delay profiles. The selected measured bands are 18 - 20 GHz, 25 - 27 GHz, 28 - 30 GHz and 38 - 40 GHz. The chosen bands are based on the candidates for future 5G frequency allocations presented in [9].

Measurement Setup

Two frequency sweeps from 18 to 27 GHz and from 28 to 40 GHz, utilizing two standard gain horn antennas for RX were performed. As the TX antenna, the biconical antenna presented in [27] is used. All the antennas used are vertically polarized. The properties of the used antennas are presented in TABLE A.1.

Both of the frequency sweeps from 18 to 27 GHz and from 28 to 40 GHz are recorded using 10001 frequency points. The four bands of interest all have a bandwidth of 2 GHz, giving a delay resolution of 0.5 ns equivalent to a spatial resolution of 0.15 m.

Two different scenarios were studied in a rich furnished laboratory as shown in Fig. A.6. The first is an LOS scenario, shown left in Fig. A.6. The second, shown right in Fig. A.6, is a obstructed line-of-sight (O-LOS) scenario, where the LOS path is blocked by an obstruction. The O-LOS scenario was created by placing a cubicle divider in the direct path between TX and RX at a distance of 4.15 m from the TX. The distance between TX and RX is 8 m for both scenarios.

The TX power for all the measurements is 9 dBm. When starting the measurement the orientation of the RX horn antennas is 90^o of bore-sight of

Table A.1: Properties for the used antennas

Antenna Type	Freq. Range [GHz]	HPBW, Azimuth [^{o}]	Gain [dB]
Biconical (1.5 - 42 GHz)	18 - 20	Omni	4.5
	25 - 27	Omni	4.8
	28 - 30	Omni	4.6
	38 - 40	Omni	3.7
Horn (18 - 27 GHz)	18 - 20	21.5	18.7
	25 - 27	15.7	21.2
Horn (27 - 40 GHz)	28 - 30	21,2	18.8
	38 - 40	15.8	21.1

Fig. A.6: Measurement scenario. Left in the figure the LOS case is shown and right in the figure the O-LOS case is shown. The biconical TX antenna, seen in the bottom of both scenarios, is encased in styrofoam as a part of its design.

the TX antenna. It is then rotated clockwise in 1^o steps between each sweep for a full 360^o measurement.

Measurement Results

The power-angle-delay profiles for the four measured bands presented in Fig. 7 - 10, are obtained via an inverse Fourier transformation of the frequency sweeps for each orientation. To suppress the effect of side lobes, a Hamming window has been applied to the data. The frequency response of the used antennas has not been removed from the recorded frequency sweeps and thus are embedded in the presented plots. The dynamic range of the plots is

set to 40 dB. The four measured bands are presented for both the LOS and O-LOS scenario. The same power scale is used to enable comparison between the scenarios.

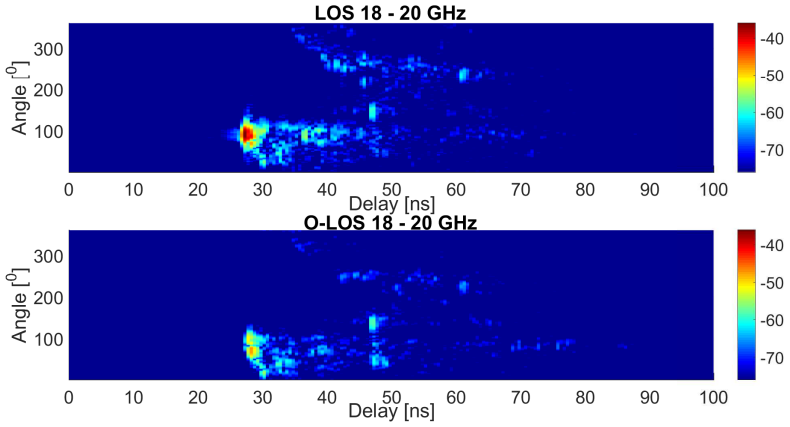

Fig. A.7: Power-angle-delay profile measured using a directional horn antenna for 18 - 20 GHz in LOS and O-LOS.

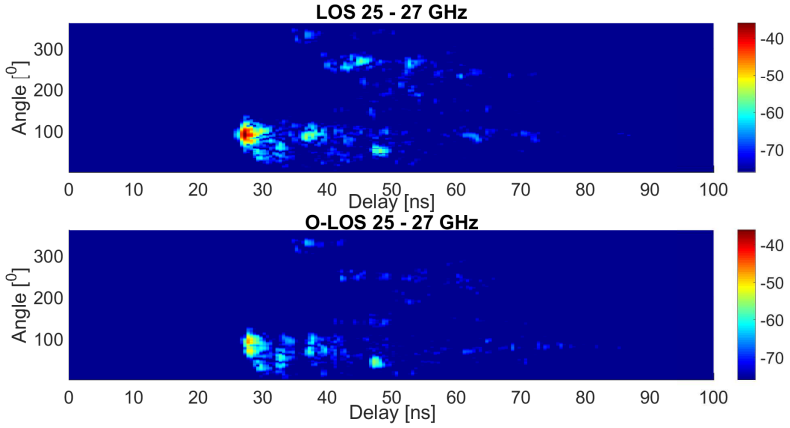

Fig. A.8: Power-angle-delay profile measured using a directional horn antenna for 25 - 27 GHz in LOS and O-LOS.

In Fig. 7 - 10, the dominant path is at 90^o, which corresponds to the LOS path between the TX and RX. The delay of the dominant path, for the LOS scenario, is 27 ns corresponding to 8.1 m in accordance with the distance between TX and RX in the chosen scenario. The delay of the dominant path for the O-LOS is 28 ns which are only 1 ns longer than for the LOS scenario. This indicates that it might be a diffraction around the edges of the obstruc-

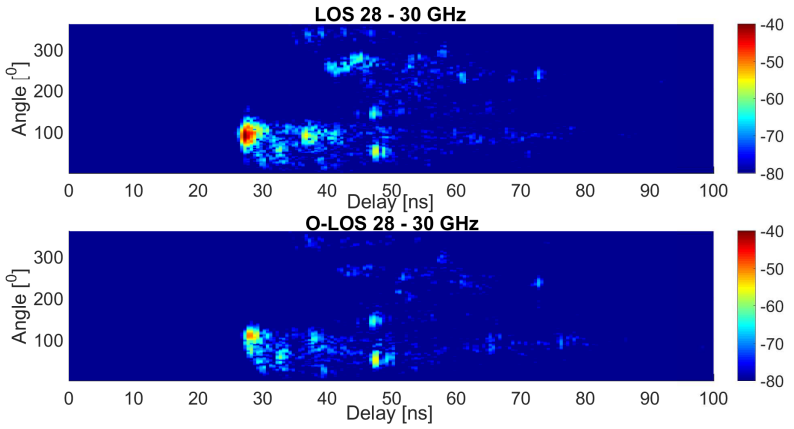

Fig. A.9: Power-angle-delay profile measured using a directional horn antenna for 28 - 30 GHz in LOS and O-LOS.

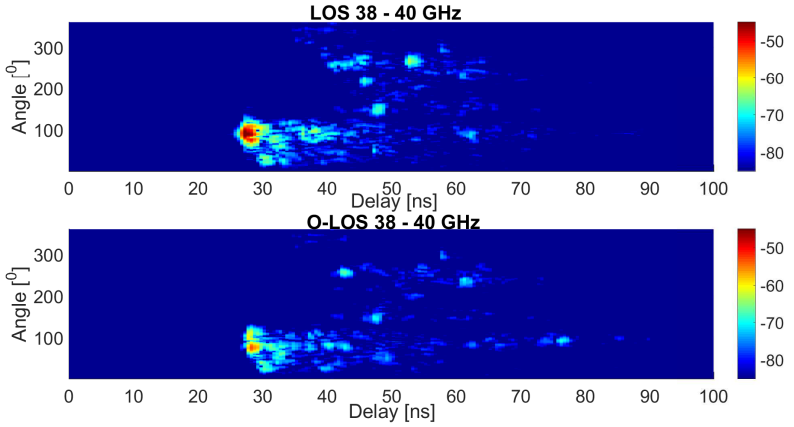

Fig. A.10: Power-angle-delay profile measured using a directional horn antenna for 38 - 40 GHz in LOS and O-LOS.

tion. The power difference between the dominant path in LOS and O-LOS is around 9 dB, varying with only 0.5 dB between the four bands.

The number of multipath components is similar for all four bands, given the chosen dynamic range. In addition, some similarity in the location of the components can be observed in the four bands. There is a tendency for the components to be located around 90^o and 270^o. The components at 270^o are presumed to be backscatters from the wall behind the RX, as seen from the TX. It can be seen in Fig. A.10 that the component arriving at 55 ns from 270^o in the LOS scenario diminishes in the O-LOS scenario. This is due to the

lower power of the dominant path, which results in a very low power of the backscatter.

A comparison of the omnidirectional power delay profile for the measured bands is presented in Fig. C.1. To enable comparison of the slope of the delay profiles, the maximum power of the LOS component have been used for normalization of each band separately. The O-LOS profiles have been normalized using the same value as for the LOS.

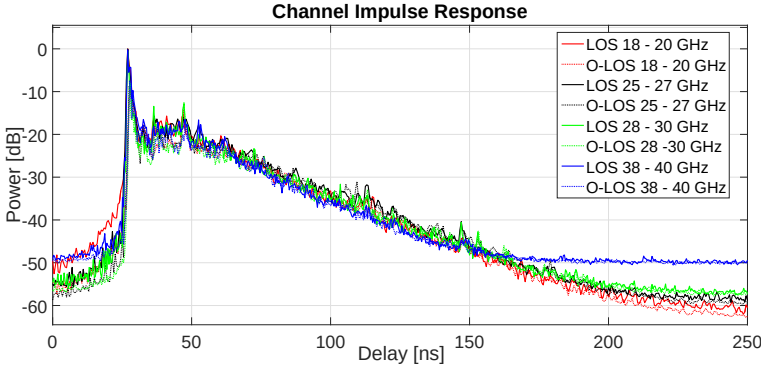

Fig. A.11: Channel impulse response for the measured bands in both LOS and O-LOS.

An interesting finding from Fig. C.1 is that all four bands in both LOS and O-LOS scenario present the same decay slope from 50 to 150 ns. In [14], it was concluded that the decay rate is independent of frequency. However, the measurements were performed in an empty basement scenario and therefore the impact of furniture in the room is not investigated. In this paper, we demonstrated that the decay rate is frequency independent for a rich furnished laboratory.

IV Conclusion

This work presents the improvement of an existing VNA based measurement system contributing with a wider frequency range and longer measurement range. The proposed system is capable of measuring from 2 to 50 GHz with a power drift of less than 0.5 dB in the whole span. The range of the system has been extended to 30 meters for measurement at 50 GHz and even further for measurement at lower frequencies.

Multi-band measurements in both LOS and O-LOS have been conducted using the proposed system Measurements. The conducted measurements showed that the frequency bands 18 - 20 GHz, 25 - 27 GHz, 28 - 30 GHz and 38 - 40 GHz have similar power-angle-delay properties. Another interesting result is the similarity in the slope of the delay decay slope for all measured

bands.

Acknowledgment

The work have been conducted under the framework of the VIRTUOSO project. The Danish National Advanced Technology Foundation supports this project together with industry partners. The authors would like to thank Kim Olesen and Anders Karstensen for assistance with measurements.

References

[1] P. Demestichas, A. Georgakopoulos, D. Karvounas, K. Tsagkaris, V. Stavroulaki, J. Lu, C. Xiong, and J. Yao, "5g on the horizon: Key challenges for the radio-access network," *Vehicular Technology Magazine, IEEE*, vol. 8, no. 3, pp. 47–53, Sept 2013.

[2] Q. Li, H. Niu, A. Papathanassiou, and G. Wu, "5g network capacity: Key elements and technologies," *Vehicular Technology Magazine, IEEE*, vol. 9, no. 1, pp. 71–78, March 2014.

[3] L. Wei, R. Q. Hu, Y. Qian, and G. Wu, "Key elements to enable millimeter wave communications for 5g wireless systems," *IEEE Wireless Communications*, vol. 21, no. 6, pp. 136–143, December 2014.

[4] Y. Kim, H. Y. Lee, P. Hwang, R. K. Patro, J. Lee, W. Roh, and K. Cheun, "Feasibility of mobile cellular communications at millimeter wave frequency," *IEEE Journal of Selected Topics in Signal Processing*, vol. PP, no. 99, pp. 1–1, 2016.

[5] W. Roh, J.-Y. Seol, J. Park, B. Lee, J. Lee, Y. Kim, J. Cho, K. Cheun, and F. Aryanfar, "Millimeter-wave beamforming as an enabling technology for 5g cellular communications: theoretical feasibility and prototype results," *Communications Magazine, IEEE*, vol. 52, no. 2, pp. 106–113, February 2014.

[6] S. Han, C. l. I, Z. Xu, and C. Rowell, "Large-scale antenna systems with hybrid analog and digital beamforming for millimeter wave 5g," *IEEE Communications Magazine*, vol. 53, no. 1, pp. 186–194, January 2015.

[7] A. Maltsev, R. Maslennikov, A. Sevastyanov, A. Khoryaev, and A. Lomayev, "Experimental investigations of 60 ghz wlan systems in office environment," *Selected Areas in Communications, IEEE Journal on*, vol. 27, no. 8, pp. 1488–1499, October 2009.

[8] W. Fu, J. Hu, and S. Zhang, "Frequency-domain measurement of 60 ghz indoor channels: a measurement setup, literature data, and analysis," *IEEE Instrumentation Measurement Magazine*, vol. 16, no. 2, pp. 34–40, April 2013.

[9] Ofcom, "Spectrum above 6 ghz for future mobile communications," Ofcom UK, Riverside House, 2a Southwark Bridge Road, London, Consultation Report, January 2015.

[10] S. Methley, W. Webb, S. Walker, and J. Parker, "Study on the suitability of potential candidate frequency bands above 6ghz for future 5g mobile broadband systems," Quotient Associates Limited, Compass House, Vision Park, Chivers Way Histon, Cambridge, CB24 9AD, UK, Technical Report, March 2015.

[11] S. Rangan, T. Rappaport, and E. Erkip, "Millimeter-wave cellular wireless networks: Potentials and challenges," *Proceedings of the IEEE*, vol. 102, no. 3, pp. 366–385, March 2014.

[12] T. Rappaport, S. Sun, R. Mayzus, H. Zhao, Y. Azar, K. Wang, G. Wong, J. Schulz, M. Samimi, and F. Gutierrez, "Millimeter wave mobile communications for 5g cellular: It will work!" *Access, IEEE*, vol. 1, pp. 335–349, 2013.

[13] T. Rappaport, F. Gutierrez, E. Ben-Dor, J. Murdock, Y. Qiao, and J. Tamir, "Broadband millimeter-wave propagation measurements and models using adaptive-beam antennas for outdoor urban cellular communications," *Antennas and Propagation, IEEE Transactions on*, vol. 61, no. 4, pp. 1850–1859, April 2013.

[14] W. Fan, I. C. Llorente, J. Ødum Nielsen, K. Olesen, and G. F. Pedersen, "Measured wideband characteristics of indoor channels at centimetric and millimetric bands," *EURASIP Journal on Wireless Communications and Networking*, vol. Pre Press, no. Special issue on Radio Channel models for higher frequency bands, 2016.

[15] A. F. Molisch, *Wireless communications*. IEEE Press, 2005, iSBN: 978-0-470-84888-3.

[16] J. Ødum Nielsen, J. B. Andersen, P. C. F. Eggers, G. F. Pedersen, K. Olesen, E. H. Sørensen, and H. Suda, "Measurements of indoor 16x32 wideband mimo channels at 5.8 ghz," in *Proceedings of the 2004 International Symposium on Spread Spectrum Techniques and Applications*, May 2004.

[17] A. F. Molisch, "Ultrawideband propagation channels-theory, measurement, and modeling," *IEEE Transactions on Vehicular Technology*, vol. 54, no. 5, pp. 1528–1545, Sept 2005.

[18] A. M. Street, L. Lukama, and D. J. Edwards, "Use of vnas for wideband propagation measurements," *IEE Proceedings - Communications*, vol. 148, no. 6, pp. 411–415, Dec 2001.

[19] S. Ranvier, M. Kyro, K. Haneda, T. Mustonen, C. Icheln, and P. Vainikainen, "Vna-based wideband 60 ghz mimo channel sounder with 3-d arrays," in *Radio and Wireless Symposium, 2009. RWS '09. IEEE*, Jan 2009, pp. 308–311.

[20] S. S. Ghassemzadeh, R. Jana, C. W. Rice, W. Turin, and V. Tarokh, "A statistical path loss model for in-home uwb channels," in *Ultra Wideband Systems and Technologies, 2002. Digest of Papers. 2002 IEEE Conference on*, May 2002, pp. 59–64.

[21] K. Sarabandi, N. Behdad, A. Nashashibi, M. Casciato, L. Pierce, and F. Wang, "A measurement system for ultrawide-band communication channel characterization," *IEEE Transactions on Antennas and Propagation*, vol. 53, no. 7, pp. 2146–2155, July 2005.

[22] Y. Rikuta, S. Fujita, F. Ohkubo, H. Hosoya, K. Hamaguchi, J. i. Takada, and T. Kobayashi, "Indoor channel measurement of 26 ghz band uwb communication

system," in *Ultra-Wideband, The 2006 IEEE 2006 International Conference on*, Sept 2006, pp. 219–224.

[23] X. Wu, Y. Zhang, C. X. Wang, G. Goussetis, e. H. M. Aggoune, and M. M. Alwakeel, "28 ghz indoor channel measurements and modelling in laboratory environment using directional antennas," in *2015 9th European Conference on Antennas and Propagation (EuCAP)*, May 2015, pp. 1–5.

[24] M. Lei, J. Zhang, T. Lei, and D. Du, "28-ghz indoor channel measurements and analysis of propagation characteristics," in *Personal, Indoor, and Mobile Radio Communication (PIMRC), 2014 IEEE 25th Annual International Symposium on*, Sept 2014, pp. 208–212.

[25] W. Fan, I. C. Llorente, and G. F. Pedersen, "Comparative study of centimetric and millimetric propagation channels in indoor environments," in *2016 10th European Conference on Antennas and Propagation (EuCAP 2016)*, April 2016.

[26] A. Karstensen, W. Fan, I. C. Llorente, and G. F. Pedersen, "Comparison of ray tracing simulations and channel measurements at mmwave bands for indoor scenarios," in *2016 10th European Conference on Antennas and Propagation (EuCAP 2016)*, April 2016.

[27] S. S. Zhekov, A. Tatomirescu, and G. F. Pedersen, "Modified biconical antenna for ultrawideband applications," in *2016 10th European Conference on Antennas and Propagation (EuCAP 2016)*, April 2016.

Paper B

Channel Sounding System for MM-Wave Bands and Characterization of Indoor Propagation at 28 GHz [Invited Paper]

Johannes Hejselbæk, Yilin Ji, Wei Fan and Gert Frølund Pedersen

The paper has been published in the
International Journal of Wireless Information Networks Vol. 24, Issue 3,
pp. 204–216, 2017.

Abstract

The aim of this work is to present a vector network analyzer (VNA) based channel sounding system capable of performing measurements in the range from 2 to 50 GHz. Further, this paper describes an indoor measurement campaign performed at 26 to 30 GHz. The sounding system is capable of receiving two channels and transmitting one. Using this feature a channel measurement has been performed using both a directional horn antenna and a virtual uniform circular array (UCA) at the same time. This allows for comparative studies of measured channels with two different antennas in a simultaneous way. The measurement has been conducted with 42 measurement positions distributed along a 10 m long path through an indoor laboratory environment. The transmitter was positioned such that measurements were conducted both in line-of-sight (LOS) and non-line-of-sight (NLOS) scenarios. The measurements showed good agreement between the measurement data collected with the horn antenna and the data collected with the UCA. The propagation environment was found to be sparse both in delay and angular domain for the given scenario. Based on the performed measurement campaign together with validation measurements of the system stability, it is found that the system works as expected.

I Introduction

The increasing growth in demand for mobile data is one of the driving factors for the industry in moving towards a fifth generation mobile communication network (5G) [1,2]. To help facilitate the demand, there is a need for unused radio spectrum, which is scarce below 6 GHz. The available spectrum of interest, which ranges from 6 GHz to 100 GHz, falls in the two bands denoted the super-high-frequency (SHF) band (3 - 30 GHz) and the extremely high-frequency (EHF) band (30 - 300 GHz). These are also referred to as the centimetre and millimetre wave bands. In this large range from 6 GHz to 100 GHz, multiple frequency bands have been suggested as candidates for 5G [2–5]. The studies point out that for larger area coverage the lower frequencies are preferable due to the frequency dependent free-space path-loss together with other physical constraints such as atmospheric attenuation. As an example, high oxygen absorption is seen at 60 GHz used for IEEE 802.11ad (WLAN) [6]. As a result, the frequency range from 15 GHz to 40 GHz which are expected to be more suitable for cellular communication has received the most attention in regards to channel measurements [7–15].

These studies mainly focus on path-loss, the angle of arrival (AoA) and the delay-spread (DS) in static or quasi-static environments. Especially the AoA has been of interest as the angular information is needed to facilitate beam forming, which is seen as one of the key enabling technologies for 5G [3,16]. The suggested use of high frequencies for 5G systems enables the

implementation of massive antenna arrays due to the small antenna elements. This allows for utilization of the spatial dimension via e.g., beamforming algorithms, which can improve the system performance in signal strength levels significantly and thereby data [17,18]. Therefore, a study of the AoAs in the given propagation environments is the focus of this paper.

Generally two different types of channel sounding systems are widely utilized in the literature, namely time-domain and frequency-domain sounders [19]. The time-domain sounders utilize a transmitted pseudo random binary sequence (PRBS) which is recovered by a correlative process. This requires dedicated equipment specially build for the purpose. The correlative channel sounders are capable of recovering an estimate of the channel impulse response (CIR) very fast and are therefore preferable for measurements of the dynamic propagation environment [20,21]. However, the complexity of generating and sampling the PRBS poses challenges if a large bandwidth is of interest [20]. Nevertheless, have bandwidths of up to 6 GHz been reported in [22,23]. The frequency-domain sounders sweep the chosen frequency band with a continuous wave (CW). Due to this frequency sweep sounders does not have the same constraints in the measurable bandwidth as for the correlative channel. The limiting factor then becomes the acceptable measurement time as the frequency sweep time has to be considered. For a static propagation environment, this is not a problem but if a dynamic environment is to be measured this has to be considered. A method to overcome this is to use very fast frequency sweeping systems known as frequency modulated continuous wave (FMCW) or chirp sounders. These have been reported in literature also with a bandwidth of up to 6 GHz for capable of measuring in a dynamic environment with speeds of up to 20 km/h [24,25]. However, again these system requires dedicated equipment which has to be modified for measurements in a given frequency range. It is costly and limited in availability to have dedicated equipment. Due to this, a more simple approach of utilizing a general purpose Vector Network Analyser (VNA) is often seen in literature [10,13,26]. A VNA based system sweeps the chosen frequency band while the channel frequency response is measured between two ports. The sweep time of the high precision CW generator used by the VNA is considerable higher than the one for the chirp sounders. Due to this VNA based sounding systems are often only used in static propagation environments.

This paper presents the work related to the development of a VNA based measurement system together with an investigation of the stability of this system. The capability of the developed system is further extended to allow for simultaneous recording of two channel frequency responses together with a reference frequency response from the transmitting test port of the VNA. The extended measurement system is utilized for a measurement campaign aiming at a comparative study between a channel sounding using a virtual uniform circular array (UCA) and a directive horn to record the power-angle-

delay profiles (PADP). Further, the system is used for a larger indoor measurement campaign intended for highlighting multipath component evolution over different spatial positions.

The paper is organized as follows. Section II describes the VNA-based channel sounding system and presents the capabilities and limitations of the system. Section III presents the extended measurement system used for the measurements presented in Section IV. Section V summarizes this work.

II Channel Sounding System

The VNA measurement system presented in this work is utilizing the *Agilent N5227A PNA*. To extend the physical range of the measurements, the VNA is used together with a distribution system, also from Agilent, including mixers and amplifiers. The basic principle of the distribution system is that via down-converting the cable loss of high-frequency signals can be reduced. The down-converting is obtained at the mixers by applying heterodyning. The cable-losses is the main limiting factor for the physical range of the measurement system. A block diagram of the system is depicted in Fig. B.1 and it contains the following blocks.

- Vector Network Analyser (VNA)
- Distribution unit for the local oscillator and intermediate frequency
- Reference mixer
- Test mixer
- Transmit (TX) and receive (RX) antennas

The distribution unit functions as an amplifier and splitter of the LO (Local Oscillator) from the VNA to the mixers. The LO signal path is marked in blue in Fig. B.1. The distribution unit also provides amplification of the IF (Intermediate Frequency) from the mixers. The IF signal path is marked in red in Fig. B.1. The test mixer multiplexes the IF signal on the LO connection allowing for only one cable being needed to connect test mixer to the distribution unit. The multiplexed LO/IF signal path is marked in orange in Fig. B.1. Due to the multiplexing the distribution unit also has to provide the demultiplexing of the IF from the test mixer before the VNA.

The system operates with two different types of mixers, namely the test and reference mixer. The purpose of both mixers is to down-convert the received high-frequency signal to IF, which for this system is 7.438 MHz. As stated the test mixer operates with only one cable and therefore includes a multiplexer besides the down-converter. The reference mixer uses separate

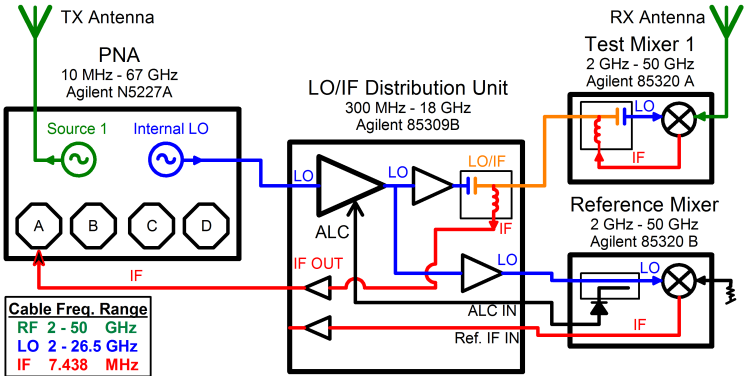

Fig. B.1: Block diagram of the measurement system using internal LO. Green is RF frequency, blue is LO frequency and red is IF frequency.

lines for the LO and IF and also provides feedback for the ALC (Automatic Level Control) in the distribution unit. Using the reference mixer enables the system to utilize leveled output power. A leveled output is a frequency independent output power as the frequency response of the amplifier together with the frequency dependent cable loss is corrected by adjusting the output power via the ALC. This is an important feature when large frequency ranges are measured.

Operating with internal VNA LO

The most straightforward way to utilize the LO is to use the internal LO from the VNA, as shown in Fig. B.1. However, as also discussed in [27], it became evident that the used VNA only utilizes the fundamental frequency up to 26.5 GHz before it switches to the 3rd harmonics of the frequency. The distribution unit only has a frequency range from 300 MHz to 18 GHz, resulting in a lack of amplification in the range of the LO from 18 to 26.5 GHz.

To study the consequences of the mismatch between the LO of the VNA and the distribution unit amplifiers, a measurement was conducted. A frequency sweep is conducted in the range from 2 GHz to 30 GHz (1001 points). The TX port is connected directly to the test mixer input and after the manufacturer specified warm-up period a normalization/calibration is performed. The VNA is set to continuous sweeping, while the drift from the normalization is recorded. In Fig. B.2 the resulting drift after 10 sweeps is presented. The power deviations up to 3 dB within 18 to 26.5 GHz is a result of the missing amplification capability of the distribution unit.

In Fig. B.2 power deviation up to 1 dB within 2 to 6 GHz is also seen. This is found to be a result of too high LO power at the test mixer. The

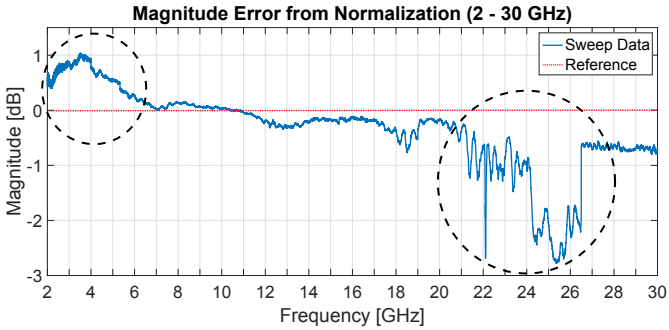

Fig. B.2: Deviation from the normalization/calibration curve for the frequency sweep from 2 to 30 GHz using the internal LO.

ALC is controlled by the reference mixer and is supposed to compensate for the frequency dependent loss of the cable connecting the mixers to the distribution unit. However, in the used setup two cables of different types and lengths are used to connect the distribution unit and the two mixers. As a result, the ALC did not function as intended. A solution is simply to use the same cabling to the reference and test mixers.

Operating with alternative LO

From the presented measurement in Fig. B.2 it is clear that an alternative source for the LO has to be used. The alternative source could be an external signal generator. However, the used VNA is already equipped with two source oscillators (signal generators). The benefit of using the internal source oscillators is that these can function in so-called phase lock which results in two synchronized frequency sweeps. It is possible to introduce a frequency offset between the two oscillators while maintaining phase lock as long as the two frequency ranges are of the same size. This enables the use of one oscillator (source 1) to generate the high-frequency signal for the TX antenna while the other oscillator (source 2) is used to generate the LO signal operating on a lower frequency harmonic. In Fig. B.3 it can be noted that the LO is now supplied to the distribution unit from source 2 in the PNA.

The same test measurement as for the setup using the internal LO has been performed. The difference is that now source 1 is set to sweep from 2 GHz to 30 GHz, while source 2 is operating on the 3rd harmonic. This means that source 2 is sweeping from 2/3 GHz to 10 GHz, which ensures that the system operates within the frequency limits of the amplifiers of the distribution unit. The resulting magnitude error is shown in Fig. B.4.

In Fig. B.4 a significant improvement in terms of power deviations is seen when compared to Fig. B.2. The only significant deviation is seen close to

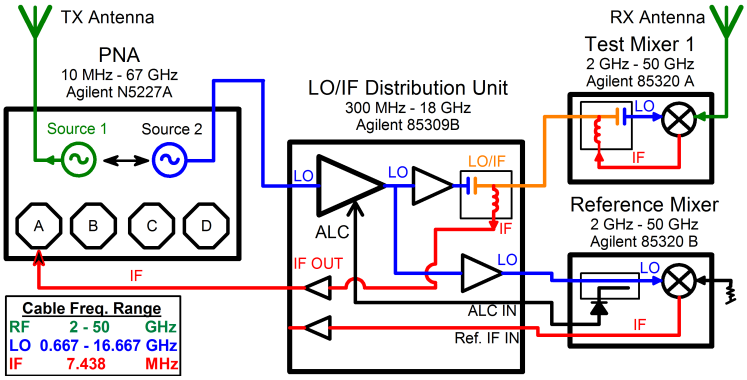

Fig. B.3: Block diagram of measurement system using source 2 to generate the LO. Green is RF frequency, blue is LO frequency and red is IF frequency.

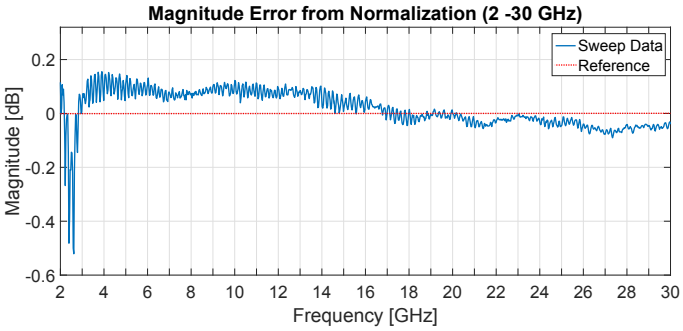

Fig. B.4: Deviation from the normalization/calibration curve for the frequency sweep from 2 to 30 GHz using the alternative LO.

2.5 GHz, which is due to the settling time of the ALC. This settling time introduces a variation of up to 0.5 dB at the low frequency. Aside from this, a variation of less than 0.1 dB is seen.

Another benefit of utilizing the 3rd harmonic is that the lowered frequency also reduces the cable losses, which can improve the operational range of the system. Lowering the frequency with higher harmonics would increase the operational range even farther. However, the use of harmonics decrease the sensitivity of the mixers and using higher harmonics will decrease the sensitivity level further.

The drift from the normalization over time is also investigated. The magnitude drift for 10 minutes, 1, 2, and 15 hours is shown in Fig. B.5.

From Fig. B.5 it is interesting to see that even though source 2 is used for the distribution unit and external mixing, it seems that the internal LO is still problematic in the range from 21 to 26.5 GHz. The magnitude error

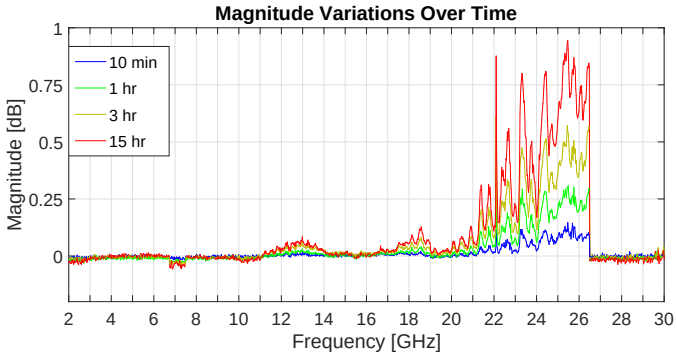

Fig. B.5: Deviation over time from the normalization/calibration curve for the frequency sweep from 2 to 30 GHz using the alternative LO.

is, however, less than 1 dB over 15 hours. If in some cases the measurement time is to exceed this long time period or the system is left for an extended period, it is clear that a new normalization/calibration has to be performed.

The phase stability of the measurement system is also investigated. The resulting plot for the unwrapped phase drift for 10 minutes, 1, 2, and 15 hours is presented in Fig. B.6.

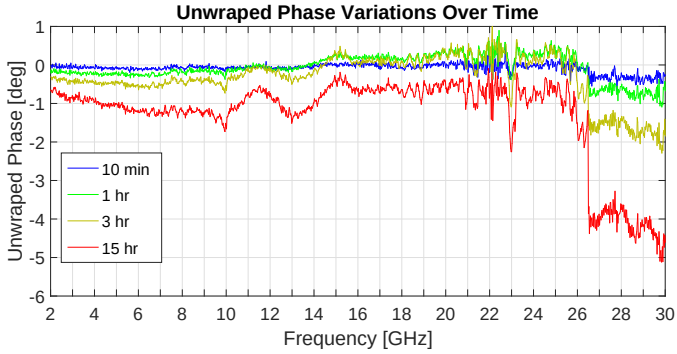

Fig. B.6: Deviation from the normalization/calibration curve for the frequency sweep from 2 to 30 GHz using the alternative LO.

The unwrapped phase plotted in Fig. B.6 also only shows small deviation over the extended period. For the part of the frequency sweep where the internal LO is running on the fundamental frequency the deviation less than 1^o. At the shift point for the internal LO harmonic shift point, a jump in the phase is seen. At the 15 hours sweep the jump is roughly 4^o but it seems the phase stabilizes again after the jump. As for the variation in magnitude, the phase variations is also tolerable.

The presented measurement of phase variations was conducted without moving the connected cables. Phase change due to cable movement while conducting high-frequency measurements is a known problem especially at higher frequencies. This is also a reason for down-converting the LO signal as this would make the system less sensitive to movement of the cables. However, using higher harmonics would, as mentioned, decrease the sensitivity level of the mixers which is also an unwanted effect. Therefore, to decrees the impact of the phase changes introduced by the cables much care have to be given to minimize movement of the cable while measurements are conducted.

System link budget

The system link budget is important to ensure the RF power requirements of the used equipment. This link budget is not to be confused with the in-the-air propagation loss, as it only factors the RF chain losses. The physical range of a VNA measurement system is mainly limited by the power requirements to the distributed LO. Therefore the focus of this system link budget is the LO power loses tolerable to obtain the maximum physical measurement range.

The used test mixers have a frequency range from 2 to 50 GHz and the lowest detectable RF input at the test mixers is given by their sensitivity level. The power requirement for the test mixers LO input is between +12 and +17 dBm. If this power requirement is met, the sensitivity level, when operating the test mixers with 3rd harmonic, is -118 dBm for 2 GHz to 18 GHz, -103 dBm for 18 GHz to 40 GHz and -100 dBm for 40 GHz to 50 GHz, respectively. The aim is then to ensure the correct power level of the LO input to the test mixer. When making the link budget the most critical case, at the highest frequency, has to be used for the loss calculations. As an example, the calculations for 30 GHz is presented here. The 3rd harmonic of 30 GHz is simply 10 GHz and according to the specifications, the maximum LO output power from the distribution unit is +23.5 dBm in the frequency range from 6.2 to 18 GHz. This is on the condition that the distribution unit is given an LO input signal of +6 dBm from the VNA. This leaves $23.5 - 12 = 11.5$ dB for cable loss between distribution unit and mixer as illustrated in Fig. B.7.

The maximum output from the VNA is +19 dBm at 10 GHz from port 3 which is used for source 2. The distribution unit required a minimum LO input of +6 dBm giving a maximum acceptable loss of 13 dB. The used LO cable (UTiFLEX UFB293C) has a loss of 0.59 dB/m at 10 GHz. This means that $13/0.59 = 22$ meters of cable can be used from VNA to distribution unit and $11.5/0.59 = 19.5$ meters of cable can be used from the distribution unit to the test mixer. In total, this gives an operational range of 41,5 meters when measuring at maximum 30 GHz. Lower measurement frequencies would result in a longer range and an optional LO amplifier would extend the range even

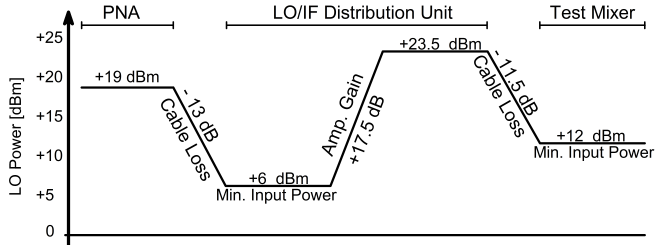

Fig. B.7: Link-budget for the LO power distribution.

farther. Alternatively an optical solution could be used for the distribution of the LO. This would allow for very long ranges due to the low loss introduced by fiber-optic cables. However, the cost of these systems is significant.

III Used measurement system

The measurement system capabilities can be further extended to simultaneously record two complex channel frequency responses. The fundamental principle is though unchanged from the system presented in the previous section.

VNA based sounding system

A block diagram of the system is seen in Fig. B.8, where the system is operating with two test mixers allowing for recording two individual complex channel frequency responses.

Besides the two test mixers, the reference mixer is also used in this setup. This means that three frequency responses are recorded by the VNA on port A, B and C. The recorded frequency response from the reference mixer is used to decrease the impact of the unwanted frequency response of the measurement system. The reference frequency response is recorded just before the port of the transmitting antenna by using an RF coupler (Agilent 87301E). The signal from source 1 until the antenna port of the transmitting antenna can be written as:

$$Y_{TX}(f) = X(f)\, G(f) \tag{B.1}$$

where $X(f)$ is the signal from source 1 and $G(f)$ is the unwanted frequency response of the measurement system.

Then the received signal from test mixer 1 is recorded at port A and can be written as:

$$A(f) = X(f)\, G(f)\, H(f)\, G_{test}(f) \tag{B.2}$$

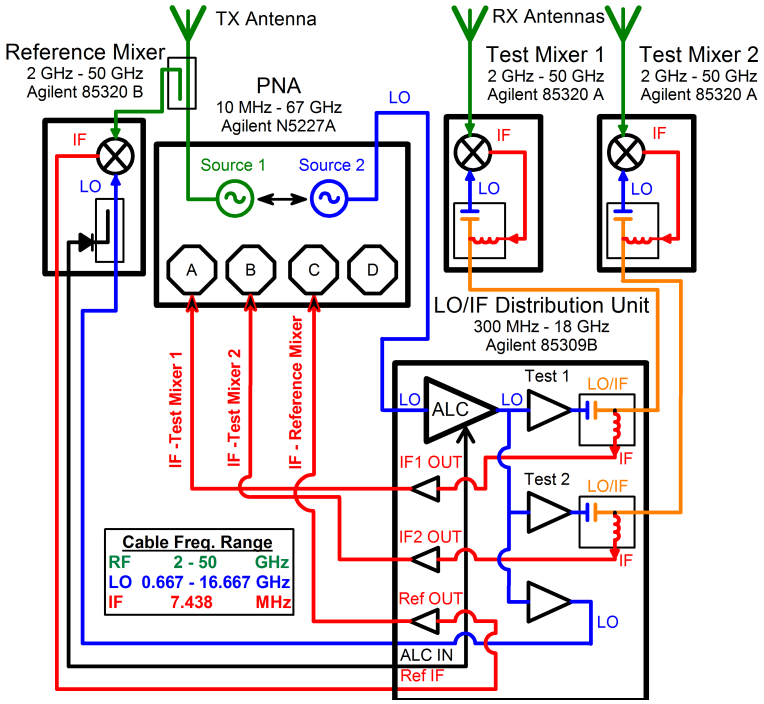

Fig. B.8: Block diagram of the used sounding system. Green is RF frequency, blue is LO frequency and red is IF frequency.

where $H(f)$ is the channel frequency response which we would like to measure and $G_{test}(f)$ is the unwanted frequency response of the test mixers RF chain.

In a similar way, the received signal from the reference mixer is recorded at port C and can be written as:

$$C(f) = X(f)\, G(f)\, G_{ref}(f) \tag{B.3}$$

where $G_{ref}(f)$ is the unwanted frequency response of the reference mixers RF chain.

Now by assuming that the frequency response of the test mixer RF chain is approximately the same as the one for the reference mixer the channel response can be found as:

$$H(f) = \frac{A(f)}{C(f)} \tag{B.4}$$

The assumption of the frequency response of the test mixer RF chain is approximately the same is justified via use of identical cabling and the fact that the system is normalized/calibrated from transmit antenna port to re-

ceiver antenna port before the measurement. The frequency response for test mixer 2 can be found in the same way as for test mixer 1.

For the used setup a horn antenna (Pasternack - PE9851/2F-10) is used at the transmit side (TX). The receive side (RX) is utilizing the possibility of recording two frequency responses by having both a horn (Flann - 22240-20) and a bi-conical antenna (AINFO - SZ-2003000/P). The reason for having a horn antenna and a bi-conical antenna as RX is to enable the use of both directional horn and virtual UCA for capturing the power-angle-delay profiles. Both the TX and RX antennas are connected via cables. The specifications of the used antennas are given together with the settings for the VNA in Table E.2.

Table B.1: Measurement System Setup

Parameter	Setting
Center Frequency	28 GHz
Bandwidth	4 GHz
Frequency Points	1500
TX power	15 dBm
TX antenna Azimuth HPBW	54°
TX antenna Elevation HPBW	53°
TX antenna gain	10 dBi
RX horn antenna Azimuth HPBW	22°
RX horn antenna Elevation HPBW	21°
RX horn antenna gain	18 dBi
RX bi-conical antenna gain	6 dBi

In Table E.2 the transmit power is also given together with the antenna gains. Using this information an estimate of the RF range of the measurement system can be given. This range is given by the maximum allowed path loss defined as the loss of the transmitted power until the given sensitivity of the receiver. For the used measurement system, the maximum leveled output power from source 1 when sweeping from 26 to 30 GHz is 15 dBm and the sensitivity of the test mixer is -103 dBm. Together this leaves a maximum tolerable path loss of 118 dB. This can however be extended by applying high gain antennas.

The aim is to ensure a good dynamic range of the system and thereby high-quality measurements performed with it. The maximum range of the measurement system operating at 30 GHz was 41,5 meters. By using Friis free space propagation loss for LOS scenario and assuming a 10 dBi TX antenna gain together with a 6 dBi RX antenna gain, the received power can be calculated to -63.35 dB. This leaves a dynamic range from received power to the sensitivity level of 39.65 dB. The propagation loss is however highly dependent on the measurement scenario, e.g. Line-Of-Sight (LOS) or Non-LOS

(NLOS). That is, the dynamic range in practice will be smaller.

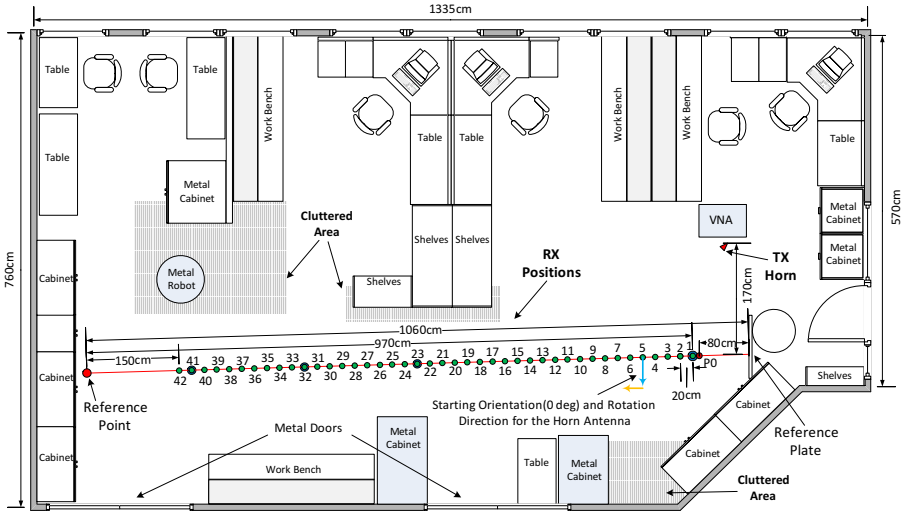

Fig. B.9: Floor plan of the measurement scenario.

Measurement Scenario

The measurement system was used an indoor scenario. The location is a laboratory located on the second floor on a contemporary building. A floor plan is shown in B.9 and a picture of the laboratory is shown in Fig. B.10.

In Fig. B.9 the TX and RX positions are marked in relation to the surroundings. The aim of the selected measurement locations together with the positioning of TX and RX is to be able to capture the change in PADP when the RX is moved farther away from the TX and from the LOS to the NLOS scenarios. For all the conducted measurements the TX antenna was oriented towards position RX-8 with a height of 100 cm. As seen in Fig. B.9, a total of 42 RX positions (green) distributed with a 20 cm distance along a reference line (red) have been used. The RX positions are located such that the points starts in the LOS scenario and moves farther and farther in the NLOS scenario. To conduct the measurements at each RX position using both the horn and bi-conical antenna, a RX setup with a turntable as shown in Fig. B.11 has been used.

As illustrated in Fig. B.11, the horn antenna was placed in a height of 90 cm, with its main beam in the azimuth plane. The starting orientation (cyan) of the horn antenna at all the RX positions was orthogonal to the reference line as indicated at RX-5, in Fig. B.9. The measurement at each RX position was conducted by rotating the horn antenna clockwise (orange) in

Fig. B.10: View of the laboratory where the measurement was conducted

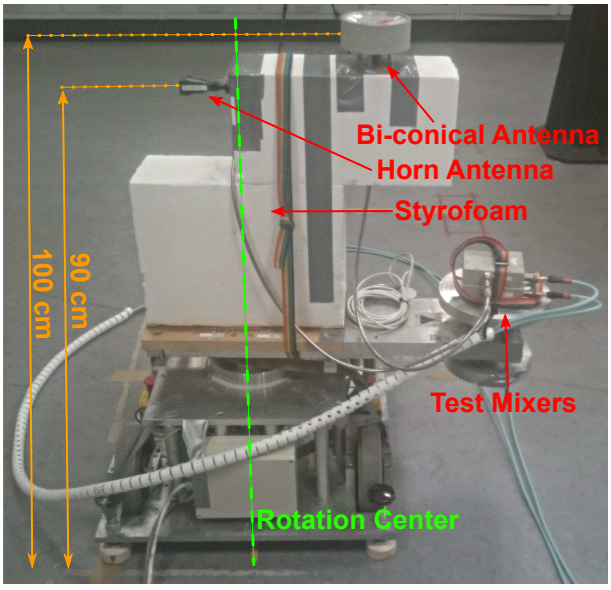

Fig. B.11: Illustration of the receiver setup with turntable together with both horn and bi-conical antenna.

the azimuth plane in steps of 1° using the turntable. For each rotation step, a complex frequency response is recorded simultaneously for both horn and bi-conical antenna.

In Fig. B.11 it can be seen that the bi-conical antenna is offset from the

rotation center and placed above the horn antenna at a height of 100 cm, which is the same height as the TX antenna. The offset from the rotation center results in the bi-conical antenna forming a circle in the azimuth plane when the turntable is rotating as illustrated in Fig. B.12.

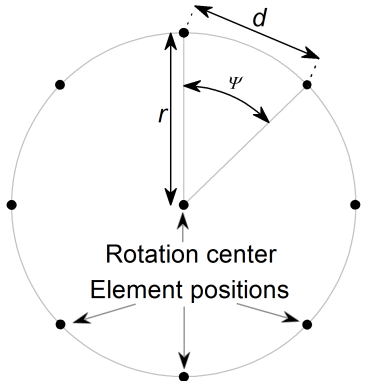

Fig. B.12: Dimensions of the Uniform Circular Array (UCA).

The bi-conical antenna is moved around along the circle while a complex frequency response is recorded for each 1° (Ψ). This results in the possibility of forming a virtual UCA with 360 elements (N). To determine the needed offset from the rotation center (r) each element can be seen as a spatial sample of the channel. To avoid aliasing the distance (d) between these samples should be less than $\lambda/2$. The distance between points on the circle can be approximated by:

$$d \approx \frac{2\pi r}{N} \tag{B.5}$$

giving that:

$$\frac{2\pi r}{N} < \frac{\lambda}{2} \Rightarrow \; r < \frac{\lambda N}{4\pi} \;\; | \; N > 0 \wedge \lambda \in \mathbb{R} \tag{B.6}$$

From this, it can be seen that a solution is to minimize r. However, the obtainable angular resolution from the measurement conducted with the UCA increases with the aperture of the UCA, giving that r is wanted as large as possible. Due to this r has been chosen to be 25 cm, which give $d \approx 0.004$, with $\lambda/2 = 0.005$ at 30 GHz.

Each of the 42 complete 360° scans with steps of 1° in the azimuth plane while collecting the complex frequency response from both both horn and bi-conical antenna took roughly 6 minutes. During the time of each scan the scenario was completely static. The measurement of all the 42 RX positions was conducted during one night ensuring nothing was changed in the almost 6 hours the measurement took.

IV Measurement Results

In this section, the results from the measurement campaign are presented. First, we briefly explain the measured data for a representative LOS position and a NLOS position respectively. After that, we intend to investigate the channel dynamics over the measurement positions and frequency dependency of the channel characteristics.

Measured data in a LOS and in a NLOS scenario

To obtain the channel impulse repose (CIR), an inverse Fourier transformation (IFT) of the complex channel frequency response can be performed for each rotation step. A Hamming window has been applied to the data to suppress sidelobe levels. The resulting CIR for each rotation step can together with the orientation of the horn antenna be used to construct the power-angle-delay profile (PADP) for the azimuth plane, as seen in Fig. B.13. The CIR from 360 positions of the bi-conical antenna can also be plotted in a similar way as seen in Fig. B.14. It should be noted that the frequency response of the used antennas has not been removed from the recorded frequency sweeps and thus are embedded in the presented results.

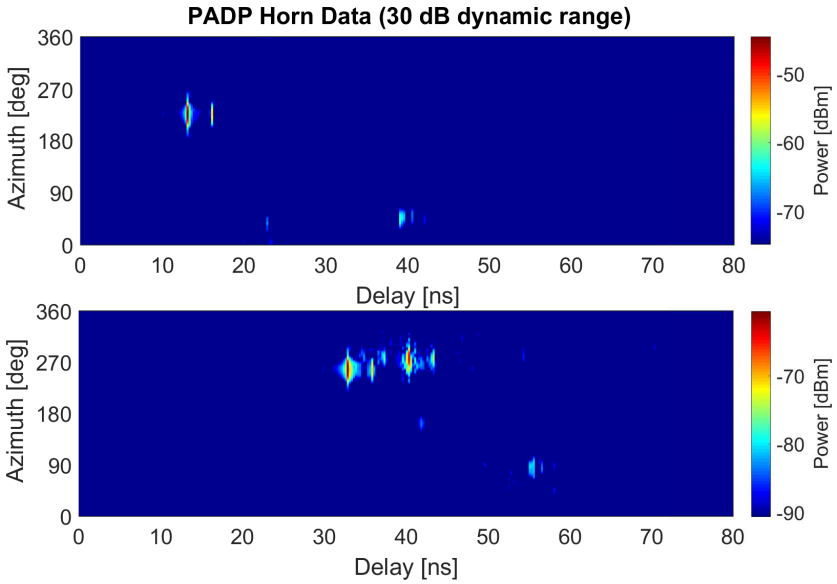

Fig. B.13: Power-angle-delay profile using the horn antenna data. Position 8 is shown in the top and position 40 is shown in the bottom. Both locations have been plotted with 30 dB dynamic range.

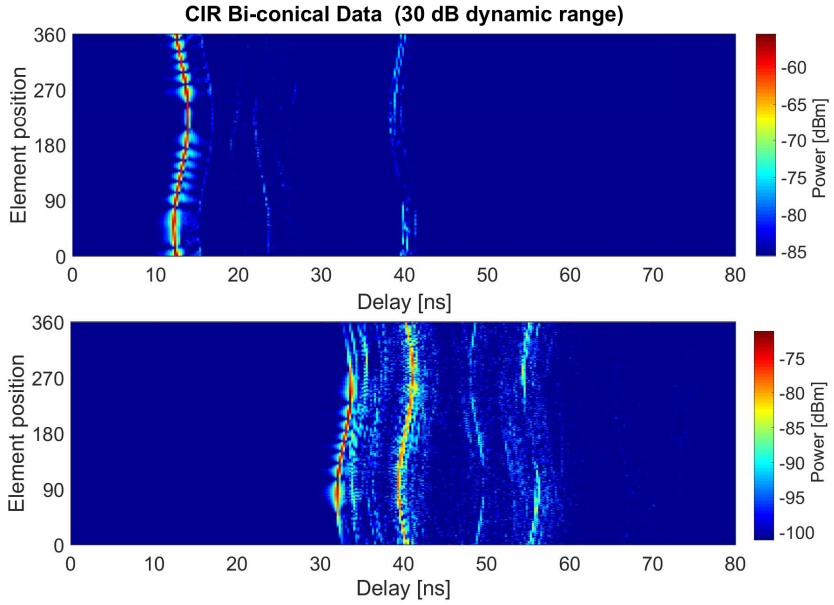

Fig. B.14: Channel impulse response for the 360 positions of the bi-conical antenna data. Position 8 is shown in the top and position 40 is shown in the bottom. Both locations have been plotted with 30 dB dynamic range.

In Fig. B.13 and Fig. B.14, position 8 and 40, shown in Fig. B.9, have been used to illustrate a LOS and a NLOS case of the measurement scenario, respectively. The measured PADP is sparse and specular, with few paths detected both in LOS and NLOS scenarios. The CIR from the bi-conical antenna seen in Fig. B.14 can not directly be related in angular domain. The delay domain can, however, be compared to the components given by the horn data. In the LOS case, shown in the top of Fig. B.14, the strongest component is located at roughly around 13 ns in delay which correspond to the horn data. The components in the NLOS case, shown in the bottom of Fig. B.14, also correspond to the components seen from the horn data.

To be able to compare the data from the bi-conical antenna in the angular domain a UCA is formed. Then the PADP can be found by applying the maximum likelihood estimator with successive interference cancellation (MLE-SIC) with a wideband and spherical-wave signal model as described in [28]. The reason for applying a spherical-wave signal model to the MLE-SIC estimation is due to the size of the used UCA. The aperture of the UCA is 50 cm resulting in the far field assumption not being valid due to the vicinity of interacting object in the chosen scenario. In addition, the used ML-based estimator has the advantages of higher estimation resolution and less sidelobes interfering in the resultant PADP compared to spectrum-based esti-

mators like delay-and-sum beamforming [13]. The resulting azimuth PADPs are presented in Fig. B.15 for position 8 and in Fig. B.16 for position 40, respectively.

The measured PADPs with the virtual UCA match well with the ones with the horn antenna, where detected multipath components with same angle and delay values are shown. Note that the power levels are different due to the difference in antenna gain of 12 dB between the horn and bi-conical antenna. The measured PADPs with the virtual UCA are used for later analysis since much higher angle resolution can be achieved for the virtual UCA with the maximum likelihood estimator.

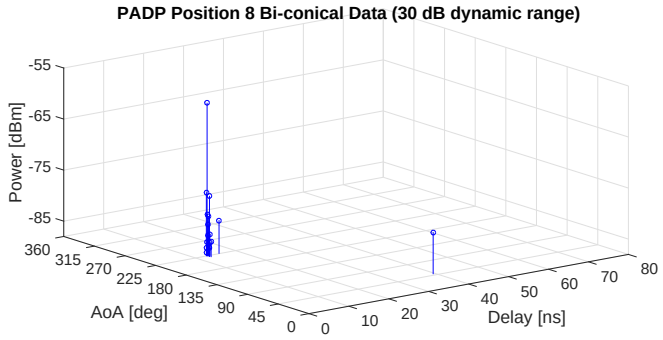

Fig. B.15: Power-angle-delay profile using the bi-conical antenna data for position 8 with 30 dB dynamic range.

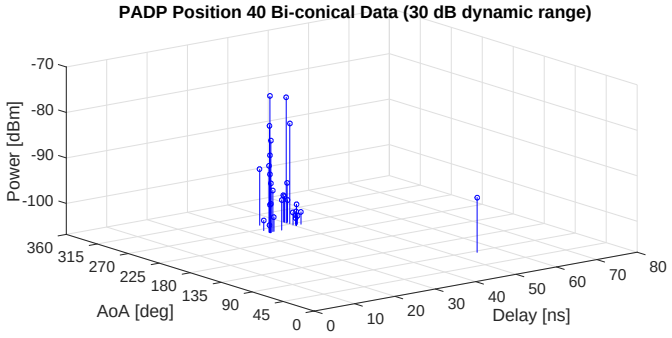

Fig. B.16: Power-angle-delay profile using the bi-conical antenna data for position 40 with 30 dB dynamic range.

The path trajectory can be constructed based on the measured PADPs in the LOS and NLOS scenarios, as shown in Fig. B.17 and Fig. B.18 for measurement position 8 and 40, respectively.

In the LOS case, shown in the top of Fig. B.13, the strongest component is

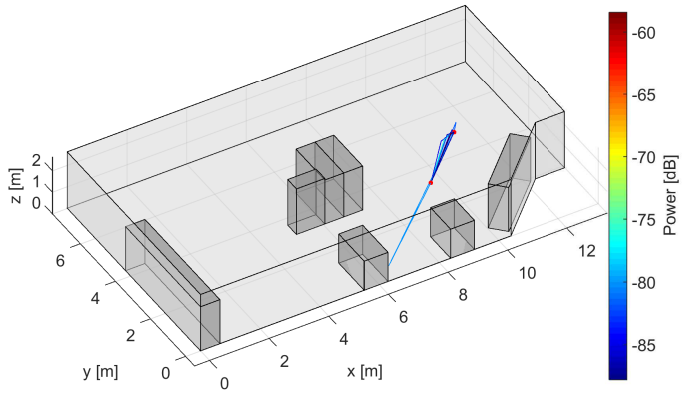

Fig. B.17: Measurement based ray-Tracing for position 8 with 30 dB dynamic range. Red dot is RX and TX.

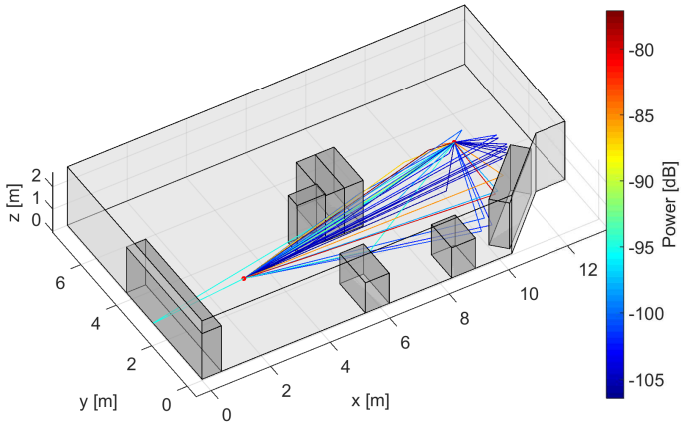

Fig. B.18: Measurement based ray-Tracing for position 40 with 30 dB dynamic range. Red dot is RX and TX.

located at roughly 230° and 13 ns in delay. This corresponds to the direct LOS path between the TX and the RX. A secondary component is seen at 50° and 40 ns in delay which corresponds to a backscatter from the metal door behind the RX as seen from the TX. In the NLOS case, the strongest component is located at 270° and 33 ns in delay which could correspond to a diffraction around the corner of the obstructing shelve seen in Fig. B.9. Both position 8 in Fig. B.17 and position 40 in Fig. B.18 show the backscatter with significant longer delay as also seen in the horn data. As shown in Fig. B.17 and Fig. B.18, the path trajectories for the LOS and NLOS scenario differ significantly. This spatial dynamics of the channel is investigated further in the following section.

Given the fact that the two measured PADP present consistent results, it can be concluded that the channel sounding system is indeed capable of capturing two responses at the same time.

Spatial Dynamics

It is important to understand how the channel profiles vary over different measurement locations. One of the practical design challenges in beamforming schemes is how often the beamforming should be updated to identify the dominant paths in the channel. With a highly dynamic channel over spatial locations, a more frequent update is needed, which would increase system cost. To investigate the spatial dynamics of the measurements, all PADP have been calculated for all the 42 measurement positions using the MLE-SIC algorithm. The delay and angular domain results are plotted in two different plots for illustration purpose. The delay characteristics are presented in Fig. B.19 and the angular characteristics in Fig. B.20. From Fig. B.19 and Fig. B.20, it can be seen that the channels are sparse for most measurement points. In the LOS region (i.e. measurement positions from 1 to 11), LOS path is dominant. In the NLOS region, most paths are concentrated in an angle region.

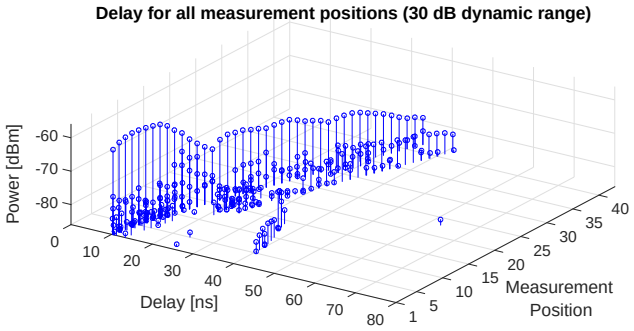

Fig. B.19: Delay domain characteristics plotted for all measurement positions with 30 dB dynamic range.

The second order characteristics have also been calculated for all the measurement positions. The resulting delay and angular spread are shown in Fig. B.21. In Fig. B.21, it is clear that the region from measurement position 1 until 11 is dominated by a LOS component, which results in a low delay and angle spread. From measurement position 12 until 26 a transition zone is seen. Components from the surroundings have a larger impact, resulting in a larger spread. After measurement position 26 the spread decreases again as the surroundings might have a guiding effect towards the RX.

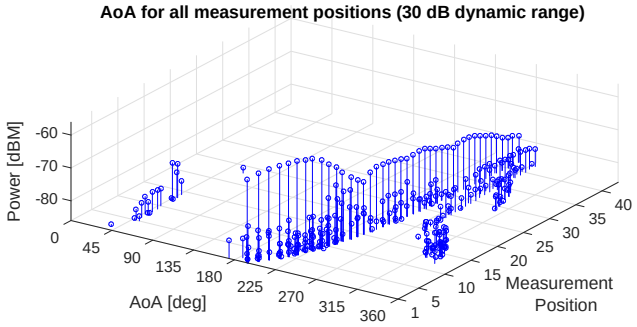

Fig. B.20: Angular domain characteristics plotted for all measurement positions with 30 dB dynamic range.

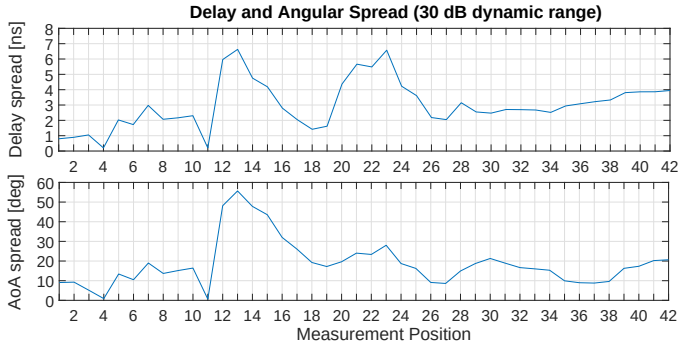

Fig. B.21: Comparison of delay and angular spread for all measurement positions with 30 dB dynamic range.

V Conclusion

This work presents the improvement of an existing VNA based measurement system operating in the frequency range from 2 to 50 GHz. A solution to address system instability at 2 to 4 GHz and 21 to 26.5 GHz is described. The measurement system is further extended to be capable of recording two independent channel frequency responses together with a reference frequency response. The proposed system is validated in the range from 2 to 30 GHz with a power drift of less than 0.5 dB in the whole span. The phase drift in the same span is less than 1° over a measurement period of 1 hour.

The proposed measurement system have been utilized for a measurement in the frequency range from 26 to 30 GHz. The measurements were conducted in both LOS and NLOS using 42 measurement positions distributed along a line through an indoor laboratory environment. Two channel frequency responses were recorded simultaneously using a directional horn an-

tenna and a virtual uniform circular array. The recorded data is used to construct power-angular-delay profiles (PADP) and a comparison between the two showed good agreement. The PADP showed a sparse propagation environment when the dynamic range of the measurement was constrained to a 30 dB range. Plotting the recorded PADPs evolution over the 42 measurements positions showed it was possible to track dominant paths.

Acknowledgment

The authors would like to thank the lab staff for valuable assistance with measurements.

References

[1] P. Demestichas, A. Georgakopoulos, D. Karvounas, K. Tsagkaris, V. Stavroulaki, J. Lu, C. Xiong, and J. Yao, "5g on the horizon: Key challenges for the radio-access network," *Vehicular Technology Magazine, IEEE*, vol. 8, no. 3, pp. 47–53, Sept 2013.

[2] Q. Li, H. Niu, A. Papathanassiou, and G. Wu, "5g network capacity: Key elements and technologies," *Vehicular Technology Magazine, IEEE*, vol. 9, no. 1, pp. 71–78, March 2014.

[3] L. Wei, R. Q. Hu, Y. Qian, and G. Wu, "Key elements to enable millimeter wave communications for 5g wireless systems," *IEEE Wireless Communications*, vol. 21, no. 6, pp. 136–143, December 2014.

[4] Ofcom, "Spectrum above 6 ghz for future mobile communications," Ofcom UK, Riverside House, 2a Southwark Bridge Road, London, Consultation Report, January 2015.

[5] S. Methley, W. Webb, S. Walker, and J. Parker, "Study on the suitability of potential candidate frequency bands above 6ghz for future 5g mobile broadband systems," Quotient Associates Limited, Compass House, Vision Park, Chivers Way Histon, Cambridge, CB24 9AD, UK, Technical Report, March 2015.

[6] ITU, *Attenuation by atmospheric gasess*, ITU-R P.676-10, Sep. 2013.

[7] T. Rappaport, S. Sun, R. Mayzus, H. Zhao, Y. Azar, K. Wang, G. Wong, J. Schulz, M. Samimi, and F. Gutierrez, "Millimeter wave mobile communications for 5g cellular: It will work!" *Access, IEEE*, vol. 1, pp. 335–349, 2013.

[8] T. Rappaport, F. Gutierrez, E. Ben-Dor, J. Murdock, Y. Qiao, and J. Tamir, "Broadband millimeter-wave propagation measurements and models using adaptive-beam antennas for outdoor urban cellular communications," *Antennas and Propagation, IEEE Transactions on*, vol. 61, no. 4, pp. 1850–1859, April 2013.

[9] A. Sulyman, A. Nassar, M. Samimi, G. Maccartney, T. Rappaport, and A. Alsanie, "Radio propagation path loss models for 5g cellular networks in the 28 ghz and

38 ghz millimeter-wave bands," *Communications Magazine, IEEE*, vol. 52, no. 9, pp. 78–86, September 2014.

[10] R. J. C. Bultitude, R. F. Hahn, and R. J. Davies, "Propagation considerations for the design of an indoor broad-band communications system at ehf," *IEEE Transactions on Vehicular Technology*, vol. 47, no. 1, pp. 235–245, Feb 1998.

[11] G. A. Kalivas, M. El-Tanany, and S. Mahmoud, "Millimeter-wave channel measurements with space diversity for indoor wireless communications," *IEEE Transactions on Vehicular Technology*, vol. 44, no. 3, pp. 494–505, Aug 1995.

[12] H. Xu, T. S. Rappaport, R. J. Boyle, and J. H. Schaffner, "Measurements and models for 38-ghz point-to-multipoint radiowave propagation," *IEEE Journal on Selected Areas in Communications*, vol. 18, no. 3, pp. 310–321, March 2000.

[13] W. Fan, I. C. Llorente, J. Nielsen, K. Olesen, and G. F. Pedersen, "Measured wideband characteristics of indoor channels at centimetric and millimetric bands," *EURASIP Journal on Wireless Communications and Networking*, vol. 2016, no. 1 - Special issue on Radio Channel models for higher frequency bands, pp. 1–13, 2016.

[14] J. Nielsen and G. F. Pedersen, "Dual-polarized indoor propagation at 26 ghz," in *2016 IEEE 27th Annual International Symposium on Personal, Indoor, and Mobile Radio Communication (PIMRC)*, September 2016.

[15] G. R. Maccartney, T. S. Rappaport, S. Sun, and S. Deng, "Indoor office wideband millimeter-wave propagation measurements and channel models at 28 and 73 ghz for ultra-dense 5g wireless networks," *IEEE Access*, vol. 3, pp. 2388–2424, 2015.

[16] Y. Kim, H. Y. Lee, P. Hwang, R. K. Patro, J. Lee, W. Roh, and K. Cheun, "Feasibility of mobile cellular communications at millimeter wave frequency," *IEEE Journal of Selected Topics in Signal Processing*, vol. PP, no. 99, pp. 1–1, 2016.

[17] W. Roh, J.-Y. Seol, J. Park, B. Lee, J. Lee, Y. Kim, J. Cho, K. Cheun, and F. Aryanfar, "Millimeter-wave beamforming as an enabling technology for 5g cellular communications: theoretical feasibility and prototype results," *Communications Magazine, IEEE*, vol. 52, no. 2, pp. 106–113, February 2014.

[18] S. Han, C. l. I, Z. Xu, and C. Rowell, "Large-scale antenna systems with hybrid analog and digital beamforming for millimeter wave 5g," *IEEE Communications Magazine*, vol. 53, no. 1, pp. 186–194, January 2015.

[19] A. F. Molisch, *Wireless communications*. IEEE Press, 2005, iSBN: 978-0-470-84888-3.

[20] ——, "Ultrawideband propagation channels-theory, measurement, and modeling," *IEEE Transactions on Vehicular Technology*, vol. 54, no. 5, pp. 1528–1545, Sept 2005.

[21] J. O. Nielsen, J. B. Andersen, P. C. F. Eggers, G. F. Pedersen, K. Olesen, and H. Suda, "Measurements of indoor 16 times;32 wideband mimo channels at 5.8 ghz," in *Eighth IEEE International Symposium on Spread Spectrum Techniques and Applications*, Aug 2004, pp. 864–868.

[22] T. S. Rappaport, G. R. MacCartney, M. K. Samimi, and S. Sun, "Wideband millimeter-wave propagation measurements and channel models for future wireless communication system design," *IEEE Transactions on Communications*, vol. 63, no. 9, pp. 3029–3056, Sept 2015.

[23] X. Chen, S. Liu, J. Lu, P. Fan, and K. B. Letaief, "Smart channel sounder for 5g iot: From wireless big data to active communication," *IEEE Access*, vol. 4, pp. 8888–8899, 2016.

[24] S. Salous, S. M. Feeney, X. Raimundo, and A. A. Cheema, "Wideband mimo channel sounder for radio measurements in the 60 ghz band," *IEEE Transactions on Wireless Communications*, vol. 15, no. 4, pp. 2825–2832, April 2016.

[25] X. Raimundo, S. Salous, and A. A. Cheema, "Indoor radio propagation measurements in the v-band," in *Radio Propagation and Technologies for 5G (2016)*, Oct 2016, pp. 1–5.

[26] W. Fan, I. C. Llorente, and G. F. Pedersen, "Comparative study of centimetric and millimetric propagation channels in indoor environments," in *2016 10th European Conference on Antennas and Propagation (EuCAP 2016)*, April 2016.

[27] J. Hejselbaek, W. Fan, and G. F. Pedersen, "Ultrawideband vna based channel sounding system for centimetre and millimetre wave bands," in *2016 IEEE 27th Annual International Symposium on Personal, Indoor, and Mobile Radio Communications (PIMRC)*, Sept 2016, pp. 1–6.

[28] Y. Ji, W. Fan, and G. F. Pedersen, "Channel characterization for wideband large-scale antenna systems based on a low-complexity maximum likelihood estimator," *IEEE Transactions on Wireless Communications*, pp. 1–1, 2018.

Paper C

Validation of Emulated Omnidirectional Antenna Output Using Directive Antenna Data

Johannes Hejselbæk, Anders Karstensen, Jesper Ødum Nielsen,
Wei Fan and Gert Frølund Pedersen

The paper has been published at the
2017 11th European Conference on Antennas and Propagation - EuCAP 2017.

Abstract

In this paper, we present validation of a method for constructing a virtual omnidirectional antenna in the azimuth plane. The virtual omnidirectional antenna utilizes a combination of data from directive horn antennas. The aim is to utilize the high gain of the horn antenna to improve the dynamic range of channel sounding measurements conducted in the centimeter and millimeter wave bands. The resulting complex impulse response from the virtual omnidirectional antenna is used to find the power-delay-profile (PDP). This is then compared to measurements conducted at the same time using a real omnidirectional antenna. The validation shows that the synthesized omnidirectional is capable of predicting main components and the slope of the PDP. Further, it is shown that by choosing angular sampling steps corresponding to the half power beam width (HPBW) of the used antenna similar power levels can be achieved.

I Introduction

Lately, there has been a great interest in channel measurements of the centimeter and millimeter wave bands [1–3]. This is a part of the process of moving towards fifth-generation cellular networks (5G) [4]. To develop statistical channel models for 5G, measurements in different scenarios have to be conducted. The proposed use of centimeter and millimeter wave bands introduces high path-losses. To overcome this, high-gain antennas are often used in measurements. The high-gain antennas are highly directive and often of the horn type. To express power at a given point for use in omnidirectional path-loss models, this directivity of the used antenna is unwanted. Due to this, synthesizing techniques have been applied to create virtual omnidirectional antennas [5–9]. The approach of synthesizing with directional elements is not new, as shown by [10,11]. However, the recent measurement endeavors have rekindled interest.

This paper presents a validation of a method for creating a virtual omnidirectional antenna in the azimuth plane. The virtual omnidirectional antenna is synthesized using data from a directive horn. The performance of the synthesizing is then compared with measurements of the power-delay-profile (PDP) conducted at the same time with a real omnidirectional antenna. Further, it is investigated what impact the choice of angular sample density has on the synthesized PDP.

The paper is organized as follows. Section II describes the measurement setup used for the validation. Section III elaborates the synthesizing technique. Section IV presents the recorded channel impulse responses and the comparison between synthesized and real omnidirectional measurements. Section V summarizes this work.

II Validation Measurement

The measurement used for this validation was conducted as a part of measurement campaign in a laboratory environment. The measurement surroundings are shown in Fig. C.1.

Fig. C.1: View of the laboratory where the measurement was conducted.

A VNA based measurement system as described in [12] has been used for the measurement campaign. The transmit side (TX) is a horn antenna (Pasternack - PE9851/2F-10). The receive side (RX) is using both a horn (Flann - 22240-20) and a bi-conical antenna (AINFO - SZ-2003000/P). The VNA system is capable of recording both complex frequency responses from the two RX antennas using two test mixers.

The specific parameters of the system are presented in TABLE E.2.

Table C.1: Measurement System Details

Parameter	Setting
Center Frequency	28 GHz
Bandwidth	4 GHz
Frequency Points	1500
TX power	15 dBm
TX antenna Azimuth HPBW	54°
TX antenna Elevation HPBW	53°
TX antenna gain	10 dBi
RX horn antenna Azimuth HPBW	22°
RX horn antenna Elevation HPBW	21°
RX horn antenna gain	18 dBi
RX bi-conical antenna gain	6 dBi

In Fig. C.2, the position of the transmitter (TX) and receiver (RX) is marked in relation to the surroundings. There are two RX positions, RX-1 in clear line-of-sight (LOS) and RX-2 in non-line-of-sight (NLOS).

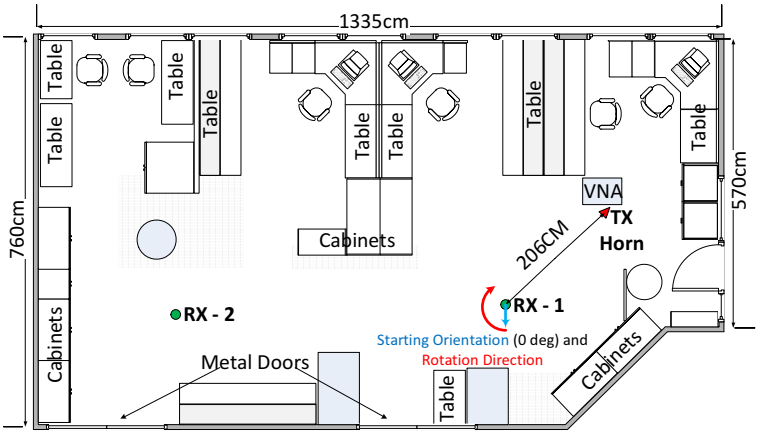

Fig. C.2: Positioning of transmitter and turntable with receiving horn and bi-conical antenna.

The TX antenna was oriented towards position RX-1 in a height of 100 cm. The bi-conical antenna was placed at the same height as the TX antenna in the rotation center of the turntable. The horn antenna was placed below the bi-conical antenna, orthogonal to the rotation axis, in a height of 90 cm. The starting orientation of the horn antenna point to the south as marked in Fig. C.2. The horn antenna is rotated clockwise in steps of 1°. A Complex Impulse Response (CIR) is recorded for both horn and bi-conical antenna for each rotation step. One complete scan of the azimuth plane took roughly 6 minutes in which the scenario where completely static.

III Synthesizing method

The common model for the CIR in the stationary case is expressed as (C.1) which follows [13]. The simplified model, in (C.1), can be expanded to include the impact of the antennas orientation as shown in (C.2).

$$h(\tau) = \sum_{k=1}^{K} a_k \, \delta\left(\tau - \tau_k\right) \, e^{j\varphi_k} \tag{C.1}$$

$$h(\tau, \phi) = \sum_{k=1}^{K} a_k \, \delta\left(\phi - \phi_k\right) \delta\left(\tau - \tau_k\right) \, e^{j\varphi_k} \tag{C.2}$$

where K is the total number of resolvable multipath components (MPC). a_k, τ_k, ϕ_k and φ_k are respectively the amplitude, arrival time, direction and phase

for the kth component.

In practice the measurement system does not have infinite bandwidth and the used antenna will have a given beamwidth. Therefore, instead of $\delta(\cdot)$, the following will use $p(\tau)$ to describe the pulse shape and $A(\phi)$ will describe the antennas radiation pattern. The resulting expression follows the one presented in [7].

$$h_l^d(\tau) = \sum_{k=1}^{K} A\left(\phi_k - \phi_l^o\right)\, G_k\, p\left(\tau - \tau_k\right) \tag{C.3}$$

where h_l^d is the directive CIR to a given direction, l. The complex radiation pattern for the used antenna is expressed by $A\left(\phi_k - \phi_l^o\right)$, where ϕ_k is direction of the incoming k'th component and ϕ_l^o is the orientation of the antenna for the l'th direction. G_k express the complex gain of the k'th component as $G_k = a_k\, e^{j\varphi_k}$.

Note that in this paper only the azimuth plane is investigated. Therefore, the complex radiation pattern function A is only dependent on the azimuth angle (ϕ) and not the elevation angle (θ).

Using (C.3) an approximation of the CIR for an omnidirectional antenna in the azimuth plane can be obtained with a summation of L responses distributed over a full rotation of the horn antenna. However, as the measurement system records a CIR for each direction (l), each CIR will include minor errors due to the nature of the measurement system. This error will present itself as small random amplitude and phase variations (V_l, v_l) and additive noise (w_l). Due to this, these are added in the approximation shown in (C.4).

$$h^o(\tau) = \sum_{l=1}^{L} h_l^d(\tau)\, V_l e^{jv_l} + w_l(\tau) \tag{C.4}$$

where $h^o(\tau)$ is the approximated omnidirectional CIR.

The purpose of approximating the omnidirectional CIR is to be able to find the omnidirectional PDP for the measurement location. The PDP is found as shown in (C.5).

$$P(\tau) = |h^o(\tau)|^2 \tag{C.5}$$

In (C.6), (C.5) is expanded and (C.3) is substituted into (C.4). The random amplitude variations (V_l) and additive noise (w_l) from the measurement system is assumed to be insignificant compared to the measured channel

response and therefore ignored here.

$$
\begin{aligned}
P(\tau) = & \sum_{l=1}^{L} \sum_{l'=1}^{L'} \sum_{k=1}^{K} \sum_{k'=1}^{K'} A\left(\phi_k - \phi_l^o\right) \, G_k \, p\left(\tau - \tau_k\right) \\
& A^*\left(\phi_{k'} - \phi_{l'}^o\right) \, G_{k'}^* \, p^*\left(\tau - \tau_{k'}\right) \, e^{j\left(v_l - v_{l'}\right)} \qquad \text{(C.6)} \\
= & \sum_{k=1}^{K} \sum_{k'=1}^{K'} \left[\sum_{l=1}^{L} A\left(\phi_k - \phi_l^o\right) e^{jv_l} \right] G_k \, p\left(\tau - \tau_k\right) \\
& \left[\sum_{l'=1}^{L'} A^*\left(\phi_{k'} - \phi_{l'}^o\right) e^{-jv_{l'}} \right] G_{k'}^* \, p^*\left(\tau - \tau_{k'}\right) \qquad \text{(C.7)}
\end{aligned}
$$

where the two terms dependent on the measurement of each direction (l) is contained by the brackets in (C.7).

Following the approach presented in [7], it is assumed that the phase error (v_l) of the measurements within the beamwidth of the used horn antenna is approximately constant. Further, it is assumed that the increments of ϕ_l^o is small compared to the beamwidth of the used horn antenna. The result of these assumptions is an approximation of the antenna and phase error term as shown in expression (C.8).

$$
\sum_{l=1}^{L} A\left(\phi_k - \phi_l^o\right) e^{jv_l} \simeq c \, e^{jv_k} \qquad \text{(C.8)}
$$

where c is the constant determined by the radiation pattern of the used horn antenna. The phase error is now included in the random variable v_k. Note the transform from l to k. This is a result of the seeing the phase error as effectively distorting the individual MPC.

The approximation in (C.8) is used to replace the bracket part of (C.7) as shown in (C.9).

$$
P(\tau) \simeq \sum_{k=1}^{K} \sum_{k'=1}^{K'} |c|^2 e^{j\left(v_k - v_{k'}\right)} G_k G_{k'}^* p\left(\tau - \tau_k\right) p^*\left(\tau - \tau_{k'}\right) \qquad \text{(C.9)}
$$

As stated, the approximation requires the measurement of the angular plane is sufficiently dense. Due to this the effect of choosing different increments of ϕ_l^o and thereby the number of directions (L) is studied in the following section.

IV Results

The measured power-angle-delay profile (PADP) using the horn antenna are shown in Fig. C.3 and Fig. C.4 for line-of-sight (LOS) and non-line-of-sight (NLOS), respectively.

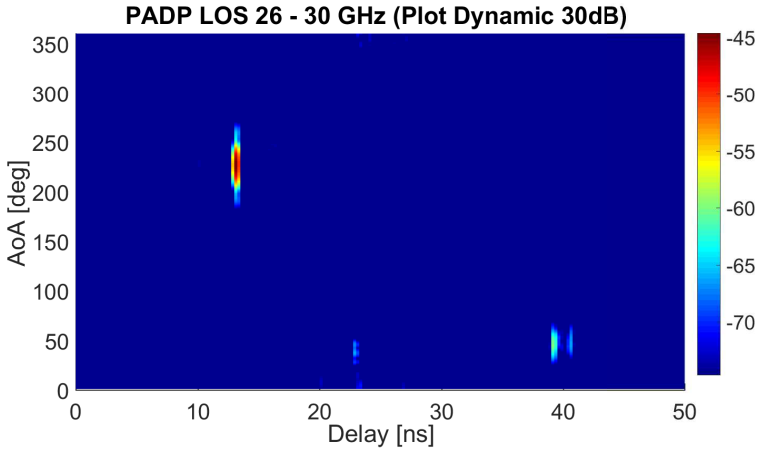

Fig. C.3: Measured power-angle-delay profile for the LOS measurement

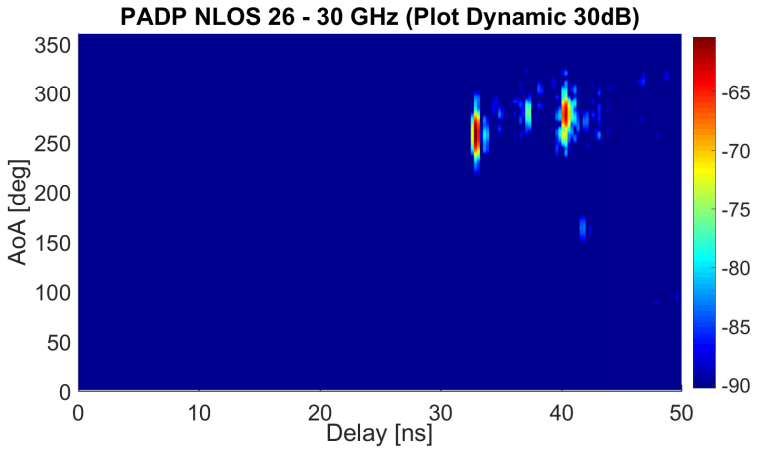

Fig. C.4: Measured power-angle-delay profile for the NLOS measurement

Emulated Omnidirectional PDP

Using the measured data from the horn antennas, the omnidirectional PDP is approximated using (C.5) and compared to the measured data from the bi-conical antenna. The approximation is done using different increments of ϕ_l^o. In specific 1, 5, 10 and 20 degrees which are all within the HPBW of the used horn antenna of 22°. To enable comparison of the shape of the PDPs they are normalize to the maximum power (main component).

The comparison for the LOS measurement is shown in Fig. C.5. Here it can be noted that the approximation using different increments show close

to no difference. To highlight the differences utilizing different angular increments, a zoomed version in shown in Fig. C.6.

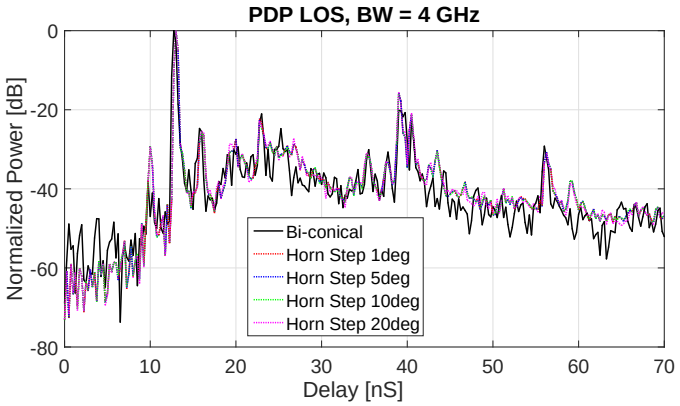

Fig. C.5: PDP for the LOS comparison

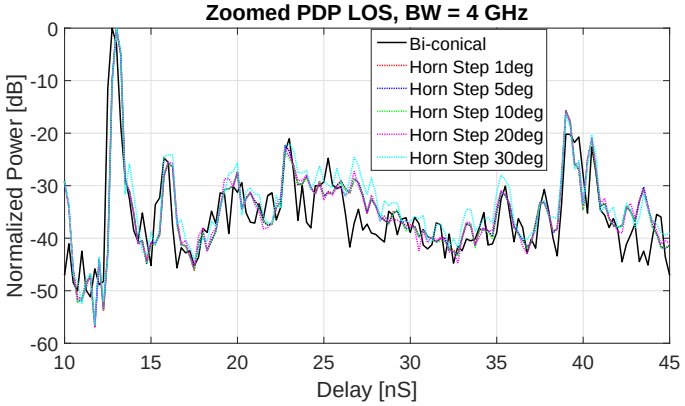

Fig. C.6: Zoomed PDP for the LOS comparison

In the zoomed version shown in Fig. C.6, an approximation using increments of 30° is also included. This trace (cyan) starts to deviate from the other approximations. This is a result of the angular spectrum now is starting to be under sampled compared to the HPBW of the used horn antenna.

Investigating the details of Fig. C.5 and Fig. C.6 shows that the main component of the bi-conical PDP and the approximated PDP is offset by 0.25ns in the delay domain. Using the geometric relation this can be explained by the small height difference of the bi-conical antenna and the horn antenna.

The comparison for the NLOS measurement is shown in Fig. C.7 together with a zoomed version in Fig. C.8.

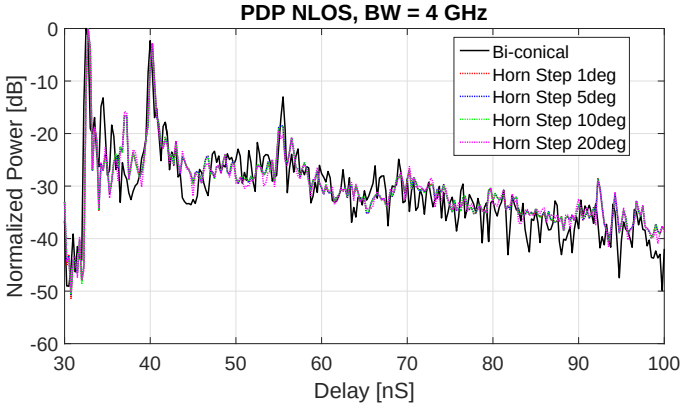

Fig. C.7: PDP for the NLOS comparison

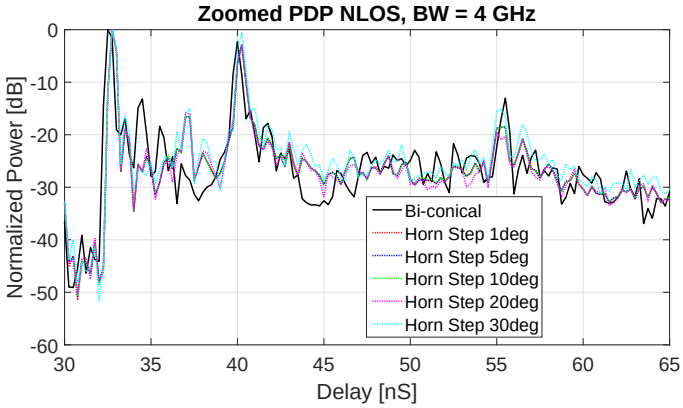

Fig. C.8: Zoomed PDP for the NLOS comparison

The two plots show that the approximation for the NLOS case also is capable of capturing the dominant components and follow the general slope of the PDP. However, there are two components at approximately 34ns and 36ns which are not captured. Instead, the approximation shows a component at approximately 37ns. The delay offset between the main component of the bi-conical PDP and the approximated PDP is again 0.25ns.

Large Angular Spread

The lack of significant difference between the approximations using 1, 5, 10 and 20 degrees angular increments could be explained by the very directional measurement data. Due to this a PADP with a larger angular spread have been constructed. This is constructed by editing the NLOS measurement and

copying the response between 225° and 325° to 25° and 125° and offsetting it by 10ns. The resulting PADP is shown in Fig. C.9.

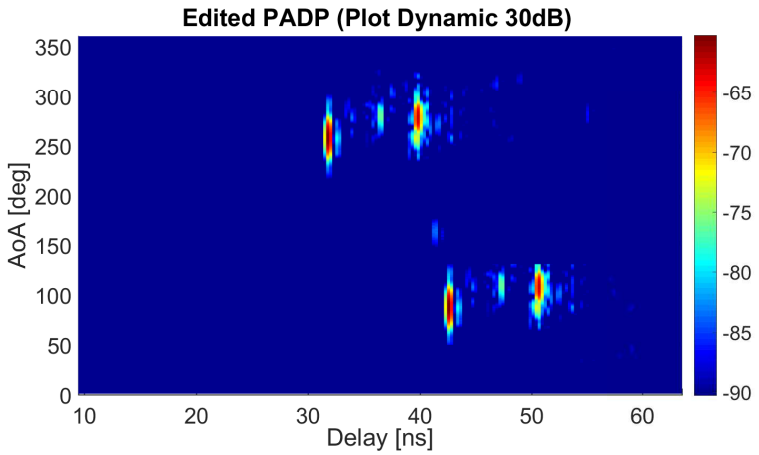

Fig. C.9: Edited power-angle-delay profile

The PDP have, as in the previous, been approximated using different angular increments as shown in Fig. C.10. It is not possible to compare the approximations to the bi-conical antenna as this is based on an edited PADP. It is however still possible to compare the approximations which show that they are close to overlapping, as in the previous comparisons. Only significant deviations are seen from the increments of 30° (cyan). This indicates that as long as the angular increments are below the HPBW of the used horn antenna the approximation shows good agreement with the measured reference.

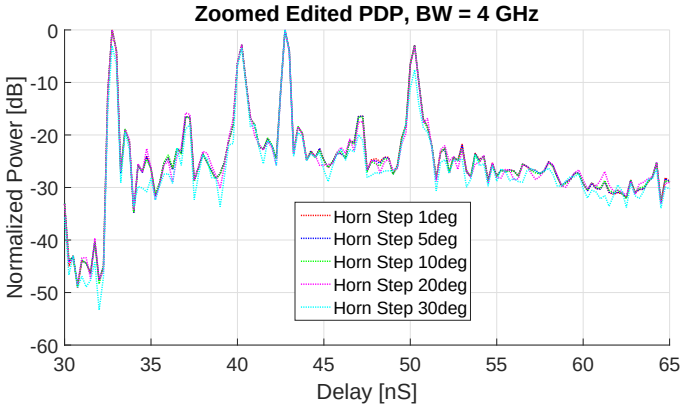

Fig. C.10: Zoomed PDP for the edited PDP comparison

Power Estimation

In the previous sections, the power has been normalized to the maximum power (main component), as the aim was to compare the shape of the PDP. If the aim is to compare the absolute power value for the measurement point, this normalization should be removed. Instead, the power levels have been scaled with the antenna gains as shown in TABLE E.2. The resulting PDP for the bi-conical measurement data is presented in Fig. C.11 together with the approximations using different angular increments.

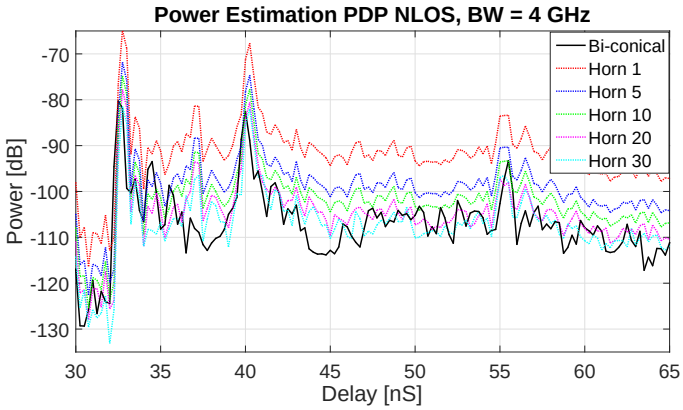

Fig. C.11: Comparison of the unnormalized power levels using the different approximations

Fig. C.11 shows that using small angular increments when sampling the azimuth plane will result in a overestimated power. This is a result of the same components being captured more than once by the broader beam of the antenna and included multiple times as seen from (C.8). A solution could be to scale the summation of power accordingly to the number of samples within a given beamwidth. This relates to the assumptions made in [5,6,8] where angular increments corresponding to the HPBW is chosen. The reason for this is to avoid the 'overlapping' of the most significant part of the radiation pattern. When investigating Fig. C.11 it is also seen that by using increments comparable to the HPBW of the used horn (22°) the power levels are quite well predicted.

V Conclusion

This paper presents a validation of a method for approximating the omnidirectional PDP using measurement data from directional horn antennas in the azimuth domain. Measurements using an omnidirectional bi-conical antenna and a directional horn antenna have been conducted at the same time and lo-

cation. The measurement data from the bi-conical antenna have been used as a reference for comparison of approximations based on the measurement data from the directional horn. It is shown in the paper that it is possible to approximate the omnidirectional PDP. The paper also shows that changing the angular increments of the horn antenna have a small impact on the approximation as long as the increments are chosen smaller or equivalent to the HPBW of the used horn antenna. Finally, it is shown that choosing angular increments of the horn antenna equivalent to the HPBW will enable estimation of the power levels with good agreement to the reference measurement.

Acknowledgment

The work has been conducted under the framework of the VIRTUOSO project. The Danish National Advanced Technology Foundation supports this project.

References

[1] T. Rappaport, S. Sun, R. Mayzus, H. Zhao, Y. Azar, K. Wang, G. Wong, J. Schulz, M. Samimi, and F. Gutierrez, "Millimeter wave mobile communications for 5g cellular: It will work!" *Access, IEEE*, vol. 1, pp. 335–349, 2013.

[2] T. Rapport, F. Gutierrez, E. Ben-Dor, J. Murdock, Y. Qiao, and J. Tamir, "Broadband millimeter-wave propagation measurements and models using adaptive-beam antennas for outdoor urban cellular communications," *IEEE Transactions on Antennas and Propagation*, vol. 61, pp. 1850–1859, April 2013.

[3] W. Fan, I. C. Llorente, J. Ødum Nielsen, K. Olesen, and G. F. Pedersen, "Measured wideband characteristics of indoor channels at centimetric and millimetric bands," *EURASIP Journal on Wireless Communications and Networking*, vol. Pre Press, no. Special issue on Radio Channel models for higher frequency bands, 2016.

[4] J. G. Andrews, S. Buzzi, W. Choi, S. V. Hanly, A. Lozano, A. C. K. Soong, and J. C. Zhang, "What will 5g be?" *IEEE Journal on Selected Areas in Communications*, vol. 32, no. 6, pp. 1065–1082, June 2014.

[5] S. Hur, Y.-J. Cho, J. Lee, N.-G. Kang, J. Park, and H. Benn, "Synchronous channel sounder using horn antenna and indoor measurements on 28 ghz," in *Communications and Networking (BlackSeaCom), 2014 IEEE International Black Sea Conference on*, May 2014, pp. 83–87.

[6] J. Liang, J. Lee, M. D. Kim, and X. Yin, "Synthesis techniques of narrow beamwidth directional antenna measurements for millimeter-wave channel characterization," in *Information and Communication Technology Convergence (ICTC), 2015 International Conference on*, Oct 2015, pp. 689–693.

[7] J. . Nielsen and G. F. Pedersen, "Dual-polarized indoor propagation at 26 ghz," in *2016 IEEE 27th International Symposium on Personal, Indoor and Mobile Radio Communications*, September 2016.

[8] S. Sun, G. R. MacCartney, M. K. Samimi, and T. S. Rappaport, "Synthesizing omnidirectional antenna patterns, received power and path loss from directional antennas for 5g millimeter-wave communications," in *2015 IEEE Global Communications Conference (GLOBECOM)*, Dec 2015, pp. 1–7.

[9] K. Haneda, S. L. H. Nguyen, J. Järveläinen, and J. Putkonen, "Estimating the omni-directional pathloss from directional channel sounding," in *2016 10th European Conference on Antennas and Propagation (EuCAP)*, April 2016, pp. 1–5.

[10] T. Rahim, "Directional pattern synthesis in circular arrays of directional antennas," Ph.D. dissertation, University College London - Department of Electronic and Electrical Engineering, Torrington Place, August 1980.

[11] T. Rahim and D. E. N. Davies, "Effect of directional elements on the directional response of circular antenna arrays," *Microwaves, Optics and Antennas, IEE Proceedings H*, vol. 129, no. 1, pp. 18–22, February 1982.

[12] J. Hejselbæk, W. Fan, and G. F. Pedersen, "Ultrawideband vna based channel sounding system for centimetre and millimetre wave bands," in *2016 IEEE 27th Annual International Symposium on Personal, Indoor, and Mobile Radio Communication (PIMRC)*, September 2016.

[13] H. Hashemi, "The indoor radio propagation channel," *Proceedings of the IEEE*, vol. 81, no. 7, pp. 943–968, Jul 1993.

Paper D

Measured 21.5 GHz Indoor Channels With User-Held Handset Antenna Array

Johannes Hejselbæk, Jesper Ødum Nielsen, Wei Fan and Gert Frølund Pedersen

The paper has been published in the
IEEE TRANSACTIONS ON ANTENNAS AND PROPAGATION Vol. 65, Issue 12, pp. 6574–6583, 2017.

Abstract

For mobile systems involving hand held devices, the influence of the user on system performance has to be considered. Extensive studies below 6 GHz have demonstrated large effects on system performance. However, the impact of user influence at potential higher frequency bands for upcoming 5G mobile networks is still to be investigated. This work investigates how the user affects the performance of a 5G handset mock-up. The user impact is studied by channel sounding in an indoor scenario, with and without the presence of different users. The mock-up handset has a uniform linear array of receive (Rx) antennas operated at 21.5 GHz. A dual-polarized horn antenna with a wide beamwidth is used as transmit (Tx) antenna and a fast channel sounder is used, allowing for recording dynamic and realistic channels. The results show that the mean influence of the user on the power varies considerably depending on the scenario, with more than 12 dB loss in some cases, while a gain of 4 dB is seen in other. An important finding is that the mean power among the seven Rx branches may be very different. Branch power ratios in the typical range of 2–10 dB were found, depending on the user and scenario.

I Introduction

The increasing demand for mobile broadband is one of the driving factors behind the development of the fifth generation (5G) mobile communication network [1,2]. To provide the required high data rate and capacity, there is a strong need for unused spectrum, which is scarce below 6 GHz. Due to this, multiple frequency bands in the centimetre- and millimetre-wave range above 6 GHz have been suggested [2–5].

Historically, frequency bands below 6 GHz have been preferred for cellular usage mainly due to generally increasing pathloss causing coverage issues at high frequency bands. However, these challenges can be overcome by applying high gain directional antennas, as explained in [6,7]. Further, the increase in frequency and thereby shorter wavelengths makes it possible to fit more antennas in a small form-factor such as a mobile terminal [8]. This allows for directive antenna arrays which can be used for beam steering/forming [9–11]. Knowledge of channel characteristics is crucial for 5G system design and performance evaluation. As a result, strong efforts on channel measurements at the proposed frequencies for 5G have been made both from industry and academia.

For the unlicensed frequency band at 60 GHz, used for IEEE 802.11ad wireless local area networks (WLANs), a significant amount of channel studies are available [12–16]. However, 60 GHz is suitable only for short-range communications because of high path loss. Due to this, lower frequencies, which are more suitable for cellular communications, have been studied,

ranging from 20 GHz to 40 GHz, see e.g. [6,11,17–26]. However, the focus of existing work has been on channel characteristics, e.g. path-loss, angle of arrival (AoA) and delay-spread (DS) in static or quasi-static environments.

The human blocking effect is a well-studied phenomenon in the 60 GHz range where it was shown that the propagation path can be attenuated by more than 20 dB due to human blocking [27,28]. The fading characteristics of human movement in a 26 GHz point-to-point indoor static scenario have been reported in [29]. The results showed that more severe received power variation occurred in the 26 GHz band compared with the 2 GHz band. The human body can effectively block the radio path at millimetre-wave bands. This implies that the user impact is important to describe in the propagation environment. In order to investigate the influence that users have on a handset antenna performance, it is necessary to use antennas and handset designs close to what they will be in the intended application. In related work [30,31], a linear phased array operating at 15 GHz was studied, and it was demonstrated that the blocking effect in talk mode was up to 25 dB. However, the focus was on antenna design, only investigating the completely static user impact in an anechoic chamber. User influence, together with propagation environments and antenna designs, determines how well multiple-input multiple-output (MIMO) handset terminals operate in true usage conditions. It is well-known that 5G systems at millimetre-wave bands will suffer rapid channel dynamics, due to the high Doppler shift and blockage. As a result, it is important to evaluate user influence on feasible 5G antenna designs in dynamic environments. This differs from other reported channel measurements as they in most cases have been utilizing horn antennas or virtual arrays. A horn antenna is not a feasible solution for an implementation in a user handset and these measurements cannot capture dynamic influences of users. As the main aim for 5G is to improve the data rates, it is most interesting to investigate the user impact in 'data mode', where the user holds the device in front of the body. The user influence on performance has been extensively investigated frequency bands below 6 GHz [32–35] and recently also at 28 GHz in anechoic conditions [36]. However, to the knowledge of the authors, a comprehensive study of user impact in a realistic dynamic environment in the millimetre-wave frequency band is missing in the literature.

The paper is structured as follows: Section II details the measurement system, measurement scenario and measurement procedure. After that the measured results are detailed in Section III and further discussed in Section IV. Finally, Section V concludes the paper.

II Measurement System and setup

Mock-up Handset Antenna

To investigate the user influence on the channel, a mock-up with a realistic size for a handset was designed. The mock-up handset consists of eight microstrip patch antenna elements on the top side of the handset. The antenna design was detailed in [37] and only briefly explained here. In [37], a phased array consisting of three identical sub-arrays, each with eight antenna elements, was proposed to enable 3D coverage. In this study, only the sub-array pointing towards the user is realized and used in the mock-up. The array elements can be seen on the top edge of the Printed Circuit Board (PCB) in Fig. D.1, left. The individual elements are connected by a matched transmission line to an absorptive switch (Pasternack PE7173) as seen in Fig. D.1, right. The center-to-center distance between the elements is around $\lambda/2$, operated at 21.5 GHz.

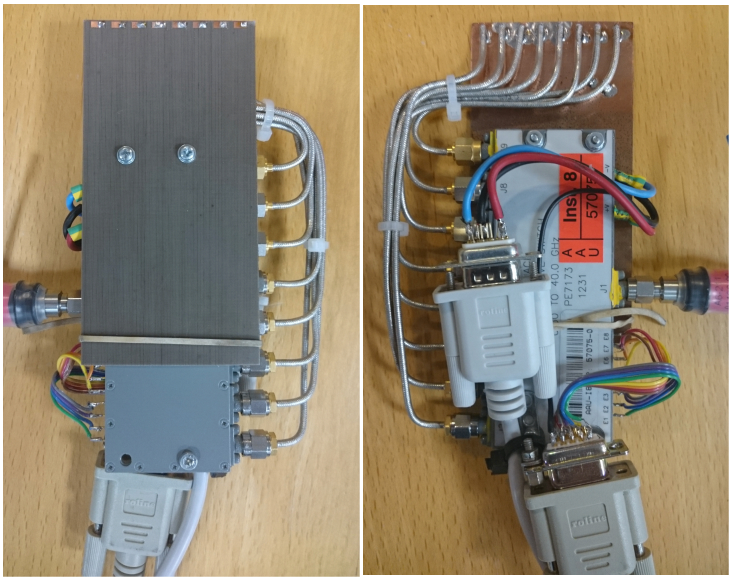

Fig. D.1: Mock-up handset. Left: the front which was pointing towards the user during the measurements. Right: back of the mock-up with the switch and control connectors.

Further dimensions of the mock-up are given in Fig. D.2. As explained in [37], the designed mock-up antenna array offers good efficiency, good S-parameters at the operating frequency, good impedance matching level and low mutual coupling. Each patch antenna element provides good radiation behavior, with a 5 dBi directive pattern towards the user direction. The radiation behavior for the constructed mock-up was validated in measurements. The added absorptive switch and cabling resulted in only minor impact on the performance of the patch elements when compared to the design pre-

sented in [37]. This is mainly due to the use of patches which will not excite strong surface currents as discussed in [38].

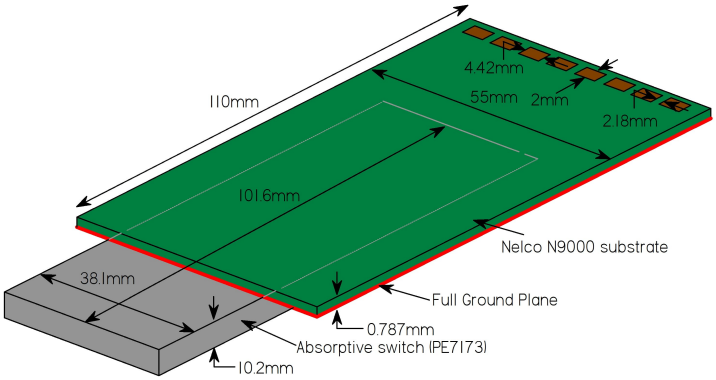

Fig. D.2: Sketch of the mock-up handset including dimensions. Partly redrawn from [37].

Tx antenna

A dual-polarized standard-gain horn antenna is utilized as the Tx antenna (A-INFO LB-SJ180400). The horn antenna covers 18 GHz to 40 GHz, with a 3 dB beamwidth 46.8° for the H-plane and 37.2° for the E-plane at 21.5 GHz. The Tx antenna gain is around 12 dBi at 21.5 GHz. The vertical and horizontal polarization of the used antenna are driven by Tx branch Tx1 and Tx2, respectively, as explained in the following.

Channel sounder

The measurements were performed using a wideband MIMO channel sounder developed at Aalborg University. The channel sounder is based on the pseudo noise (PN) correlation principle; its fundamentals are described in [39]. The latest version, covering carrier frequencies up to 40 GHz, was used in [40]. The specific parameters of the system as used in the current work are presented in Fig. D.3.

As explained in [39], the wideband channel sounder can support quasi-simultaneous measurements, via parallel branches at both the Tx and Rx, combined with fast switching. In the current measurement campaign, two Tx branches were recorded in parallel for each Rx, and this was repeated 7 times via a fast switch at the Rx. Note that only 7 Rx antenna elements of the mock-up array were utilized due to limitations of the practical setup (one antenna on the edge not used).

The total measurement time to record 2×7 complex channel impulse

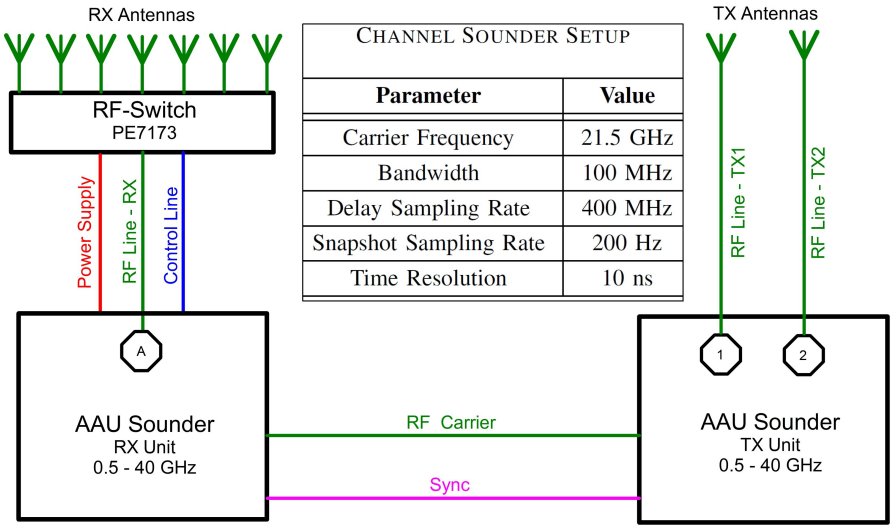

CHANNEL SOUNDER SETUP

Parameter	Value
Carrier Frequency	21.5 GHz
Bandwidth	100 MHz
Delay Sampling Rate	400 MHz
Snapshot Sampling Rate	200 Hz
Time Resolution	10 ns

Fig. D.3: Schematic and settings for the channel sounder setup. Note that the two Tx antennas shown are the two different polarization feeds of the same dual polarized horn antenna.

responses (CIRs) for all Tx and Rx branches is about 573 μs. The channel was measured at a rate of 200 Hz and a total of 50 snapshots of the channel were collected for each measurement.

Measurement Scenarios

The measurement campaign was conducted in a typical indoor corridor scenario in a modern office building. The floor plan of the scenario is shown in Fig. D.4 and pictures are shown in Fig. D.5.

As indicated in Fig. D.4, the Tx antenna was placed in the corridor at a height of 205 cm on a wooden pole, with the main beam pointing towards the Rx locations in the corridor, mimicking an indoor access point scenario. The Tx was kept in the same position throughout the entire measurement campaign.

Both line of sight (LOS) (i.e. locations L7 to L10) and non-line of sight (NLOS) (i.e. locations L1 to L6) scenarios were considered for the Rx, as shown in Fig. D.4. The measurement locations were distributed following a reference line from left to right in Fig. D.4. Most measurement locations were placed in the middle of the corridor except L5 and L7, which were placed closer to the walls.

At every location, four orientations (O) of the user with handset were considered, as shown in the top right corner of Fig. D.4. O1 was orientated such that the user looked away from the Tx, and the other three orientations

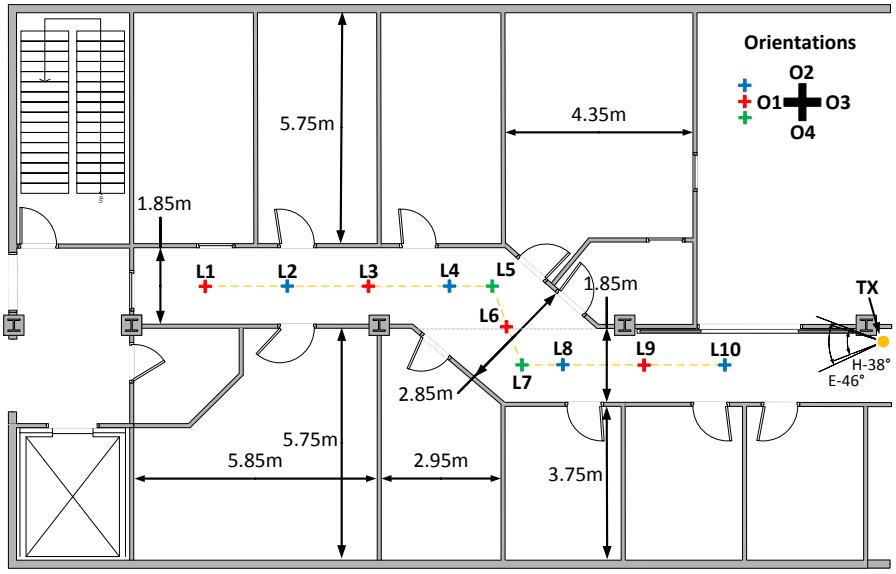

Fig. D.4: Floor plan showing the locations for the measurements. In the top right corner a reference for the orientations (O) used at the different locations (L) is shown.

(O2-4) were obtained, with 90^o step in a clockwise way, as shown in Fig. D.4. The different Rx locations and orientations were measured using different operation modes of the mock-up handset, as explained in the following.

Operation modes

Two different operation modes were investigated, free space mode and user influence mode. As for the user influence mode, so-called 'data mode' was considered, where the user holds the DUT in both hands, as shown in Fig. D.6.

Free Space Mode

The free space mode represents the case where no user is present. This was realized by placing the mock-up on a column of expanded polystyrene (EPS - $\epsilon_r \approx 2.25$) with minimal influence on the fields. As shown in Fig. D.6 (left), the mock-up was placed at the height of 120 cm and slanted 30^o with respect to the azimuth plane, similar to the height and angle as when held by a user.

The EPS column, with mock-up, was placed with its center at each measurement location and orientation, as explained above. During each measurement, the EPS column was moved in a circular manner without changing the orientation of the mock-up. The radius for the movement was roughly

Fig. D.5: Pictures of the corridor where the measurement was conducted. Left is seen the setup for measuring in free space. Right is seen a measurement including a user.

5 cm, which is equivalent to slightly more than 3.5 wavelengths at 21.5 GHz. The movement during the measurement allows for different realizations of the multipath channel. Note that measurement locations L5 and L7 were repeated 10 times for each orientation.

User influence mode

In the user influence mode, we intend to follow the same procedure as described in the free space mode. To achieve this, each user was instructed to move the handset in a circular fashion with the similar radius (i.e. 5 cm) as in the free space mode. To ensure a comparable height of the Rx, the user's wrist was guided by a stick of polyethylene (PE - $\epsilon_r \approx 2.25$), as illustrated in the middle of Fig. D.6. Further, the elevation angle of the mock-up handset was aligned to 30° before the start of the measurement. However, due to the different styles of grip, as seen in the right photos in Fig. D.6, variations between users might be present. This is intentional since this kind of variation must be expected for practical devices. The measured environment was kept largely static, except that the user holding the mockup was moving as instructed.

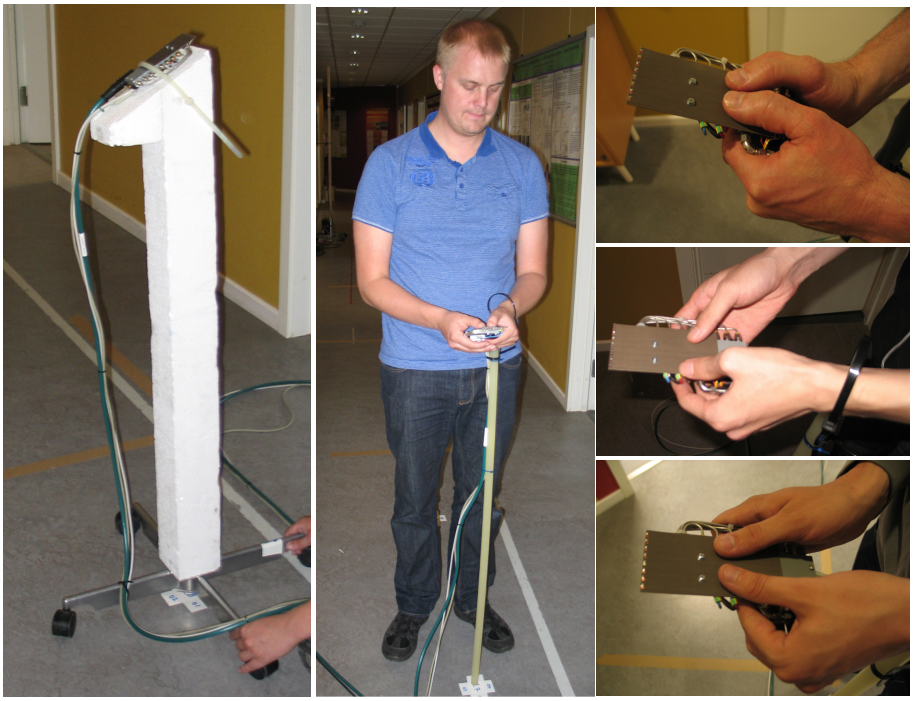

Fig. D.6: The left picture shows the pedestal for measuring in the free space mode. The middle picture illustrates the positioning with a user. Note that the guide stick is centered at the same point as the free space pedestal. Right pictures show how different users holds the mock-up handset.

A total of 5 users were involved in the measurement campaign to allow for a study of the impact of different users. All 5 users were of similar height and body shape. At location L5 and L7, 10 repetitions of each measurement were conducted with user 1 and 2, and 3 repetitions for user 3, 4 and

III Measurement Results

A total of 504 measurements, including repetitions at some locations, was conducted and used for the presented results. The datasets contains the following parameters:

- 10 Locations (L1-10)
- 4 Orientations (O1-4)
- 6 Operation Modes (FS and U1-5)
- 2 Polarizations (Tx1 and Tx2)

- 7 Array elements (Rx1-7)

where L denotes location, O orientation, FS free-space and U denotes user. Tx1 and Tx2 denotes, respectively, the horizontal and vertical Tx polarization. Rx1-7 denotes the 7 elements/branches in the used linear array.

The current work focuses on the mean power gain defined as

$$P(t,r) = \frac{1}{NM} \sum_{n=1}^{N} \sum_{m=1}^{M} |h(t,r,n,m)|^2 \tag{D.1}$$

where $h(t,r,n,m)$ is the complex impulse response at the n-th time-index, the m-th delay-index, where $t \in \{1,2\}$ is the Tx index, and $r \in \{1,\dots 7\}$ is the Rx branch index. Thus, $P(t,r)$ is the mean wideband power of the instantaneous channel between the t-th transmitter and r-th receiver antenna element. The number of channel snapshots in each measurement is $N = 50$ and $M = 500$ is the number of samples in delay.

Five studies are presented in the following sub-sections. The first is focusing on the mean power in free space conditions, then mean influence of the user is studied, followed by the differences in power due to the users, then the branch power ratios (BPRs) of the Rx array, and finally differences due to the Tx polarization.

Free Space

In the following study, the presented total mean power is found as the mean power over all seven Rx elements. For the measurement locations including repetitions (L5 and L7) the expressed power is given as the mean power of the repetitions.

The resulting mean total power for the free space measurement is presented in Fig. D.7 for all the measurement locations. As expected the received power decreases with distance, given that the lower the location number, the further away from Tx, as seen in Fig. D.4. This is emphasised by the added interpolation between measurement locations in Fig. D.7. In strict sense data is only available for the individual measurement locations and the added curves must therefore only been seen as an estimation of the expected power between measurement locations.

The mean power variation in free space due to the change of orientation is up to 10 dB in the same polarization. The variation between polarizations, even for the same orientations, is up to 14 dB. The power difference between polarizations tends to diminish with distance to the Tx except for L3. Here the vertical polarization shows significantly higher power. This could be a result of favorable geometry for this specific location and orientation of the antenna.

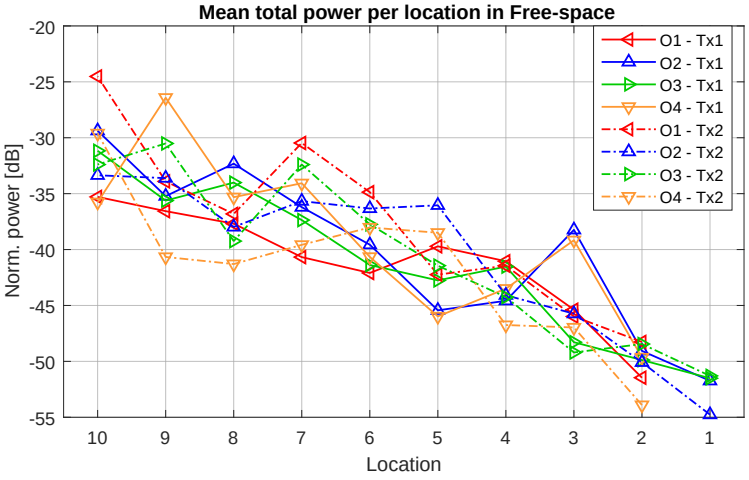

Fig. D.7: Mean total power in the free space scenario for the four orientations (O) shown for all the locations and both polarizations (Tx1 and Tx2). The points indicate measured values, while the connecting lines are only for visualization

For especially O4 - Tx1, in Fig. D.7, it seems like L10 has much lower power than L9. This is explained by the proximity of L10 to the Tx and the height of the Tx and Rx. In this scenario the Rx is below the main lobe of the Tx antenna and therefore not illuminated to the same degrees as it is the case for Rx in L9.

Note that some values in Fig. D.7 (and later plots) are missing, since they were discarded due to a too low quality of the measurements (typically a low dynamic range).

Mean Influence of the User on Power

The mean influence of the user is computed as the mean of the total power obtained with the different users and normalized with the total power gain obtained in free space for the same location and orientation combination. Fig. D.8 shows the results for Tx1, while Fig. D.9 shows similar reults for Tx2.

An interesting finding is that the power in many cases is higher in the measurements with a user than for free space measurements, corresponding to positive values in Fig. D.8 and Fig. D.9. This is especially the case for O4 - Tx1. For L9 the power is the same in the two scenarios but from L8 to L2 the power is up to 8 dB higher when the user is present.

This is explained by seeing the user as an added scatterer in the scenario. The user will reflect some power towards the Rx and in the case of O4, this is most pronounced. The linear patch array elements in the mock-up handset

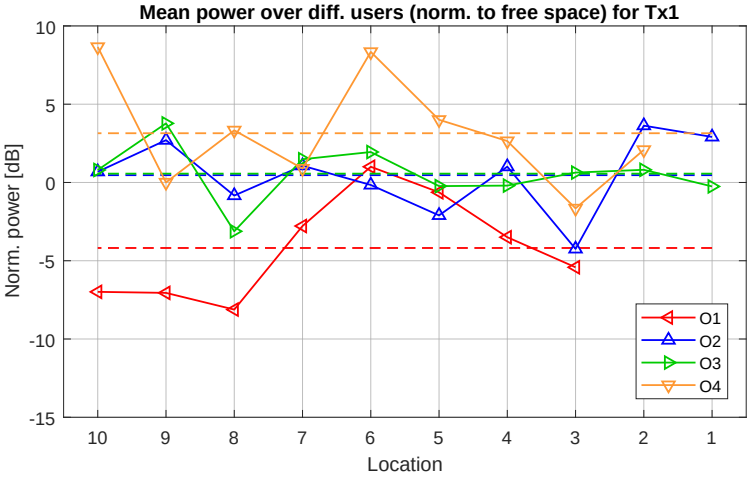

Fig. D.8: Total power gain for Tx1, averaged over the five users and normalized to the similar channel in free space with same location and orientation. The points indicate measured values, while the connecting solid lines are only for visualization. The dashed lines indicate mean values.

have maximum directivity perpendicular to its plane and therefore focused towards the user when held in front. In the case of O4, the user is orientated towards the west corridor wall, as seen in Fig. D.4. This orientation will give the least blocking and the user will reflect some of the power back towards the direction of maximum antenna directivity, overall improving the gain. A similar phenomena was seen in the measurements presented in [36]. In this study the user effect on the handset antenna was studied in the anechoic chamber.

From both Fig. D.8 and Fig. D.9, it is clear how the users introduce a significantly higher loss for O1 at the locations L10 to L7, which correspond to the LOS part of the measurement scenario. O1 is the orientation where the user has its back to the Tx and therefore imposes the largest blocking for the Rx. For Tx2, a large loss is also seen for O2 at L5 and L6. In this location, O2 corresponds to having the user in between the reflected path from the Tx and the Rx. In L4 and L3 O1 is again the orientation with the highest blocking effect.

As evident from the two figures, the user impact is highly dependent on both orientation and location, with both positive up to about 9 dB for Tx1-L10-O4 and negative down to about -12 dB for Tx2-L10-O4. These cases are observed for the shortest distance where the LOS will be dominant compared to any multipath.

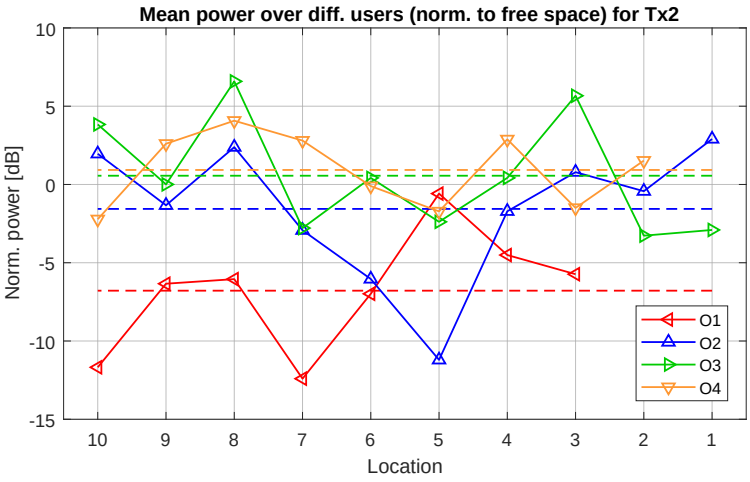

Fig. D.9: Total power gain for Tx2, plotted in the same manner as Fig. D.8.

Power Variation with User

The user influence on the power gain is likely to depend on the individual user, due to different ways of holding the mockup handset, different size, *etc.* This is analyzed in the following.

As described in section II, measurements are obtained with five users for all locations and orientations. Fig. 10 – 11 shows the mean power for each individual user, normalized to the mean value of all users for each location-orientation case. The normalization to the mean power is conducted in order to illustrate the variation in mean power between users.

In Fig. D.10 and Fig. D.11 the data is sorted according to the orientation (O) as shown in the left vertical axis. For each combination the results from the measurements with each of the five users are shown with symbols, according to the normalized power. Even though five users were used for all orientations, some measurements were discarded, as mentioned previously, and thus no points were shown (e.g. for O1-L1). The number of users per orientation-location combination is indicated by the right vertical axis. Also note that only a single repetition is shown for each user, i.e., no repeated values are included.

From Tx1, in Fig. D.10, it can be noted that almost all the values are in the range ± 6 dB with the majority within ± 4 dB. For Tx2, in Fig. D.11, the values are slightly less spread with the majority of values within ± 2 dB. In both cases no general pattern is evident between the different users when sorted according to the orientation. It is noted that sorting the data according to location neither resulted in any general pattern.

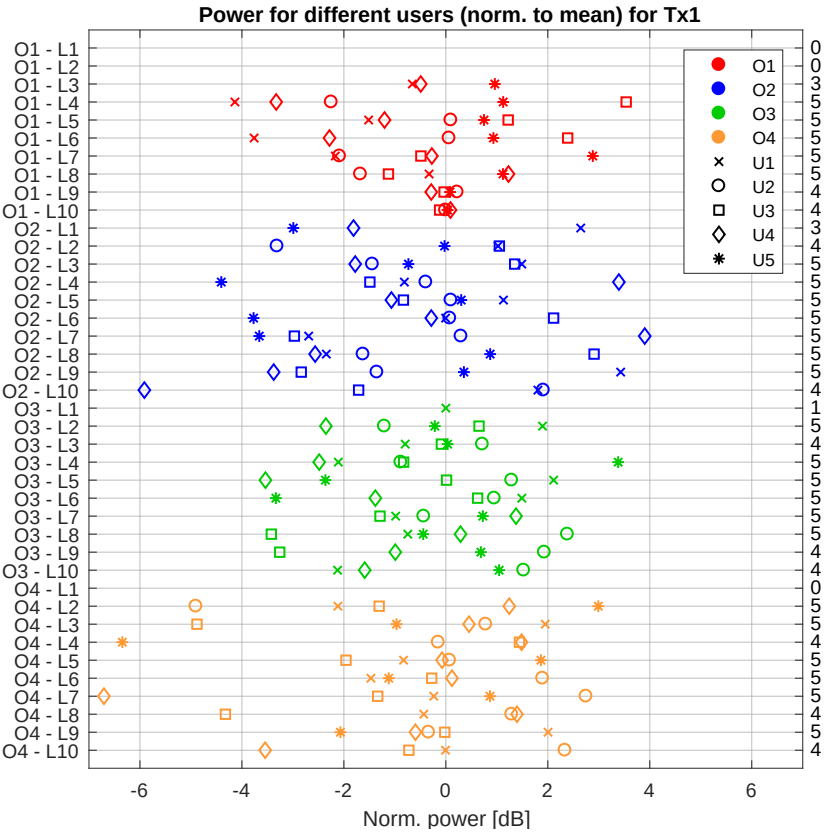

Fig. D.10: The mean power for Tx1 for different users sorted by orientation, as seen in the left vertical axis. The data points are normalized to the mean power of the users. Only one measurement repetition per user is included. The orientation (O) has been indicated by colors and the five different users (U) by different symbols. The number of successful measurements for each orientation-location combination in shown on the right vertical axis.

To investigate the repeatability of the measurements, the repeated measurement at location L5 and L7 with user U1 and U2 have been used. These user-location combinations are used as they are numerous enough for a boxplot, showing the statistical properties.

The repetition measurement was conducted in a sequential manner to limit the impact of other factors rather than the slight change in grip-styles among different users between measurements.

From Fig. D.12 it can be seen that the variation of the mean power was up to 5 dB. The majority of the measurement repetitions showed a variation of less than 1 dB. An interesting observation is the larger variation between repetitions of the same measurement using O1 and O2. This could indicate

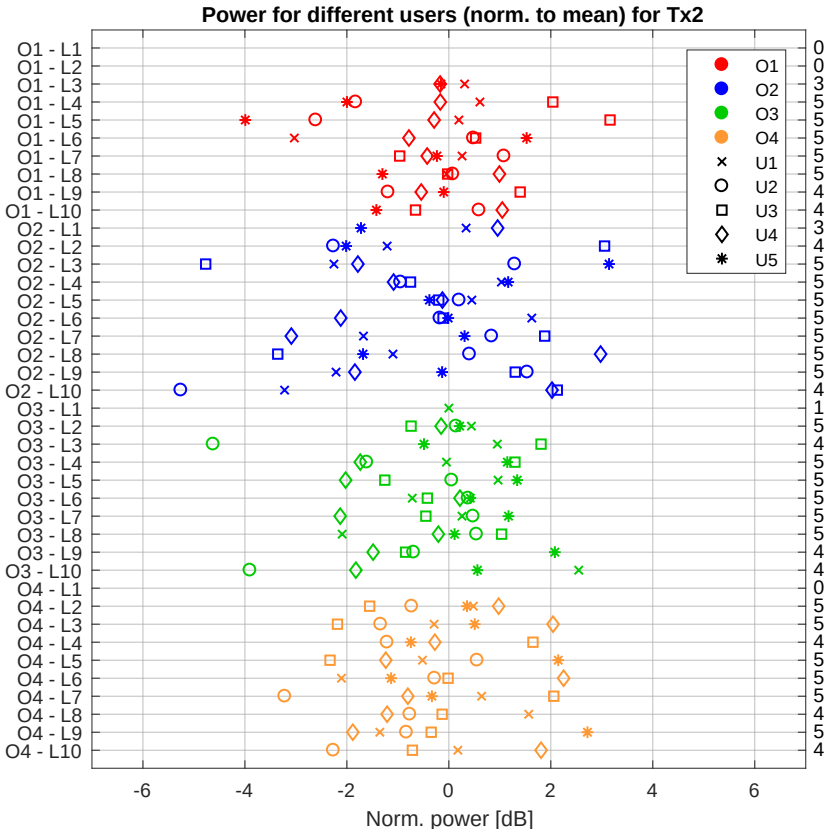

Fig. D.11: The mean power for Tx2, plotted in the same manner as Fig. D.10.

that the specific location-orientation combination is especially susceptible to slight changes of the grip-style.

Rx Element Power Ratio

An array of antenna elements may potentially be used for either diversity or to form beams, which is generally envisioned as very important for utilizing millimetre- and centimetre-waves in cellular systems.

In practice, the antenna elements can not be expected to be identical and in addition, the element properties may be changed in the presence of the user and other parts of the surroundings. The effectiveness of diversity schemes depends highly on the Rx branches having approximately equal power. Similarly, for beamforming to work any differences in the element properties may have to be known, possibly from estimation.

To illustrate the variation between the received power of the 7 Rx ele-

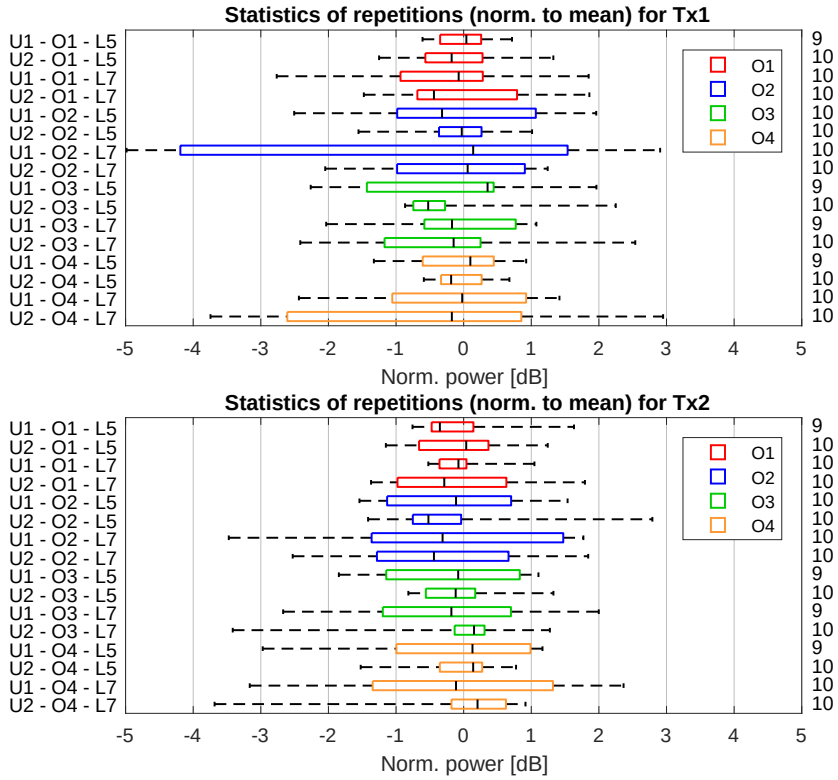

Fig. D.12: The power variation of different repetitions, normalized to the mean of the repetitions. Plotted for user (U) 1 and 2 at location (L) 5 and 7 for all orientations (O) as shown on the left vertical axis. The right vertical axis indicates the number of data points used for the box-plot. The maximum variation of the data is shown using the whiskers while the box indicates the lower 25- and upper 75-percentile limits. The black marker in the boxes indicates the median.

ments, they have been plotted for location L7 and L5 in, respectively, LOS and NLOS. The plots for the two locations are shown in Fig. D.13 and Fig. D.14, where the measured average power for the different Rx elements are shown both in free space and with a user.

Fig. D.13 and Fig. D.14 clearly indicate that mean power is not uniform among the elements. The element power for the used array shows variations up to 13 dB in the free-space scenario and 7 dB including a user. The largest variation between elements is seen in free-space (FS) at L7 for O2 in the Tx1 polarization between element Rx1 and Rx7 as seen in Fig. D.13. For the user scenario (U) the largest variation is seen at L5 for O3 in the Tx1 polarization between element Rx1 and Rx5 as seen in Fig. D.14.

The most pronounced user influence is seen at O1 in Fig. D.13 and at O2 for TX2 as seen in Fig. D.14. When the blocking occurs, it can be seen

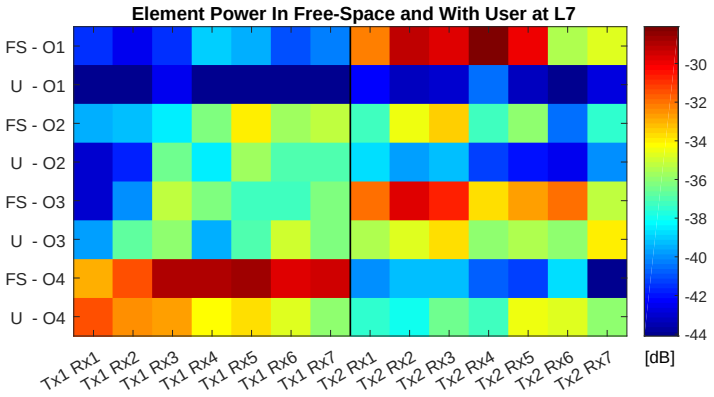

Fig. D.13: Plot of the variation in mean power for the seven elements (Rx) in free space (FS) and with a user (U) for the different orientations (O) and the two polarizations (Tx1/Tx2) for L7.

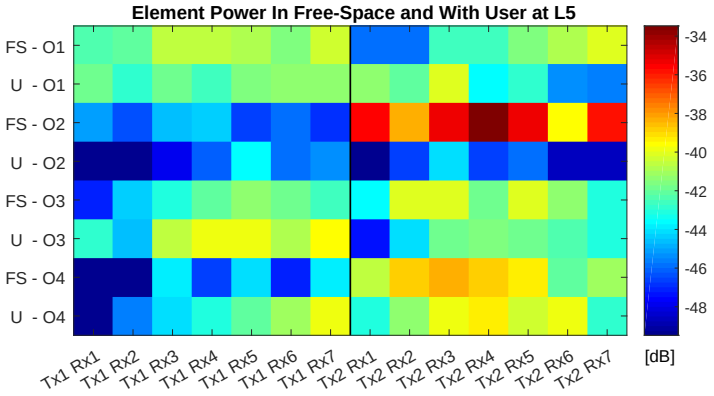

Fig. D.14: Plot of the variation in mean power for the seven elements (Rx) in free space (FS) and with a user (U) for the different orientations (O) and the two polarizations (Tx1/Tx2) for L5.

that all the elements are affected. The blocking causes more than 10 dB drops in power for some elements, while some elements show more than 10 dB increase when the user is present. Note that this improvement of the performance of the array is only possible if the users' hand is not in the vicinity of the antenna, hence affecting the radiation performance.

A simple and first approach to statistically evaluate the challenges in using array techniques for user held equipment is to study the branch power ratio (BPR) between the antenna elements. For simplicity, only the maximum BPR (mBPR) is studied here. Denoting the average channel gain by

$P(Tx, Rx)$, as in (D.1), the mBPR is defined as:

$$\beta(t) = \frac{\max\limits_{r} P(t,r)}{\min\limits_{r} P(t,r)} \tag{D.2}$$

where $t \in \{1,2\}$ is the Tx index, and $r \in \{1,\ldots 7\}$ is the Rx branch index. The mBPR will be determined by a combination of the antenna properties and the propagation in the channel.

To maximize the amount of measurement data used for calculating the mBPR, both data from the free-space and user scenario together with any repetitions have been used. Due to this large dataset, the individual points have not been indicated with user symbols as inFig. D.10 and Fig. D.11 but only simple points as seen in Fig. D.15. The data presented in Fig. D.15 shows the complete data set but can be difficult to read. Due to this, box-plots have been used to describe the statistical properties, as seen in Fig. D.16. Special attention should be given to the number of used data points for each orientation-location combination. This is indicated along the right vertical axis in the figures allow the reader to judge the underlying data, especially for the orientation-location combinations with few data points.

Fig. D.16 and Fig. D.17 shows that the majority of the mBPR values are in the range 2–10 dB. The figures also show that large variations in mBPR are present, even for the different measurements obtained with the same location and orientation combination. The highest mBPR, for both Tx1 and Tx2, is found for O3 and O4 at L7-10. This corresponds to the locations (L) closest to the transmitter (LOS) and the user facing the north wall and towards the transmitter, as seen in Fig. D.4. Interestingly, it seems that the LOS locations experience more severe power variations. The largest difference in mean values, as seen when comparing Fig. D.16 and Fig. D.17, is found for Tx1. Hence, Tx1 corresponding to the vertical polarization, is more sensitive to the orientation than Tx2 for the chosen propagation scenario.

Tx Polarization Influence on Rx Power

From the previous studies, it has become evident that there is a measurable difference between the vertical and horizontal polarization, denoted by Tx1 and Tx2, respectively. Even if a system transmits in only one polarization, some of the power in many cases will be coupled in the channel to the other polarization. While in practice most handset antennas will receive in both polarizations, depending on the design and usage, especially the orientation of the device, it is complicated to predict which is preferable, if any. This is jointly determined by the antenna/handset properties, the random influence of the user, as well as the channel.

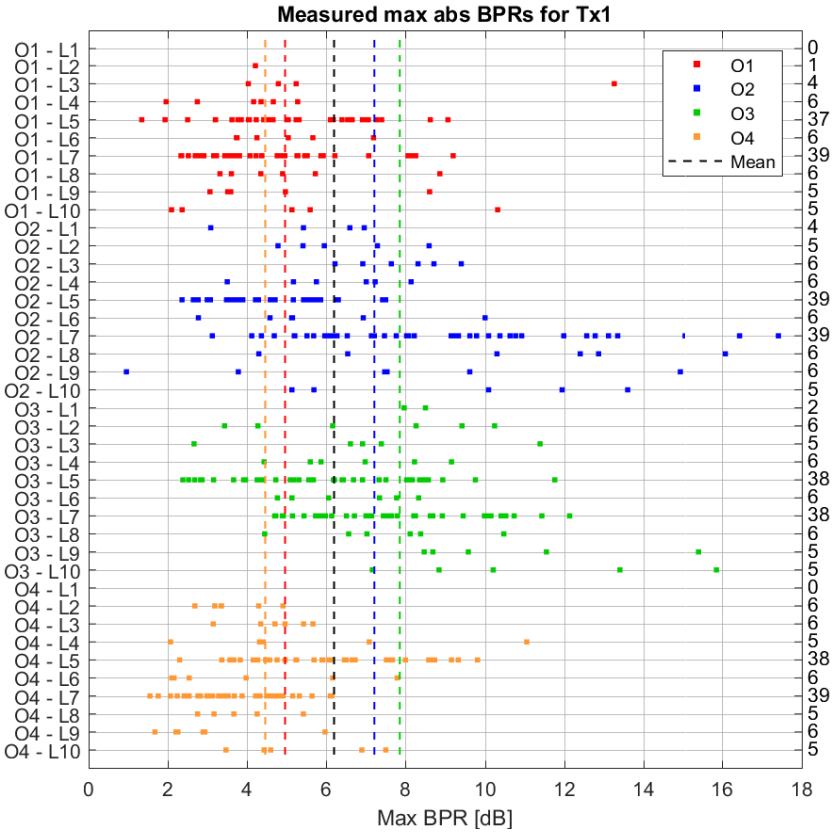

Fig. D.15: The maximum absolute branch power ratio observed for Tx1. Data points are shown for both free space and user cases, including repetitions, for the given orientation-location combination shown on the left vertical axis. The right vertical axis indicates the number of data points. The used colors corresponds to the four orientations (O) which mean mBPR is indicated with a dashed line. The mean for all data points is marked by a black dashed line.

The polarization power ratio (PPR) γ is defined as the ratio of the average power received when transmitting in the two different polarizations as:

$$\gamma = \frac{\sum_{r_1=1}^{R} P(t=1, r_1)}{\sum_{r_2=1}^{R} P(t=2, r_2)} \tag{D.3}$$

where $R = 7$ is the total number of Rx antennas and $P(\cdot)$ is defined as previously in connection with (D.1).

With the current measurements, the channels for Tx1 and Tx2 are measured at the same time physically so it is possible to evaluate the PPR in the exact same conditions with the user location and orientation. Like for the BPR study in section III, the results for both free space, users and all repeti-

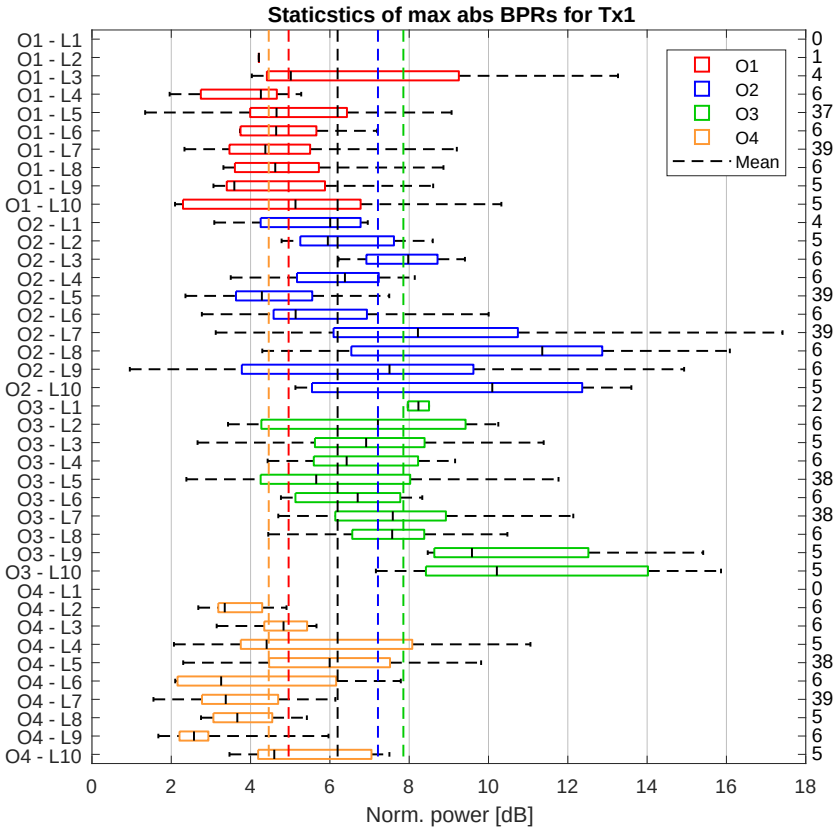

Fig. D.16: The statistics of the maximum absolute branch power ratio observed for Tx1 plotted as box-plots following the same practice as Fig. D.15. The maximum variation of the data is shown using the whiskers while the box indicates the lower 25- and upper 75-percentile limits. The black marker in the boxes indicates the median for the given orientation-location combination.

tions are included to use as large a data set as possible. The resulting PPR plot is therefore also presented in Fig. D.18 as a box-plot. Each orientation-location combination is a line in the box-plots and the mean values for the four orientations are indicated by dashed lines.

Fig. D.18 shows that most measurements have a PPR within a range of ± 10 dB, with large variations among the different measurements for the same orientation-location combinations. Thus, the polarization state is highly sensitive to the exact channel conditions. Further, Fig. D.18 shows that there is a tendency of a lower PPR for O1 when getting closer to the Tx (higher number), probably because of a more pure polarization in the channel. A similar tendency is found for O3, while it is more mixed for O2 and O4.

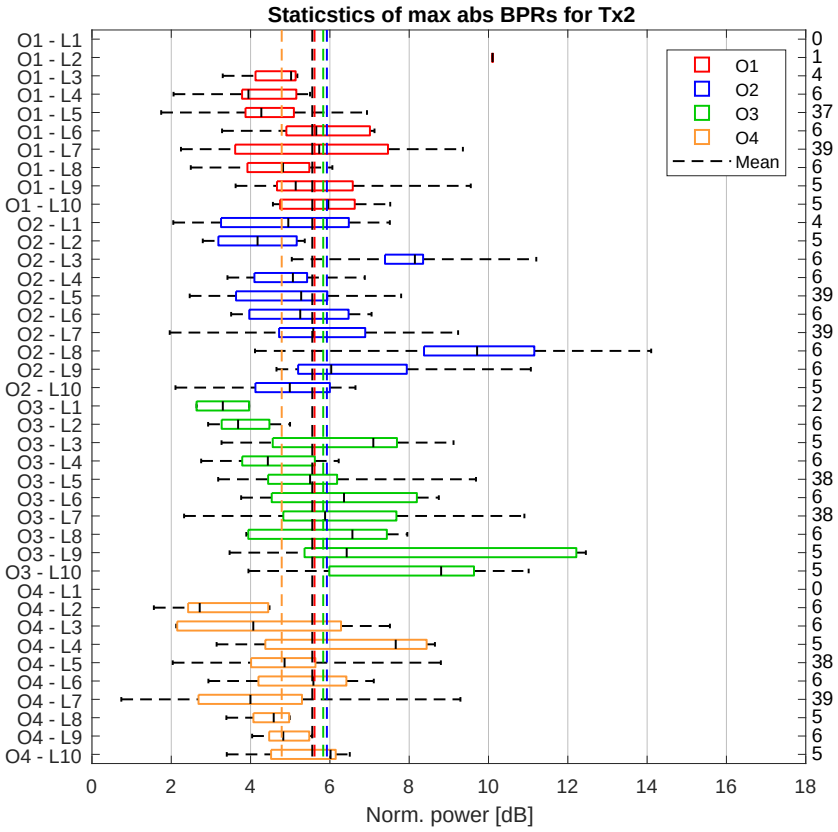

Fig. D.17: The statistics of the maximum absolute branch power ratio observed for Tx2, plotted in the same manner as Fig. D.16.

IV Discussion

Based on the results presented in the previous section some discussions and speculations can be made on the impact of the findings. This is presented in the following section.

In section III the measurements showed, as expected, that an increasing distance from Tx to Rx results in an increasing path-loss. The path-loss at especially the NLOS locations are high. However, the signal is still reaching locations deep in NLOS, likely mainly via reflections. The measurements presented in section III shows that the user blocks the LOS component in the LOS scenario and the expected dominant path in the NLOS scenario. The large impact on received power caused by the user blocking needs to be considered in future system designs.

section III describes variation in the received mean power of up to almost

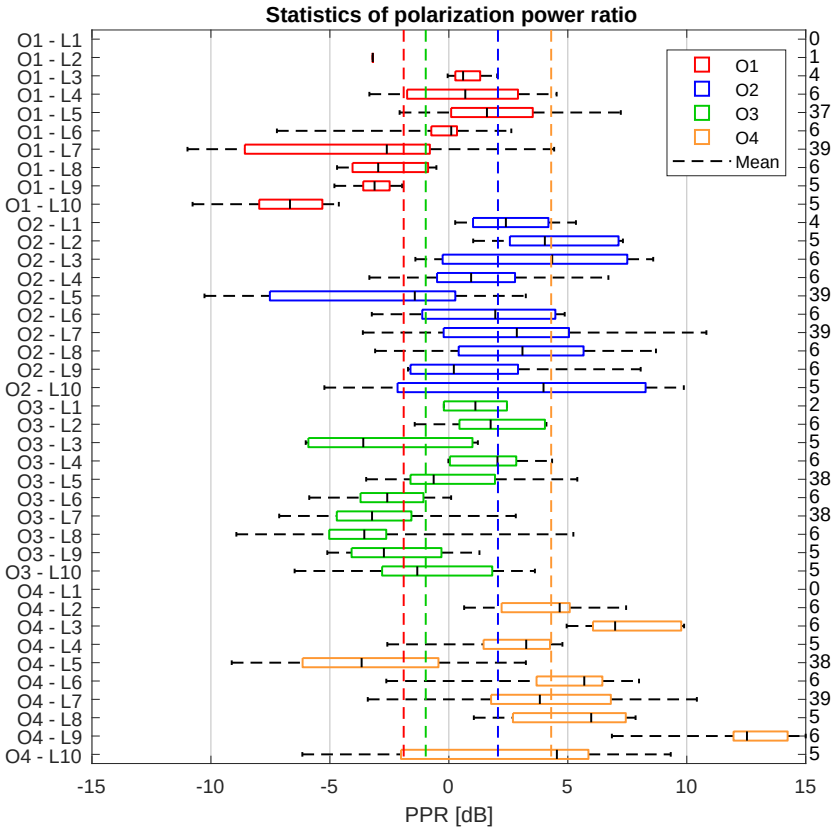

Fig. D.18: The statistics of the polarization power ratio for all the measured scenarios and users, including free space plotted in the same manner as Fig. D.16.

7 dB among the 5 different users, as seen in Fig. D.10. It is noted that the variation in mean power for repetitions of the measurement was up to 5 dB, as seen in Fig. D.12. As expected, the measurements with a user generally had higher losses when compared to a free-space measurement. However, in some cases, a gain was found. This can be explained by the user acting as an added scatterer, which in some specific scenarios can improve the link. The data obtained with the different users showed no apparent pattern, even when measured at the same orientation-location. This indicates that the user influence can be seen as a random factor.

The high path-loss together with the possible added losses due to the user has to be overcome to enable a future millimetre-wave system. One method is to apply beamforming facilitating a high gain. As shown in section III, the measurements showed large variations in BPR of up to almost 18 dB, as seen in Fig. D.15 and Fig. D.16. Overall, these variations can be caused

by fading over the array due to multipath in the channel, by the influence of the user, or a combination. Beamforming would be effective in the case of multipath, but if the power variations are caused by other mechanisms, such as absorption in the users' fingers or changes in the element radiation pattern, implementing effective beamforming could be difficult.

The investigation of the two polarizations described in section III showed a PPR of up to 15 dB, indicating that there is a large gain to be obtained if future systems utilize both polarizations at the access point. However, it is also important to realize that the PPR changes both due to the environment and the user. The handset will, in most cases, transmit or receive in a mixture of both polarizations and the user will likely also change the orientation of the handset. Therefore, the system needs to adapt to the polarization coupling in the channel.

V Conclusion

Based on 21.5 GHz channel measurements performed in an indoor scenario the impact of the user holding the receiving handset antenna is studied.

The measurement campaign includes both free space conditions and users. Five different users have been measured in an indoor corridor scenario at ten different locations and with four different orientations. The users hold the mock-up handset in data mode.

The mean influence of the user's on the power vary significantly depending on the location and orientation of the user, with a loss of more than 12 dB in some cases. The mean power loss is among the different locations less than 7 dB, depending on the orientation.

The measurements also indicate that the user can also help the link by acting as a scatterer, given that the user is not in a direct blocking position. This gain from the user is up to about 4 dB for the most favorable orientation. However, the effect is less than 2 dB for the other orientations.

Among the five users, considerable variation in the mean power was also found. The variation was typically within ± 4 dB.

The mock-up handset was equipped with a 7-element array, potentially useful for e.g. beamforming or diversity. For such applications, differences in average power among the elements may be critical. Therefore, the maximum branch power ratio (mBPR) was investigated for the measured data. Large variations were found, with absolute mBPR values typically in the range 2–10 dB, mostly depending on the individual user or measurement.

With the chosen handset mock-up the difference in received power when transmitting in either vertical or horizontal polarization depends highly on the exact measurement condition, with ratios of mean power in the range ± 10 dB. Thus, both Tx polarizations are needed in practice for best power

transfer.

Acknowledgment

The authors would like to thank Kim Olesen, Anders Karstensen, Yilin Ji and Stanislav Zhekov for valuable assistance with the measurements. Further the authors would like to thank Ming Shen for providing the mock-up antenna used for the measurement.

References

[1] P. Demestichas, A. Georgakopoulos, D. Karvounas, K. Tsagkaris, V. Stavroulaki, J. Lu, C. Xiong, and J. Yao, "5g on the horizon: Key challenges for the radio-access network," *Vehicular Technology Magazine, IEEE*, vol. 8, no. 3, pp. 47–53, Sept 2013.

[2] Q. Li, H. Niu, A. Papathanassiou, and G. Wu, "5g network capacity: Key elements and technologies," *Vehicular Technology Magazine, IEEE*, vol. 9, no. 1, pp. 71–78, March 2014.

[3] L. Wei, R. Q. Hu, Y. Qian, and G. Wu, "Key elements to enable millimeter wave communications for 5g wireless systems," *IEEE Wireless Communications*, vol. 21, no. 6, pp. 136–143, December 2014.

[4] Ofcom, "Spectrum above 6 ghz for future mobile communications," Ofcom UK, Riverside House, 2a Southwark Bridge Road, London, Consultation Report, January 2015.

[5] S. Methley, W. Webb, S. Walker, and J. Parker, "Study on the suitability of potential candidate frequency bands above 6ghz for future 5g mobile broadband systems," Quotient Associates Limited, Compass House, Vision Park, Chivers Way Histon, Cambridge, CB24 9AD, UK, Technical Report, March 2015.

[6] T. Rappaport, S. Sun, R. Mayzus, H. Zhao, Y. Azar, K. Wang, G. Wong, J. Schulz, M. Samimi, and F. Gutierrez, "Millimeter wave mobile communications for 5g cellular: It will work!" *Access, IEEE*, vol. 1, pp. 335–349, 2013.

[7] S. Rangan, T. Rappaport, and E. Erkip, "Millimeter-wave cellular wireless networks: Potentials and challenges," *Proceedings of the IEEE*, vol. 102, no. 3, pp. 366–385, March 2014.

[8] W. Hong, K. H. Baek, Y. Lee, Y. Kim, and S. T. Ko, "Study and prototyping of practically large-scale mmwave antenna systems for 5g cellular devices," *IEEE Communications Magazine*, vol. 52, no. 9, pp. 63–69, September 2014.

[9] W. Roh, J.-Y. Seol, J. Park, B. Lee, J. Lee, Y. Kim, J. Cho, K. Cheun, and F. Aryanfar, "Millimeter-wave beamforming as an enabling technology for 5g cellular communications: theoretical feasibility and prototype results," *Communications Magazine, IEEE*, vol. 52, no. 2, pp. 106–113, February 2014.

[10] S. Han, C. l. I, Z. Xu, and C. Rowell, "Large-scale antenna systems with hybrid analog and digital beamforming for millimeter wave 5g," *IEEE Communications Magazine*, vol. 53, no. 1, pp. 186–194, January 2015.

[11] T. Rappaport, F. Gutierrez, E. Ben-Dor, J. Murdock, Y. Qiao, and J. Tamir, "Broadband millimeter-wave propagation measurements and models using adaptive-beam antennas for outdoor urban cellular communications," *Antennas and Propagation, IEEE Transactions on*, vol. 61, no. 4, pp. 1850–1859, April 2013.

[12] H. Xu, V. Kukshya, and T. S. Rappaport, "Spatial and temporal characteristics of 60-ghz indoor channels," *IEEE Journal on Selected Areas in Communications*, vol. 20, no. 3, pp. 620–630, Apr 2002.

[13] N. Moraitis and P. Constantinou, "Indoor channel measurements and characterization at 60 ghz for wireless local area network applications," *IEEE Transactions on Antennas and Propagation*, vol. 52, no. 12, pp. 3180–3189, Dec 2004.

[14] P. F. M. Smulders, "Statistical characterization of 60-ghz indoor radio channels," *IEEE Transactions on Antennas and Propagation*, vol. 57, no. 10, pp. 2820–2829, Oct 2009.

[15] S. Geng, J. Kivinen, X. Zhao, and P. Vainikainen, "Millimeter-wave propagation channel characterization for short-range wireless communications," *IEEE Transactions on Vehicular Technology*, vol. 58, no. 1, pp. 3–13, Jan 2009.

[16] S. Salous, S. M. Feeney, X. Raimundo, and A. A. Cheema, "Wideband mimo channel sounder for radio measurements in the 60 ghz band," *IEEE Transactions on Wireless Communications*, vol. 15, no. 4, pp. 2825–2832, April 2016.

[17] A. Sulyman, A. Nassar, M. Samimi, G. Maccartney, T. Rappaport, and A. Alsanie, "Radio propagation path loss models for 5g cellular networks in the 28 ghz and 38 ghz millimeter-wave bands," *Communications Magazine, IEEE*, vol. 52, no. 9, pp. 78–86, September 2014.

[18] R. J. C. Bultitude, R. F. Hahn, and R. J. Davies, "Propagation considerations for the design of an indoor broad-band communications system at ehf," *IEEE Transactions on Vehicular Technology*, vol. 47, no. 1, pp. 235–245, Feb 1998.

[19] G. A. Kalivas, M. El-Tanany, and S. Mahmoud, "Millimeter-wave channel measurements with space diversity for indoor wireless communications," *IEEE Transactions on Vehicular Technology*, vol. 44, no. 3, pp. 494–505, Aug 1995.

[20] H. Xu, T. S. Rappaport, R. J. Boyle, and J. H. Schaffner, "Measurements and models for 38-ghz point-to-multipoint radiowave propagation," *IEEE Journal on Selected Areas in Communications*, vol. 18, no. 3, pp. 310–321, March 2000.

[21] W. Fan, I. C. Llorente, J. Ødum Nielsen, K. Olesen, and G. F. Pedersen, "Measured wideband characteristics of indoor channels at centimetric and millimetric bands," *EURASIP Journal on Wireless Communications and Networking*, vol. 2016, no. 1 -Special issue on Radio Channel models for higher frequency bands, pp. 1–13, 2016.

[22] G. R. Maccartney, T. S. Rappaport, S. Sun, and S. Deng, "Indoor office wideband millimeter-wave propagation measurements and channel models at 28 and 73 ghz for ultra-dense 5g wireless networks," *IEEE Access*, vol. 3, pp. 2388–2424, 2015.

[23] M. D. Kim, J. Liang, H. K. Kwon, and J. Lee, "Path loss measurement at indoor commercial areas using 28ghz channel sounding system," in *2015 17th International Conference on Advanced Communication Technology (ICACT)*, July 2015, pp. 535–538.

[24] P. B. Papazian, K. A. Remley, C. Gentile, and N. Golmie, "Radio channel sounders for modeling mobile communications at 28 ghz, 60 ghz and 83 ghz," in *Millimeter Waves (GSMM), 2015 Global Symposium On*, May 2015, pp. 1–3.

[25] S. Hur, Y.-J. Cho, J. Lee, N.-G. Kang, J. Park, and H. Benn, "Synchronous channel sounder using horn antenna and indoor measurements on 28 ghz," in *Communications and Networking (BlackSeaCom), 2014 IEEE International Black Sea Conference on*, May 2014, pp. 83–87.

[26] S. Salous and Y. Gao, "Wideband measurements in indoor and outdoor environments in the 30 ghz and 60 ghz bands," in *2016 10th European Conference on Antennas and Propagation (EuCAP)*, April 2016, pp. 1–3.

[27] S. Collonge, G. Zaharia, and G. E. Zein, "Influence of the human activity on wide-band characteristics of the 60 ghz indoor radio channel," *IEEE Transactions on Wireless Communications*, vol. 3, no. 6, pp. 2396–2406, Nov 2004.

[28] S. Obayashi and J. Zander, "A body-shadowing model for indoor radio communication environments," *IEEE Transactions on Antennas and Propagation*, vol. 46, no. 6, pp. 920–927, Jun 1998.

[29] K. Saito, T. Imai, and Y. Okumura, "Fading characteristics in the 26ghz band indoor quasi-static environment," in *Electromagnetics (iWEM), 2014 IEEE International Workshop on*, Aug 2014, pp. 135–136.

[30] J. Helander, K. Zhao, Z. Ying, and D. Sjöberg, "Performance analysis of millimeter-wave phased array antennas in cellular handsets," *IEEE Antennas and Wireless Propagation Letters*, vol. 15, pp. 504–507, 2016.

[31] K. Zhao, J. Helander, D. Sjoberg, S. He, T. Bolin, and Z. Ying, "User body effect on phased array in user equipment for 5g mm wave communication system," *IEEE Antennas and Wireless Propagation Letters*, vol. PP, no. 99, pp. 1–1, 2016.

[32] J. Toftgard, S. N. Hornsleth, and J. B. Andersen, "Effects on portable antennas of the presence of a person," *IEEE Transactions on Antennas and Propagation*, vol. 41, no. 6, pp. 739–746, Jun 1993.

[33] G. F. Pedersen and J. O. Nielsen, "Radiation pattern measurements of mobile phones next to different head phantoms," in *Vehicular Technology Conference, 2002. Proceedings. VTC 2002-Fall. 2002 IEEE 56th*, vol. 4, 2002, pp. 2465–2469 vol.4.

[34] G. F. Pedersen, K. Olesen, and S. L. Larsen, "Bodyloss for handheld phones," in *Vehicular Technology Conference, 1999 IEEE 49th*, vol. 2, Jul 1999, pp. 1580–1584 vol.2.

[35] J. B. Andersen, J. Ø. Nielsen, and G. F. Pedersen, "Absorption related to handheld devices in data mode," *IEEE Transactions on Electromagnetic Compatibility*, vol. 58, no. 1, pp. 47–53, Feb 2016.

[36] I. Syrytsin, S. Zhang, G. Pedersen, K. Zhao, T. Bolin, and Z. Ying, "Statistical investigation of the user effects on mobile terminal antennas for 5g applications," *IEEE Transactions on Antennas and Propagation*, vol. Pre Press, 2017, "TO APPEAR".

[37] N. Ojaroudiparchin, M. Shen, S. Zhang, and G. Pedersen, "A switchable 3d-coverage phased array antenna package for 5g mobile terminals," *IEEE Antennas and Wireless Propagation Letters*, vol. 15, pp. 1747–1750, 2016.

[38] S. Zhang, X. Chen, I. Syrytsin, and G. F. Pedersen, "A planar switchable 3d-coverage phased array antenna and its user effects for 28 ghz mobile terminal applications," *IEEE Transactions on Antennas and Propagation*, vol. PP, no. 99, pp. 1–1, 2017.

[39] J. Ø. Nielsen, J. B. Andersen, P. C. F. Eggers, G. F. Pedersen, K. Olesen, E. H. Sørensen, and H. Suda, "Measurements of indoor 16x32 wideband mimo channels at 5.8 ghz," in *Proceedings of the 2004 International Symposium on Spread Spectrum Techniques and Applications*, May 2004.

[40] J. Ø. Nielsen and G. F. Pedersen, "Dual-polarized indoor propagation at 26 ghz," in *2016 IEEE 27th International Symposium on Personal, Indoor and Mobile Radio Communications*, September 2016.

Paper E

Propagation Measurements for Device-to-Device Communication in Forest Terrain

Johannes Hejselbæk, Jesper Ødum Nielsen, Christian Drewes, Wei Fan and Gert Frølund Pedersen

The paper has been published at the
2018 12th European Conference on Antennas and Propagation - EuCAP 2018.

Abstract

In this paper, we present a measurement campaign conducted in forest terrain with focus on path-loss. The aim of the measurement campaign is to study the coverage in a Device-to-Device (D2D) communication scenario. The measurement campaign was conducted in the LTE band 8 at 917.5 MHz with measurement ranges extending to more than 2.5 km. The measurements have been conducted using a purpose-developed measurement system with a dynamic range of 180 dB. The measurements showed that a D2D system with transmit and receive antenna at heights of 1.5 m could achieve a range of approximately 2 km using the 164 dB path-loss limit specified for Narrow Band Internet-of-Things (NB-IoT).

I Introduction

Unlike conventional cellular communication Device-to-Device (D2D) communication is the capability of a device to communicate directly with other devices by bypassing the network infrastructure [1]. The capability is described in the standard for long term evolution-advanced (LTE-A) mobile communication release 12 (Rel-12) by the 3rd generation partnership project (3GPP) [2] and also included as an important technique for the Next Generation Mobile Communication (5G) [3–5]. D2D communication is especially mentioned in relation to Internet-of-Things (IoT) where small devices might not have the ability or need to communicate with conventional cellular network infrastructure. A scenario where D2D communication could be used is a hiking trip with multiple participants. A small device could exchange the location information of the different participants allowing everyone keeping track of each other for either competition or safety reasons. These small devices should operate over a fair distance without consuming too much power. This together with the limited amount of information/data they have to exchange suggests a narrowband communication system as a solution. Such communication system is, in the contents of LTE-A, referred to as Narrow Band IoT (NB-IoT) in the literature [5–7].

The aim of this work is to study the communication range of an NB-IoT device utilizing D2D communication. The operation frequency is chosen to be in the lower range for LTE around 900 MHz. The antenna heights are chosen to be close to the ground due to the D2D scenario. Existing path-loss studies around 900 MHz close to the ground exist, as seen in [8–12]. However, they do not extend to the full 164 dB path-loss which is specified in the standard for NB-IoT [6]. Due to this the measurement campaign presented in this work has been conducted.

The paper is organized as follows. Section II describes the planning of the measurement and presents the area in which the measurements were

conducted. Section III describes the measurement system used for the measurements. Section IV presents the results of the measurement campaign. Section V summarizes this work.

II Measurement Planning

Measurement Frequency

It is wanted to measure a quite considerable path-loss of 164 dB which, for practical limits, results in a quite high transmit power. The high transmit signal power could cause interference in other communication systems operating in the same frequency band. Due to this, a study of the licensed frequencies in and around LTE band 8 (880 - 960 MHz) has to be conducted. In Denmark, the frequency range from 790 MHz - 960 MHz is mainly reserved for mobile communication while the range from 960 MHz - 1164 MHz is used for aeronautical navigation and communication [13]. The use of the frequency range from 840 MHz - 1000 MHz is shown in Fig. E.1. The frequency allocation of the Danish spectrum is found in the government database [14].

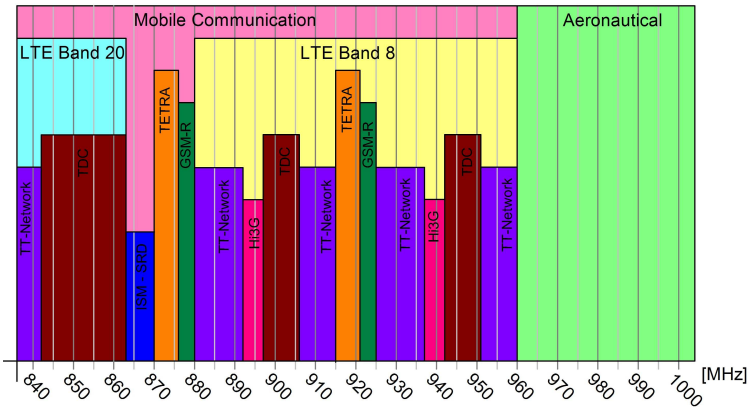

Fig. E.1: Frequency allocation diagram.

Reading from the top of Fig. E.1, the two overall allocations of mobile communication and aeronautical navigation/communication are marked as the background color. In the mobile communication allocation, LTE Band 20 and 8 are illustrated as overlaid color. The subdivisions in the bands are marked by blocks of different heights and colors. From Fig. E.1 it is clear that allocations have been made for the entire LTE band 8. Most of the allocations belong to the mobile operator's networks in Denmark:

- TT-Network (Telia and Telenor)

- TDC (YouSee)
- Hi3G (3)

The licenses to the mobile operators are 'technology neutral', meaning that the operator is free to use different wireless telephone technologies fitting their need. It is currently mostly used for GSM and LTE. As all of the mobile operator's spectrum blocks are heavily used and under licenses, it is not possible to transmit our measurement signal here.

The spectrum from 915 MHz - 925 MHz is allocated to TETRA (Terrestrial Trunked Radio) and GSM-R (Global System for Mobile Communications - Railway). The 921 MHz - 925 MHz range, allocated to GSM-R, is licensed to the national railway service (Banedanmark) and is in active use which is also restricting the use of this. The spectrum from 915 MHz - 921 MHz is allocated to TETRA type communication. In Denmark TETRA is used for the SINE (SIkkerhedsNEttet) network which is the primary communication platform for emergency services. However, currently, the SINE network is confined to the frequency range 380 MHz - 400 MHz. The TETRA allocation in the 915 MHz - 921 MHz range is available for professional radio communication companies but there is no one currently holding the license. This means that this frequency range could be used for research purposes following the Listen Before Transmit (LBT) principle [13].

To investigate if there is a current use of the 915 MHz - 921 MHz frequency range, in the area where the measurement is intended to be conducted, a spectrum analyzer together with a dipole antenna was used to sweep the frequency range. A measurement where the maximum power spectrum over 24 hours was recorded. The resulting power spectrum is shown in Fig. E.2.

From Fig. E.2 it can be seen that there is activity in the band, even though no one is licensed to use it. This restricts the measurement signals to narrowband and, to minimize interference, single tone signals. No activity was recorded at 917.5 MHz. Due to this, it is chosen to use this frequency to transmit our measurement signal as a single tone.

Measurement Area

The target application scenario is, as mentioned in the introduction, hiking in the forest. A forest called Rold Skov is located approximately 25 km south of Aalborg, Denmark. A large part of Rold Skov is so-called state forest meaning that it is governed by the government agency Naturstyrelsen. An area in this forest with only slow changes in terrain height and good access conditions were identified following the route indicated with yellow in Fig. E.3.

To conduct the measurements an official permit, allowing for entering the forest with a motor vehicle and conducting the measurements, had to be

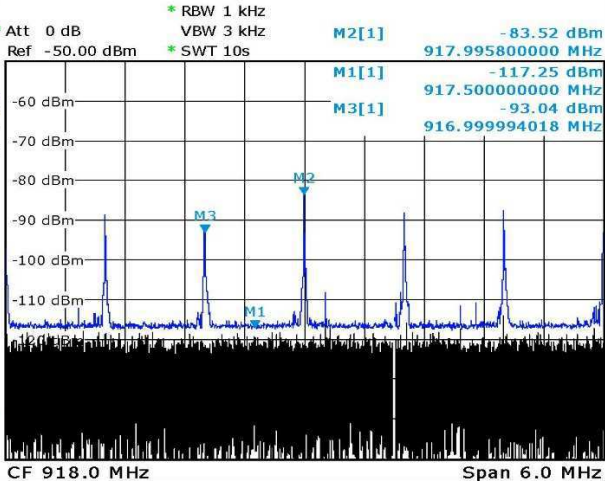

Fig. E.2: 24 hours spectrum sweep of the 915 - 921 MHz frequency range.

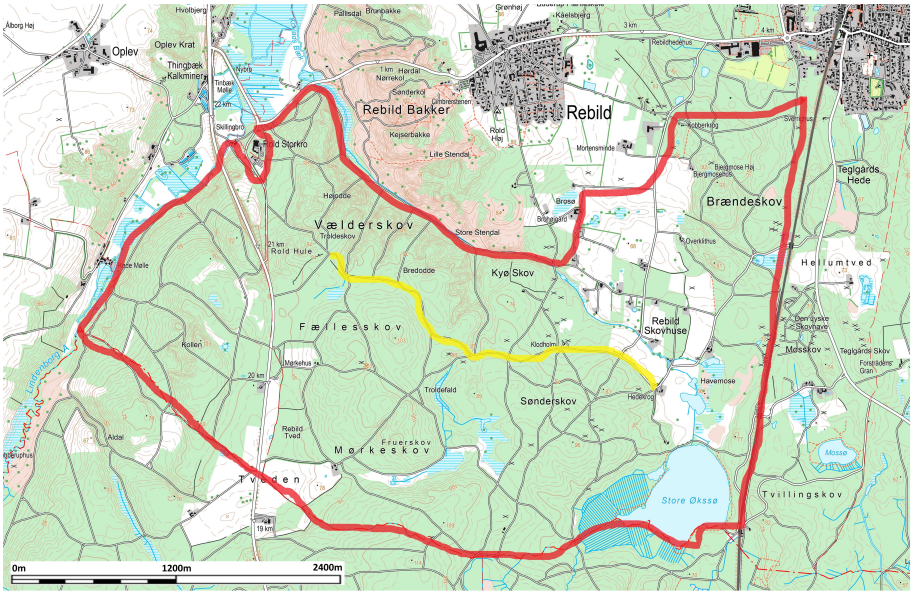

Fig. E.3: Measurement area, boundary marked in red and used route in yellow. Map source: [15].

acquired. The acquired permit is valid for the area inside the red line shown in Fig. E.3 allowing for the measurements to be conducted.

Measurement Positions

The measurement positions were recorded with the Global Navigation Satellite System (GNSS) using Leica GPS1200 surveyor equipment. The equipment utilizes the Differential Global Positioning System (DGPS) where Real Time Kinematic (RTK) corrections are applied to improve precision, which allows for centimeter precision in ideal conditions. Due to the terrain and possible tree canopies, the expected uncertainty of the measured 3D coordinates will be less than 1 meter. The used geodetic datum is UTM zone 32 (UTM32V - ETRS89/DVR90) for the recorded coordinates. The recorded coordinates can be translated to latitude, longitude position in the WGS84 system for showing the position in other map systems as described in [16].

A total of 71 different measurement positions is used for the measurements. The recorded measurement positions numbering is shown in Fig. E.4 starting at the transmitter (Tx) in the upper left corner and then distributed towards the furthest point at the lower right corner. The measurement points have been distributed such that they are most dense close to the transmitter (Tx) and at the furthest measurement positions. The furthest measurement position is 71 where the straight line distance to Tx is 2580 m.

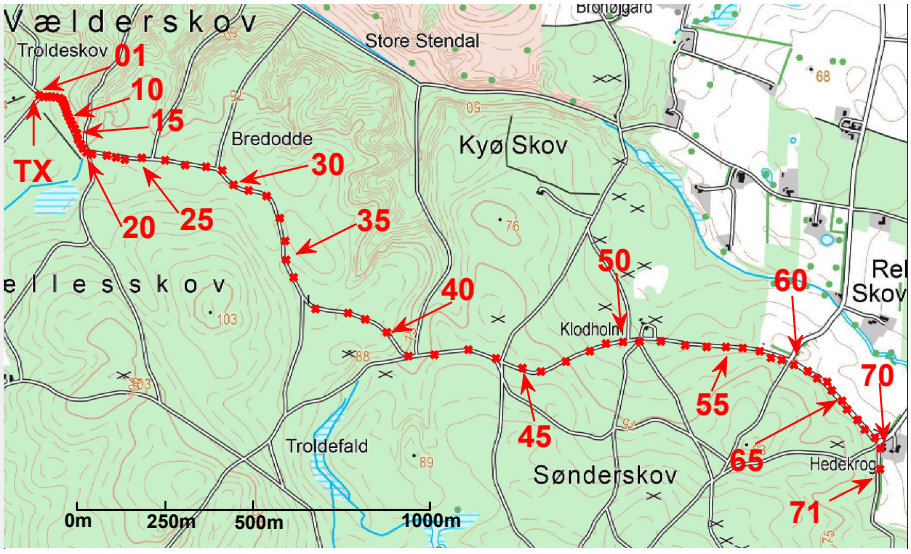

Fig. E.4: Measurement locations. Tx position is marked at the left top in the figure. Map source: [15].

The changes in terrain elevation of the 71 measurement points have been plotted in Fig. E.5. Note that the line between the measurement positions, marked with crosses, in Fig. E.5 are added only to aid readability.

The transmitter is placed on a 1.5 m mast and the transmit position is

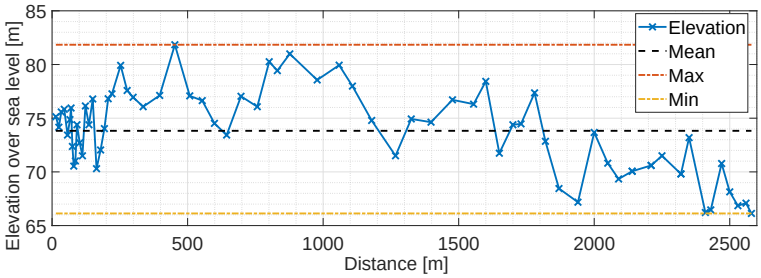

Fig. E.5: Terrain elevation over sea level versus LOS distance to the Tx.

located at an elevation of 76.8 m. The receiver is also placed on a 1.5 m mast which is moved to the 71 measurement positions. The mean elevation of the measurement positions is at approximately 74 m and from Fig. E.5 it can be seen that the variations in terrain elevation are restricted to ± 8 m from the mean elevation.

III Measurement System

The aim of this work is to establish the range of an NB-IoT D2D communication system. For this purpose, a system capable of transmitting a test signal and recording the power at the receiver is needed. Such a measurement system has been developed as illustrated in Fig. E.6, using the equipment listed in TABLE E.1.

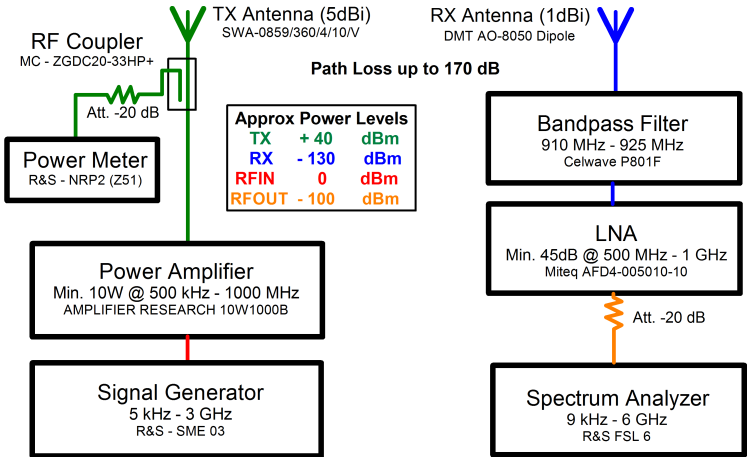

Fig. E.6: Blockdiagram of the measurement system

The test signal is generated as a single frequency tone at 917.5 MHz by the

Table E.1: Measurement System Equipment

Type	Model	Note
Signal Generator	Rohde & Schwarz SME03	
Power Amplifier	Amplifier Research 10W1000B	Min. 10 W @ 500 kHz - 1 GHz
Power Meter	Rohde & Schwarz NRP2	Using a Z51 sensor
RF Coupler	Mini-Circuits ZGDC20-33HP+	
TX Antenna	HUBER+SUHNER SWA-0859/360/4/10/V Folded Monopole	5 dBi @ 917.5 MHz
RX Antenna	DMT A0-8050 Dipole	1 dBi @ 917.5 MHz
Band-pass Filter	Celwave P801F	Tuned to CF 917.5 MHz
Low Noise Amplifier (LNA)	Miteq AFD4-005010-10	Min. 45 dBm @ 500 MHz - 1 GHz
Spectrum Analyzer	Rohde & Schwarz FLS6	

signal generator. Following this, the test signal is amplified to 10 W (40 dBm) before transmitted. This power amplification is needed to overcome the intended path loss scenario for the measurement campaign of 164 dB. Just before the transmit (TX) antenna, a Radio Frequency (RF) coupler allows the attached power meter to record the actual input power at the TX antenna. This is needed as the power amplifier might drift in amplification during the measurement. Recording an accurate TX power level is needed to determine the correct path loss throughout the measurement. Before the input of the power meter, a linear RF attenuator is added to lower the RF power to the range acceptable by the power sensor. The receiver (RX) antenna is connected through a band-pass filter and a Low Noise Amplifier (LNA) to the spectrum analyzer (FSL6). The LNA is used to amplify the signal to a level within the dynamic range of the spectrum analyzer. The band-pass filter is used to protect the LNA and spectrum analyzer for unwanted high-powered signals. The linear RF attenuator just before the spectrum analyzer is added to ensure that the RF power does not exceed the specified maximum accepted input power of the spectrum analyzer. Finally, the spectrum analyzer records the zero-span received power at the chosen measurement frequency.

As seen in Fig. E.6 there is no connection between the TX and RX side of the measurement system. This is possible as only the power is recorded and therefore there is no need for phase/time synchronization between TX

and RX. Any offset between the asynchronous oscillators is accounted for when the frequency for the zero-span measurement is chosen at the spectrum analyzer. The settings of the spectrum analyzer are shown in TABLE E.2.

Table E.2: Spectrum Analyzer Setup

Parameter	Setting
Center Frequency	$\approx 917.5\,\text{MHz}$
Resolution bandwidth (RBW)	1 kHz
Sweep Points	501
Sweep Time	5 s
Detector Mode	Root Mean Square (RMS)
Noisefloor (with LNA)	$-140\,\text{dBm}$

As seen in TABLE E.2 the Resolution bandwidth (RBW) is chosen 1 kHz. Choosing a smaller RSB would lower the noise floor of the system. However, as the system is asynchronous it is needed to choose the RSB large enough to allow for small drifts during the 5 s sweep of the 501 points. The long sweep time is needed as a single tone will be used for the measurement. This means multipath fading cannot be averaged in the frequency domain. As a result, multiple snapshots of the channel, given by the different sweep points, have to be recorded distributed over an area corresponding at least one wavelength of the recorded frequency. This allows for an averaging of the multipath fading in the spatial domain. In practice the spatial averaging was done by moving the antenna around in a circle with a diameter of 35 cm during the 5 s sweep.

IV Results

A total of 265 measurements were performed over three different days. Each day the entire measurement route were measured together with some repetitions at key points. This means that each of the 71 different measurement positions was measured between 2 and 5 times. At each measurement, the collected data consisted of 501 sweep points. All the collected sweep points for each measurement position have been concatenated and used to calculate mean power and power variance for that given measurement position. Before the concatenation of the sweep points, each power reading has been corrected by using known values of the measurement systems gains and losses. The system gains and losses were found by RF power measurements throughout the system chain. The Tx power was tracked during the measurement and the LNA gain was verified at the start and end of each measurement day. The cable, coupler, filter and connector losses were verified using vector network analyzer (VNA) measurements.

The plots shown in Fig. E.7 describe the measured received power. The plot shows the received power without added gains from antennas and LNA. For reference, the calculated Friis path-loss, shown in (E.1), and the Two-ray model, shown in (E.2), have been plotted. The Friis path-loss is plotted for both path-loss exponents 2 and 4 giving free space and 4th power loss [17].

$$P_{Friis} = P_{Tx} + G_{Tx} + G_{Rx} + \gamma\, 10\, log_{10}\left(\frac{\lambda}{4\pi d}\right) \quad [dBm] \tag{E.1}$$

$$P_{2Ray} = P_{Tx} + 10\, log_{10}\left(G_{Tx} G_{Rx} h_{Tx}^2 h_{Rx}^2\right) - 40\, log_{10}\left(d\right) \quad [dBm] \tag{E.2}$$

where P_{Friis} and P_{2Ray} is the received power for the two models. P_{Tx} is the transmit power. G_{Tx} and G_{Rx} is the antenna gain for the transmit and receive antenna. The wavelength is expressed by λ and γ is the path-loss exponent. The distance between transmitter and receiver is denoted by d while h_{Tx} and h_{Rx} denotes the height of the transmit and receive antenna.

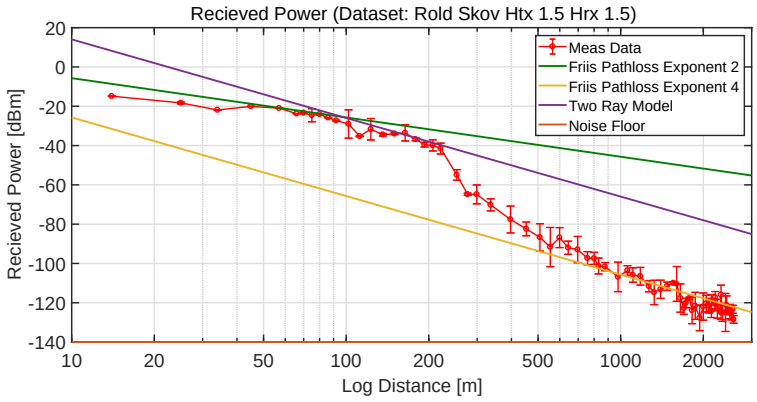

Fig. E.7: Received power plotted against logarithmic distance scale.

In Fig. E.7 it can be seen that the measured received power seems to follow the curve for free space loss from 10 m to 90 m. From 90 m to 220 m it fits quite well with the Two-ray model. Then there is a transition from 220 m to 800 m where after it settles and starts following the modeled 4th power loss.

The first approximately 200 m of the measurement route is quite open resulting in almost clean line-of-sight (LOS) conditions. This corresponds to the finding that the received power in this region follows what is expected for free space path-loss. After this, the forest gets denser which in the mea-

surements can be seen as a transition towards the 4th power path-loss model. The measurements indicate that from approximately 800 m until the furthest measurement at 2580 m the received power can be fairly well predicted using the 4th power path-loss model.

The path-loss is given by the relation between the transmitted and received power, in dB expressed as $P_L = P_{Tx} - P_{Rx}$. Using the measurement data presented in Fig. E.7 together with the transmit power of 40 dBm the mean path-loss can be found. A plot of this is shown in Fig. E.8.

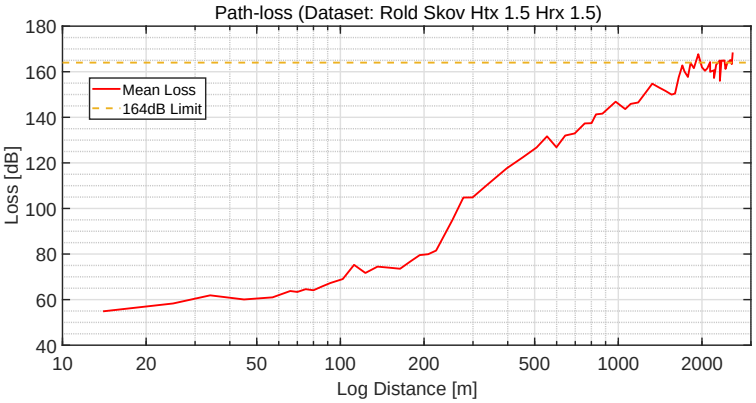

Fig. E.8: Path-loss plotted against logarithmic distance scale.

From Fig. E.8 it can be seen that the 164 dB path-loss limit, which is specified for NB-IoT, supports a distance between transmitter and receiver of approximately 2000 m.

V Conclusion

This paper presents a path-loss measurement campaign intended to illustrate the coverage range of a Device-to-Device (D2D) Narrow Band Internet-of-Things (NB-IoT) communication system in a forest scenario. A measurement system capable of high dynamic range was designed, as presented in this paper. Using the designed measurement system, measurements have been conducted at ranges up to 2580 m at 917.5 MHz. A total of 265 measurements were conducted at 71 different positions with both transmit and receive antenna in a height of 1.5 m above the terrain. The measurements showed that for the path-loss limit of 164 dB, specified for NB-IoT, a coverage range of approximately 2000 m could be achieved.

Acknowledgment

The authors would like to thank Ph.D. students: Carla Di Paola, Yilin Ji, Rocio Rodriguez Cano, Stanislav Zhekov and Jin Zhang for help during the measurements. The authors would also like to thank lab engineers Kristian Bank and Kim Olesen for valuable assistance in the development of the measurement system. Further the authors would like to thank Erik Jakobsen from Intel Mobile Communications, Aalborg, Denmark for being point of contact and enabling this measurement campaign.

The work presented in this paper has been conducted under the framework of the VIRTUOSO project. The Innovation Fund Denmark supports this project together with industry partners: Telenor, Keysight, and Intel Mobile Communications.

References

[1] A. Asadi, Q. Wang, and V. Mancuso, "A survey on device-to-device communication in cellular networks," *IEEE Communications Surveys Tutorials*, vol. 16, no. 4, pp. 1801–1819, 2014.

[2] 3GPP, *TR 36.843 (v12.0.1) - Study on LTE device to device proximity services; Radio aspects*, 2014.

[3] J. G. Andrews, S. Buzzi, W. Choi, S. V. Hanly, A. Lozano, A. C. K. Soong, and J. C. Zhang, "What will 5g be?" *IEEE Journal on Selected Areas in Communications*, vol. 32, no. 6, pp. 1065–1082, June 2014.

[4] B. Badic, C. Drewes, I. Karls, and M. Mueck, *Rolling Out 5G: Use Cases, Applications, and Technology Solutions*. Apress, 2016, ISBN: 978-1-4842-1507-4 DOI: 10.1007/978-1-4842-1506-7.

[5] Editors: Osseiran, Afif and Monserrat, Jose F. and Marsch, Patrick, *5G Mobile and Wireless Communications Technology*. Cambridge University Press, 2016, ISBN: 978-1-107-13009-8 DOI: 10.1017/CBO9781316417744.

[6] 3GPP, *TR 45.820 (v13.1.0) - Cellular system support for ultra-low complexity and low throughput Internet of Things (CIoT)*, 2015.

[7] M. Lauridsen, L. C. Gimenez, I. Rodriguez, T. B. Sorensen, and P. Mogensen, "From lte to 5g for connected mobility," *IEEE Communications Magazine*, vol. 55, no. 3, pp. 156–162, March 2017.

[8] I. Z. Kovacs, P. C. F. Eggers, and K. Olesen, "Radio channel characterisation for forest environments in the vhf and uhf frequency bands," in *Gateway to 21st Century Communications Village. VTC 1999-Fall. IEEE VTS 50th Vehicular Technology Conference (Cat. No.99CH36324)*, vol. 3, 1999, pp. 1387–1391 vol.3.

[9] K. Konstantinou, S. Kang, and C. Tzaras, "A measurement-based model for mobile-to-mobile umts links," in *2007 IEEE 65th Vehicular Technology Conference - VTC2007-Spring*, April 2007, pp. 529–533.

[10] Y. S. Meng and Y. H. Lee, "Investigations of foliage effect on modern wireless communication systems: A review," in *Progress In Electromagnetics Research (PIER)*, vol. 105, 2010, pp. 313–332.

[11] S. Chandrasekharan, A. Al-Hourani, K. Magowe, L. Reynaud, and S. Kandeepan, "Propagation measurements for d2d in rural areas," in *2015 IEEE International Conference on Communication Workshop (ICCW)*, June 2015, pp. 639–645.

[12] I. Z. Kovács, "Radio channel characterisation for private mobile radio systems : Mobile-to-mobile radio link," Ph.D. dissertation, Aalborg University, 2002.

[13] Danish Ministry of Energy, Utilities and Climate, *BEK nr 571 af 30/05/2017 - Law of Danish frequency allocation*, 2017.

[14] ——, *Spectrum auctions, frequency legislation and frequency planning.*, 2017, [Available Online] https://ens.dk/en/our-responsibilities/spectrum.

[15] Geodatastyrelsen, *Danish Geological Service.*, 2017, [Available Online] http://gst.dk/.

[16] J. P. Snyder, *Map projections: A working manual.*, 1987, washington, D.C.: U.S. Government Printing Office.

[17] A. Goldsmith, *Wireless communications*. Cambridge University Press, 2005, ISBN: 978-0-521-83716-2.

Paper F

Empirical Study of Near Ground Propagation in Forest Terrain for Internet-of-Things type Device-to-Device Communication

Johannes Hejselbæk, Jesper Ødum Nielsen, Wei Fan and Gert Frølund Pedersen

The paper has been submitted to:
IEEE ACCESS, 2018.

Abstract

This paper presents continuous wave power measurements conducted in forest terrain with focus on path-loss in a Device-to-Device (D2D) communication scenario. The measurements have been conducted at 917.5 MHz with measurement ranges extending to more than 2.5 km using a purpose-developed measurement system with a dynamic range of 180 dB. The impact of different antenna heights has been investigated by placing antennas at 1.5, 2.5 and 3.5 meters elevation over the terrain. The measurements showed that the antenna elevation in the given scenario did not have a significant impact on the received power. The measurements also showed that the dominant path of propagation is through the foliage for the first approximately 1000 meters why foliage excess loss is dominant in this region. After approximately 1000 meters the measured received power tend to follow the fourth-power law indicating that the excess loss due to foliage has to be limited. The measurement results have been compared to models proposed in the literature based on empirical data, as well as modes proposed by ITU and COST. The comparison showed that only two models predicted the, in the measurement data observed, limit in foliage excess loss. By applying these excess loss models in combination with path-loss models it was possible to model the measured total path-loss with an RMS error of less than 10 dB. This was archived by either applying a model proposed by Tewari or a combination between the two-ray path-loss model and the ITU-R P.2108 clutter loss model.

At the time of the creation of this PDF, the paper was still under review and is therefore not included in this public version. The reader is therefore referred to the publication channel or if needed to contact the author for a copy of the paper.

ISSN (online): 2446-1628
ISBN (online): 978-87-7210-260-3

AALBORG UNIVERSITY PRESS